INSTITUTO SUPERIOR TÉCNICO
Universidade Técnica de Lisboa

Modeling of a fixed bed industrial hydrotreating unit

Improvements in the deactivation mechanism

Pedro Miguel Carriça de Oliveira

Dissertação para obtenção do Grau de Mestre em

Licenciatura em Engenharia Química

Júri

Presidente: Professor João Bordado

Orientador: Professor Fernando Ramôa Ribeiro

Vogais: Professor Francisco Lemos

Setembro de 2007

Acknowledgements

This report is the result of six months traineeship in IFP during 2007 and I like to dedicate these words to all the people which directly or indirectly helped me in the accomplishment of this work.

I start to express gratitude to Professor Fernando Ramôa Ribeiro, from Instituto Superior Técnico, since this traineeship only was possible because of his contacts inside IFP. I also thank him for his trust on my capabilities and his concerns about my work during these six months.

I also dedicate a special gratitude to my traineeship supervisor, Jan Verstraete, for all the help that he granted me in the code modifications and for the ideas that he has suggested me.

I want to be grateful to my family and especially to my girlfriend for all the support that they gave me.

At last, but not least, I want to express my gratitude for the moments passed during this period to all my work companions.

Abstract

A simulation model for residue hydrotreating called THERMIDOR was developed over the last decade at IFP. It was implemented in FORTRAN and simulates a complete hydrotreating unit. The software consists of a kinetic model for residue hydrotreating based on 8 chemical families (gas, saturates, aromatics-, aromatics+, resins-, resins+, asphaltenes and metal deposits), which are further decomposed into sub-species to track the atomic composition (C, H, S, N, O, Ni, V) of each chemical lump. Between these various sub-species, a total of 87 reactions were taken into account. This kinetic model was integrated into a fixed bed reactor model that accounts for intraparticle transport by molecular, Knudsen and configurational diffusion. During this development, it was shown that, for these heavy petroleum feeds, significant intraparticle diffusion of heavy molecules needs to be explicitly accounted for.

The objective of this traineeship at IFP was to extend the process model by improving the representation of catalyst deactivation through coke laydown and metals deposition, while simultaneously incorporating their effects on catalyst activity and selectivity. The model contained a module that accounted for catalyst ageing, but its predicted effects did not correctly represent the observed phenomena, more specifically the initial rapid catalyst deactivation observed during the first two months after unit start-up.

Some modifications were successfully implemented in the code to improve it. The results obtained are more realistic and now the model predicts well the deactivation process. Other modifications were proposed with the objective of improving the program and to be used as an optimization tool.

Keywords: hydrotreatment, hydrodesulfuration, hydrodemetallization, residues, model

Resumo

Um programa de simulação chamado THERMIDOR foi desenvolvido durante a ultima década no IFP. Este foi implementado em FORTRAN e simula por completo uma unidade de hidrotratamento. O programa consiste num modelo cinético de hidrotratamento de resíduos baseado em 8 famílias químicas (gases, saturados, aromáticos^{-}, aromáticos^{+}, resinas^{-}, resinas^{+}, asfaltenos e depósitos de metal) que são ainda divididas em subespécies para se poder seguir a composição atómica (C, H, S, N, O, Ni, V) de cada família. Foram consideradas 87 reacções entre as subespécies. O modelo cinético foi integrado no modelo de um reactor de leito catalítico fixo tendo em conta o transporte intraparticular molecular, de Knudsen e de difusão configuracional. Durante o desenvolvimento do modelo foi demonstrado que para as fracções pesadas do petróleo, a difusão intraparticular limita significante as moléculas pesadas e precisa de ser considerada.

O estágio no IFP tinha como objectivos melhorar o processo de desactivação do catalisador provocada pela deposição de coque e metais assim como acoplar estes efeitos na actividade e selectividade do catalisador. O modelo já continha um módulo para considerar a desactivação do catalisador mas os resultados previstos não representavam correctamente os fenómenos observados, mais especificamente a desactivação inicial rápida do catalisador que se verifica nos primeiros dois meses após o arranque da unidade. Assim, foram implementadas com sucesso algumas modificações no código cujos resultados obtidos são mais realísticos que os anteriores. Pode-se agora considerar que o modelo prevê bem o processo de desactivação. Foram também propostas outras modificações de forma a melhorar o programa para que este possa ser usado como uma ferramenta de optimização.

Palavras-chave: hidrotratamento, hidrodesulfuração, hidrodemetalização, resíduos, modelização

Table of Contents

List of Tables

List of Figures

Abbreviations and acronyms

AR – Atmospheric residue

ARDS – Atmospheric residue desulfurization

Aro^{+} – Aromatics plus

Aro^{-} – Aromatics minus

Asp – Asphaltenes

BET – Physical adsorption method of gas molecules on a solid surface to determine the surface area

FCC – Fluid Catalytic Cracking

HDAs – Hydrodeasphalting

HDC – Hydrocracking

HDCC – Hydrogenation of Conradson carbon promoters

HDM – Hydrodemetallization

HDN – Hydrodenitrogenation

HDS – Hydrodesulfuration

HVB – Hydrovisbreaking

IFP – Institut Français du Pétrole

LSFO – Low Sulfur Fuel Oil

PNA – Polynuclear aromatics

RCM – Random Coins Model

Res^{+} – Resins plus

Res^{-} – Resins minus

RNM – Random Needles Model

RSM – Random Spheres Model

SARA – Saturates, Aromatics, Resins and Asphaltenes

Sat – Saturates

SEM – Scanning electron microscopy

TEM – Transmission electron microscopy

THERMIDOR – THERmal Monitoring for Isoperformance Demetallization of Oil Residua

VR – Vacuum residue

Context and objectives

Context:

Crude oils contain a very large fraction of heavy products for which only few outlets exist. Refining processes converting heavy oil fractions into more valuable products are therefore vital to a refinery. However, the heaviest cuts, termed residues, contain large amounts of impurities, such as sulphur, nitrogen and metals. Hence, these residues need to be purified before feeding them to heavy oil conversion processes.

Residue hydrotreating is industrially carried out at high temperature and under a high hydrogen partial pressure in units comprising several fixed bed adiabatic reactors in series. Under these conditions, a catalyst promotes a complex network of parallel and consecutive reactions among which are hydrodemetallisation, hydrodesulfurisation, hydrodenitrogenation, hydrocracking and hydrogenolysis reactions. In order to concurrently enable all these chemical transformations, the residue feed successively passes over fixed beds containing different types of catalysts.

The reactivity of a residue feed depends both on the concentration and the nature of the various species (saturates, aromatics, resins and asphaltenes) and more specifically on the size of the asphaltenes. The latter are colloid structures whose radius of gyration typically lies between 10 Å and 500 Å. Asphaltenes can therefore only penetrate into the outer layers of porous catalysts, depending on its nature, the operating conditions and the environment of the asphaltene species. Their penetration is not only governed by molecular and Knudsen diffusion, but also by so-called configurational diffusion. Hence, the performances of residue hydrotreating catalysts strongly depend on their porous texture.

The optimization of the operating conditions of a residue hydrotreating unit necessarily needs to be based on a model translating the various physical and chemical phenomena. The hydrodynamic description has to account for transport of the species by convection as well as by the various diffusion mechanisms inside the catalyst pellets, while the kinetic model needs to account for the influence of the feed composition and the operating conditions of the unit

Objectives of the traineeship:

During previous work at IFP, a kinetic model for residue hydrotreating was developed based on 8 chemical families (gas, saturates, aromatics-, aromatics+, resins-, resins+, asphaltenes and metal deposits), which are further decomposed into sub-species to track the atomic composition (C, H, S, N, O, Ni, V) of each chemical lump. Between these various sub-species, a total of 87 reactions were taken into account. This kinetic model was integrated into a fixed bed reactor model that accounts for intraparticle transport by molecular, Knudsen and configurational diffusion. During this development, it was shown that, for these heavy petroleum feeds, significant intraparticle diffusion of heavy molecules needs to be explicitly accounted for. Based on experimental data acquired within the framework of a PhD thesis, the various

parameters of the kinetic model were estimated. The model correctly predicts the evolution along the reactor of the concentration profiles of the various lumps, the impurities in the total liquid effluent, and the atomic composition of each family.

The proposed traineeship at IFP aims at completing this process model by accounting for catalyst deactivation through coke laydown and metals deposition, while simultaneously incorporating their effects on catalyst activity and selectivity. The model currently contains a module that accounts for catalyst ageing, but its predicted effects do not correctly represent the observed phenomena, more specifically the initial rapid catalyst deactivation observed during the first two months after unit start-up.

The traineeship program will start with a literature review on catalyst deactivation of hydrotreating catalysts and on the various modeling approaches that can be used to describe these deactivation phenomena. In a second step, the existing deactivation model will need to be improved and validated against available experimental data. Finally, time permitting, a complete run cycle of an industrial unit will be simulated and compared to the actual reactor performance in order to validate the modeling approach and its hypotheses.

1. Literature Review

1.1. Introduction

In the last thirty years, the world petroleum market suffered big changes. The demand for heavy products has decreased and the need for lighter products (e.g. for transportation use) has gone in the opposite way [1]. Besides this, some countries approved regulations that restrict the content of metals, sulfur and nitrogen in fuels to reduce the pollutant emissions. To achieve these objectives, the flowsheets of refineries has been changed to reduce the production of heavy fuel oil and residues and to lower the contents of metals and sulfur in the products. This was obtained with the introduction of new thermal and catalytic conversion such as *visbreaking*, *coking*, *catalytic cracking* (FCC, HDC) and *hydrotreating* (HDM, HDS, HDN…) that can convert a fraction of the atmospheric and vacuum residues into lighter and less polluted distillates. Since many of the conversion processes in a refinery are catalytic and contaminants like metals, sulfur and nitrogen deactivate the catalysts, *hydrotreating* has gained a considerable importance not only to improve the quality of the products but also to extend the life of the catalysts which permit longer runs of the units resulting in economical benefits for the refiners.

1.2. Residue Hydroprocessing

The term *resid* (residue) is used in petroleum refining for the bottom of the barrel and generally is the bottom stream of the atmospheric or vacuum distillation towers, AR and VR, respectively [2]. Naturally, these streams contain higher concentrations of sulfur, nitrogen and metals when compared with the crude oil from which they were obtained. These concentrations are higher in VR than AR since the impurities are predominantly in the heaviest fractions. Since the *resids* have a low hydrogen/carbon ratio, indicated by the *Conradson and Ramsbottom carbon residues*, they have high potential for coke formation that causes rapid catalyst deactivation and high catalyst costs. Consequently, catalytic processes for converting *resids* usually use AR as their feeds while VR are in most cases processed by noncatalytic processes.

1.2.1. Generalities on hydroprocessing

Hydroprocessing includes the processes that work with hydrogen pressure like *hydrotreating* and *hydrocracking*. Hydrotreating is a catalytic process that reduces metals, sulfur and nitrogen contents as well as saturates olefins and aromatics. Since the primary objective of hydrotreating in refineries typically is to reduce the sulfur content, the process is also commonly called *hydrodesulfurization*. On the other hand, the aim of hydrocracking is reduce the boiling range what means that most of the feed is converted (cracked) to lighter products. It is important to notice that cracking and desulfuration always occur simultaneously and we refer to hydrotreating or hydrocracking accordingly to the extent of the conversion reactions.

1.2.2. Chemical reactions

The *hydrogenolysis* of the more accessible C-S and C-N bonds by classical *hydrorefining* no longer sufficient to achieve the quality demands concerning sulfur and nitrogen. Additionally, catalytic cracking of the residues has created the need to reduce the nickel and vanadium content, contained within more complex chemical structures [3]. The main goal of hydroprocessing is therefore to promote the cracking reactions to obtain lighter compounds and the reactions that reduce the impurities (HDS, HDM, HDN) to achieve cleaner products and increase the catalysts life [4].

HDS

The removal of the sulfur is the principal objective of hydrotreating because it is a poison for the catalysts present in refineries and automobiles. Besides this, the environmental laws strongly limit the sulfur content in fuels (10 wtppm in 2009 for diesel and gasoline).

The major fraction of sulfur in *resids* is present in two forms: sulfide and thiophenic [5]. The sulfides are found in the form of condensed naphtheno-aromatic rings connected by sulfur (Figure 1.1). Since the C-S bond has low energy, it can be decomposed thermically. On the other hand, thiophenic compounds can be only decomposed catalytically and this can occur through parallel reactions with or without an intermediate hydrogenation step, followed by hydrogenolysis of the C-S bond [6] (Figure 1.2).

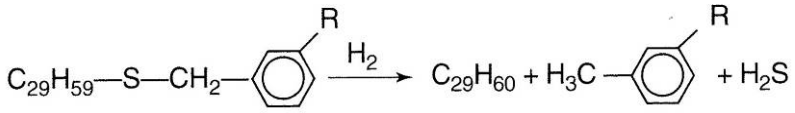

Figure 1.1 Hydrodesulfurization of sulfides present in residues.

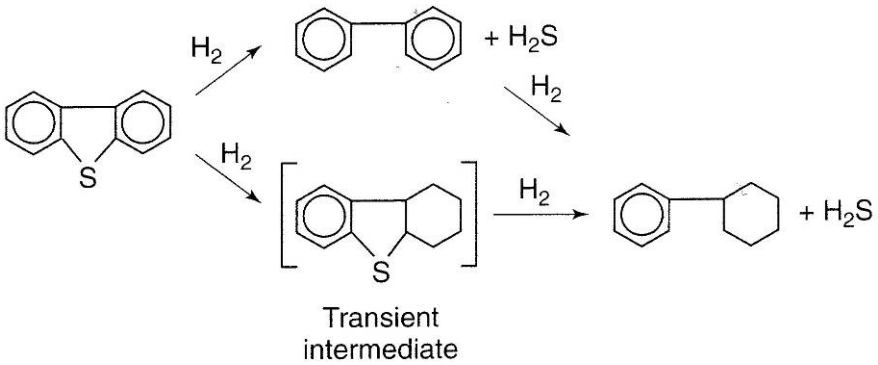

Figure 1.2 Hydrodesulfurization of thiophenic compounds present in residues.

HDM

The metals contained in the residues constrain the use of these heavy fractions. For example, the catalysts can only tolerate a low content of metals. Besides this, if there are metals in the hydrotreated residue, its use as LSFO will cause vanadium corrosion in furnaces and promote dust formation in combustion gases [6].

The metals in *resids* are in the form of soluble organometallic complexes. The micelles, which contain metal atoms, form planar structures with distances between them of about 12 Å. These structures can not easily be separated although they are not bound to each other by valence bonds [3]. The porphyrins are the most common of these organometallic complexes. All these complexes are present in the resin and asphaltene fractions of vacuum residues.

Demetallation requires a hydrogenolysis and a preliminary hydrogenation in order to expose the metal atoms. Since the vanadium atoms are situated closer to the periphery of the molecules, they are easier to remove than the nickel atoms [3]. The reaction products are metallic sulfides of the NiS or V_3S_4 type. The sulfides are deposited in the catalyst pores, covering its surface and gradually plugging up the pores, making the center of the grain less accessible to reactants. This effect, along with coke, contributes to the deactivation of the catalyst [6].

HDN

Pyrrole and pyridine are the principal families of compounds that contain nitrogen in *resids*. Although the pyridines are less reactive than pyrroles, these last ones become more easily adsorbed on the catalyst, inhibiting its activity. Since European regulations specify a maximum for NO_x emissions in combustion off gases, heavy fuel oils must have nitrogen content between 0.2 and 0.4 %wt. If the residue will be used as a FCC feed, the nitrogen content is preferably lower than 0.2 %wt to reduce the inhibition of the catalyst acid sites. Denitrogenation is therefore a desired reaction, however, very difficult to accomplish. Denitrogenation commonly varies from 20 to 60% [6].

Denitrogenation reactions are catalytic in nature. Contrary to the desulfuration of thiopenic compounds, denitrogenation always includes a prior aromatic ring hydrogenation step (limiting step) followed by hydrogenolysis of the C-N bond (Figure 1.3) [6].

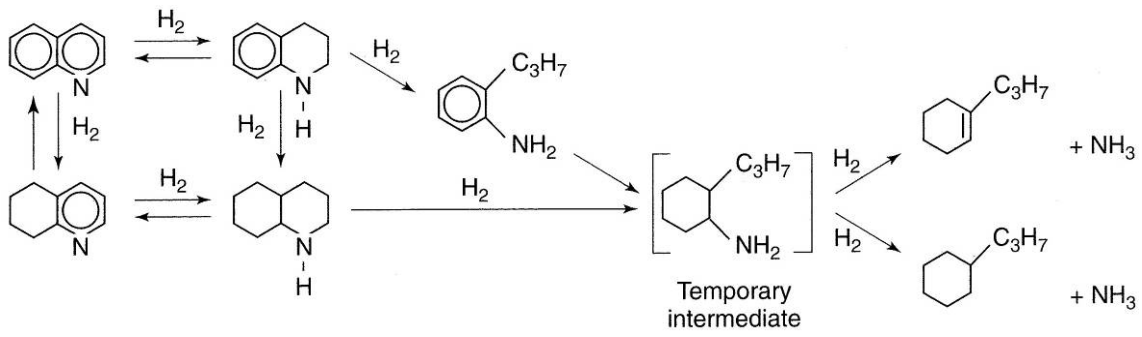

Figure 1.3 Hydrodenitrogenation of quinoline

Hydrogenation of aromatic rings and heterocyclic compounds

Hydrogenation reactions result in a higher H/C ratio in the product and 50 to 80% decrease in the Conradson carbon. If the product will be used as an FCC feed, this decrease is very advantageous since the maximum Conradson carbon content must be between 6 and 10% wt [6]. It is known however that the benzene ring is very difficult to hydrogenate.

Hydrogenations are intermediate steps that make heterocyclic compounds stabilized by resonance more reactive. This step is indispensable for the HDM and HDN reactions and promotes HDS and decyclization reactions.

Furthermore, hydrogenation reactions also affect the saturation of olefins and the capture of free radicals formed by thermal cracking, reducing the coke formation which causes catalyst deactivation.

Hydrogenation reactions along with the *hydrogen transfer* mechanism work as a *donor solvent* process. This way, polyaromatic compounds are hydrogenated to naphthenoaromatics that transfer hydrogen to free radicals in the voids of the catalytic bed before being catalytically rehydrogenated once again (Figure 1.4) [6].

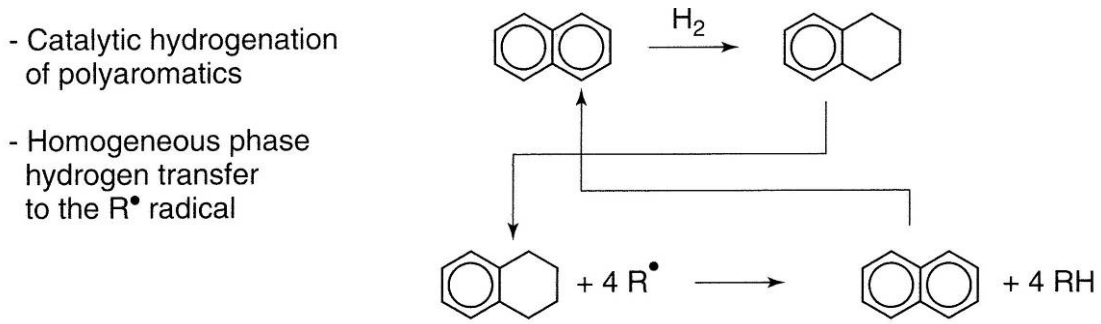

Figure 1.4 Hydrogen transfer mechanism

Cracking reactions

In resids and heavy oil processing, the cracking reactions are crucial since they produce light and valuable products (gases, gasoline, gas oils and vacuum distillates). The residue conversion rate depends on the process used but can go up to 90% [6].

Hydrogenation and hydrogenolysis reactions are responsible for generating products whose molecular weight and boiling temperature is somewhat lower. Conversion into lighter products comes from splitting C–C bonds by catalytic hydrocracking. However, the biggest fraction converted into lighter products is the result of thermal cracking at high temperature that occurs in the voids of the catalytic bed.

Thermal cracking reactions cause splitting of C-C bonds in compounds with sufficiently labile bonds and a weak tendency to be adsorbed on the catalyst surface. Aliphatic C–C bonds and, to a lesser extent, C–C naphthenic ring bonds are mainly involved. Monoaromatic ring C–C

bonds are stabilized by resonance and are therefore less apt to be thermally cracked. The same is true of polyaromatics, resins and asphaltenes, which are additionally strongly adsorbed on catalyst [6].

Condensation reactions and coke formation

There are some other types of reactions that occur. For example, the thermal cracking reactions proceed according to a free radical chain mechanism that results in the formation of polyaromatic coke precursors by condensation of heavy radicals. These heavy radicals can in turn be captured by the activated hydrogen on the catalyst, thereby reducing their tendency to condense and consequently form coke that cause a deactivating effect on the catalysts [6].

Hydrogenolysis of oxygenated compounds

There is not much information about hydrogenolysis of oxygenated compounds and the effect of these in the catalysts. The hydrogenolysis of the studied compounds, simple alcohols and carbonic acids, do not have any thermodynamic limitations [3] what suggests that the conversion of these is nearly total.

1.2.3. Catalysts

In the hydroprocessing of residues, different catalysts are used, that are placed in series. These catalysts activate the reactions described above (chapter 1.2.2), albeit to different extents. The first section of the reactor is loaded with a catalyst optimized for demetallization of the feed and for the disaggregation of asphaltenes and resins. The second section is optimized to promote conventional hydrorefining reactions like HDS and HDN. It is important that the catalysts possess good hydrotreating activity to ensure proper decarbonization (HDCC) and delay coke formation [1]. Table 1.1 **[6]** presents the general characteristics of the catalytic system.

Table 1.1 Example of characteristics of supported catalysts for residue hydroconversion

Type	Guard material	HDM catalyst	HDS catalyst
Main functions	Trap particles	HDM, Trap Ni + V, disaggregation of asphaltenes and resins	HDS HDN HDCC
Shape	Spheres-rings	Spheres -extrudates	Extrudates
Grain diameter (mm) **Surface area (m^2/g)** **Total pore volume (cm^3/g)** **Average pore diameter (Å)** **Active phase** **% of total catalyst volume**	3-10 < 1 < 0.25 10^5-10^6 - < 5	0.8-3 80-180 0.7-1.2 200-1000 NiMo-Mo 30-70	0.8-1.6 150-250 0.4-0.8 80-200 NiMo-CoMo 30-70

The catalysts are in most cases in the form of extrudates or spheres. In moving bed reactors is better to use spherical particles since they flow more readily. The use of small grains improves performance since the diffusional limitations are reduced. However the pressure drop in the reactor is increased. The catalyst grains also need to have very good mechanical strength if they are used in ebullating beds [6].

Guard material

Residues contains many solid particles that can have many origins: organic or inorganic iron, sodium chloride, coke from furnace tubes or the reactor, sediments, thermal degradation products from storage tanks, solids formed by reactions with additives present in the feed or catalyst fines from upstream units. These particles can reach 100 μm and since they do not enter into the catalyst grains, they lay down on the outer surface or between catalyst grains. This fills the inter-grain voids (increasing pressure drop) and bonds the catalyst grains together (making it difficult to unload the catalyst). To reduce these effects, the use of specific guard material before the catalysts can effectively trap the particles in its large pores increasing the life of the catalytic system [6].

HDM and HDS catalysts

The HDM catalysts are optimized to reduce Ni and V metals included in the feed. They need to be sufficiently active to enable HDM reactions and also have enough retention capacity to accommodate the metals sulfides deposited on the grain, preserving a satisfactory activity to achieve satisfactory run lengths. They also enable HDS reactions, but to a lesser degree when compared with HDS catalysts (Figure 1.5). On the other hand, besides promoting the HDS reactions, the HDS catalysts must perform deep refining reactions: hydrogenation, HDN and HDCC. Since they are placed after HDM catalyst, they receive a mostly demetallized feed and do not need a high metals retention capacity (Ni + V < 20% wt) [6].

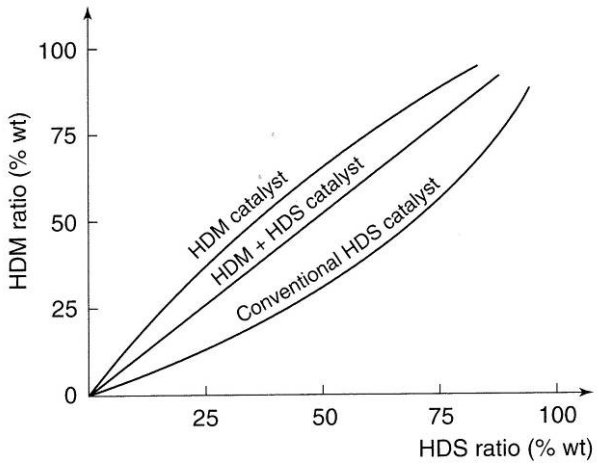

Figure 1.5 HDM/HDS selectivity of catalysts

To achieve these objectives, HDM and HDS catalysts have a completely different pore distribution (Figure 1.6). It is well known that microporosity promotes HDS reactions while mesoporosity favors HDM reactions and asphaltenes decomposition.

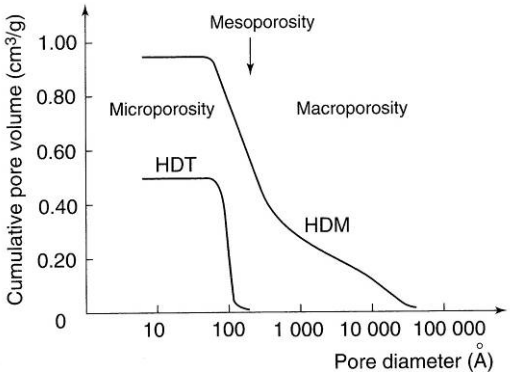

Figure 1.6 Catalyst pore distribution

Retention capacity of the HDM catalyst for metals sulfides (essentially Ni and V) can reach up to 100% of its fresh catalyst weight. This implies that HDM catalysts must have a relatively large fraction of macroporosity. This macroporosity also make possible that the large molecules, which contain the metals (resins and mainly asphaltenes), enter into the mesopores located inside the catalyst grains [6].

The catalyst's intrinsic activity comes from its active phase deposited on the support. For the HDM catalysts, its activity must not be too strong as it would cause metals to be laid down preferentially on the peripheral part of the catalyst grain. This deposit would plug the pores and consequently reduce the metals retention (Figure 1.7). However, its activity must be sufficient, since good hydrogenation slows down coke deposition on the catalyst. The choice of intrinsic catalytic activity is a balance between metals retention capacity and hydrogenating activity.

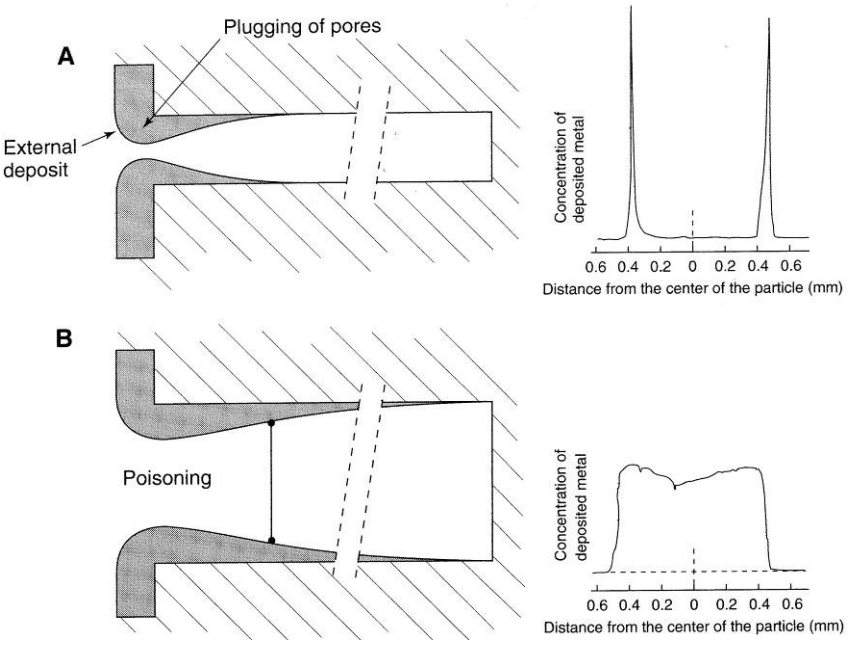

Figure 1.7 Effect of pore diameter on metals deposition

HDM and HDS ratios versus advancement in the fixed bed reactors with HDM and HDS are illustrated in Figure 1.8.

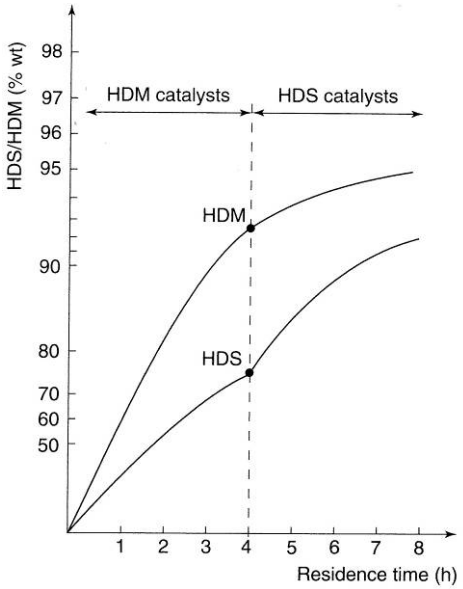

Figure 1.8 Variations in HDM and HDS for a vacuum residue versus advancement in the reactor

1.2.4. Operating conditions and kinetics

A detailed kinetic analysis of hydroprocessing is difficult because the composition of petroleum residues and the hydroconversion products is extremely complex. However, a global approach to the behavior of each reaction family is possible.

Thermal cracking reactions have high apparent activation energy (> 160 kJ/mol). The low conversion at 320ºC is virtually total at a temperature 100ºC higher. This is why these reactions are more significant in processes working at high temperature (ebullating and entrained beds). The higher the molecular weight of the various residue components, the more crackable they are and their crackability decreases going from paraffins to olefins, naphthenes and aromatics. Pressure has only a slight effect on thermal cracking reactions [6].

The reactions of polynuclear aromatics polymerization and condensation that are associated with thermal cracking are considerably felt above 410ºC. As a result, products are unstable and catalyst coking is faster and more severe. The higher the feed asphaltenes content, the stronger this tendency is. A high hydrogen pressure will therefore be necessary to hydrogenate the many radicals created when feeds are rich in asphaltenes and thereby prevent polycondensation [6].

HDS, HDN, HDM and asphaltenes disaggregation reactions occur according to kinetics with an apparent order between 1.5 and 1.7 in relation to the compounds under consideration [1]. Apparent activation energies are related to diffusional limitations in the catalyst grains. Their approximate value is 100kJ/mol. The HDS reactions are considered to be irreversible. The respective reaction rates of HDM and HDS reactions depend on the nature of the catalyst. The rate of elimination is faster for vanadium than for nickel [6].

Hydrogen pressure promotes reactions of aromatics hydrogenation, of denitrogenation and of free radical stabilization. The last reaction limits free radical condensation, thereby resulting in reduced Conradson carbon, better product stability, less catalyst coking and consequently a longer catalyst life [6].

In practice, the operating conditions used for hydroprocessing residues involve the following ranges:

- Space velocity 0.2 to 0.5 h^{-1}
- Total pressure 150 to 200 bar
- Hydrogen recycle rate 500 to 1200 m^3 (STP)/m3 of feed
- Temperature 380 to 440ºC

1.2.5. Hydrotreating processes

Hydrotreating of residues for desulfurization, denitrogenation, and demetallation is a process that recently underwent significant improvement. In combination with the catalytic cracking of the hydrotreated residues, it represents today one of the most attractive methods for converting heavy residues to motor fuels with high yields and relatively low hydrogen consumption.

Compared to the direct catalytic cracking of the residual fractions, the preliminary hydrotreating has two major advantages: it eliminates the poisoning of the catalytic cracking catalyst by Ni, V and sulfur and makes it possible to produce without difficulties gasoline that meets the increasingly more severe specifications for sulfur.

Four types of processes exist for the residues hydrotreating:

- Systems with fixed catalyst bed
- Systems with moving bed
- Systems with ebullated bed
- Systems with entrained bed

In all the systems the pressure is of the order of 150 to 200 bar [3, 6].

Fixed bed processes

The general scheme of such a unit is given in Figure 1.9 [1]. In this scheme, several reactors connected in series are used, instead of one reactor with cooling between the beds as uses for the processing of distilled feeds. The reason for this design is the fact that the deposition of the metals on the catalyst takes place rapidly, so that they are concentrated on the first portion of the contact zone, therefore in the first reactor and especially in its upper portion.

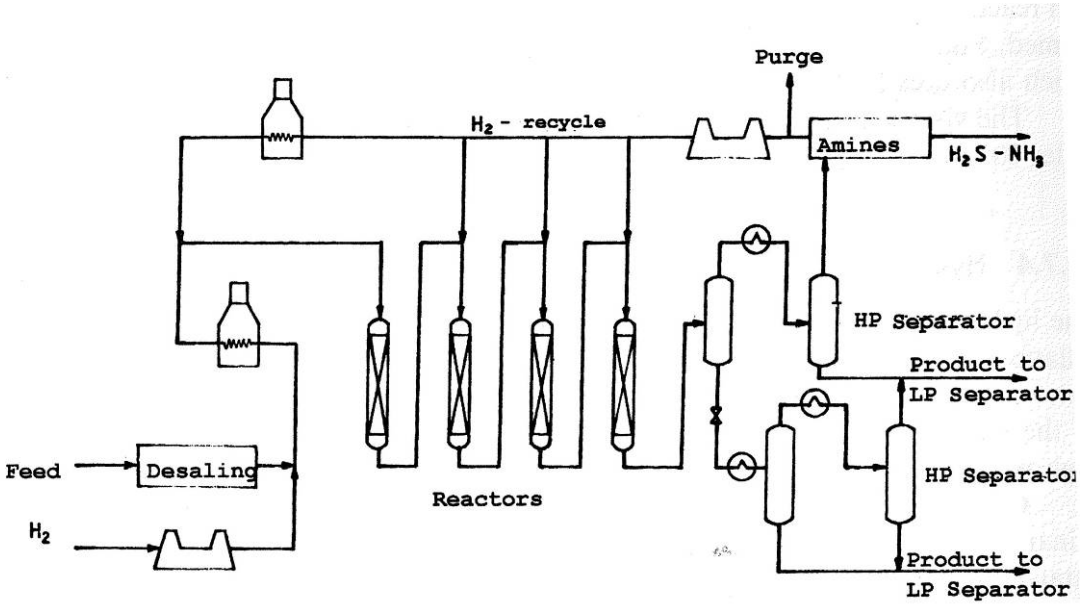

Figure 1.9 Fixed bed residue hydrotreating unit

Since the catalyst poisoned with metals can not be regenerated in place, the use of several reactors in series allows taking the first reactor out of circuit and replace the catalyst, without having to stop the operation of the unit.

The flow of the feeds in the reactors is downwards, with the gaseous phase being the continuous phase.

An essential problem for a good operation of the units is the uniform distribution and good dispersion of the liquid at the reactor inlet.

In operation, high attention is paid to the temperature profile and to the injection of the adequate amounts of cold recycled gases between the reactors, and possibly between the catalyst beds. Following each injection, the liquid must be redistributed by using a system similar to that of Figure 1.10.

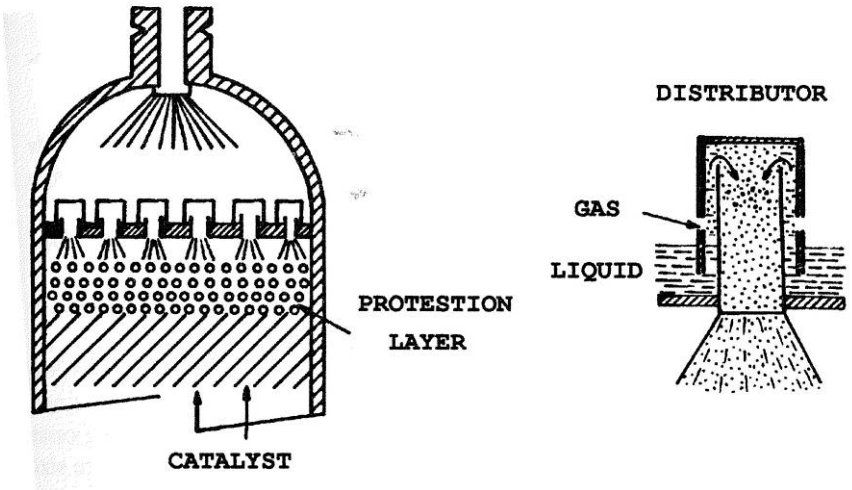

Figure 1.10 Liquid dispersion at the top of a residue hydrotreating reactor

As the coke and metals deposits in the catalyst increase, the temperature is increased to recover the catalyst activity, without however being allowed to exceed 425ºC at the end of the cycle.

The length of a cycle for a feed containing 150-200 ppm metals is typically 11 months. For feeds with a metal content up to 400ppm, two reactors that can be switched with each other on the top of the system. The length of the cycle is also 11 months. For higher metals content, the employed reaction systems are moving bed, or ebullated bed systems [3].

The system used in the fixed bed units is rather complex. Three classes of materials are used:

- Guard material
- HDM catalyst
- HDS catalyst that also promotes HDN and HDCC

In general, two types of catalyst are used: the first is for breaking the asphaltene molecules and demetallation, while the second is for hydrorefining. The proportion between the two catalysts depends on the properties of the feed and on the quality requirements of the finished product.

For good operation of the fixed bed catalyst, a good two-step desalting of the crude oil is needed, followed by a filtration of the feed to the unit, in order to prevent that the salt plugs the pores of the catalyst.

In the HYVAHL process of IFP, feed with up to 400 ppm V+Ni can be used. The system uses two interchangeable guard reactors located ahead of the main reactors. The feed passes first through the guard reactors containing demetallation catalyst. The other reactors contain both demetallation and desulfurization catalysts.

The sizes of catalysts extrudates must be sufficiently large for maintaining a reasonable pressure drop through the bed and for avoiding coke deposits that prevent circulation through the bed.

The advantages of the process in fixed bed are the absence of catalyst attrition and low risk of plugging of the bed, which can be of concern in system with moving bed or ebullating bed.

These advantages led to the situation that worldwide, in 1993, there were 30 operating units using fixed beds representing 80% of the operating units [6].

Moving bed processes

The system is similar to moving bed catalytic cracking, from which it borrows many traits.

The circulation of the catalyst is downwards. The circulation of the feed and hydrogen is cocurrent with the catalyst in the Shell process, and countercurrent in the ASVAHL IFP's process. In the latter case the velocities of the gas and liquid phases should not exceed those that would disturb the downwards plug flow of the catalyst particles of the bed.

In both cases, the metals are gradually deposited on the catalyst particles. In the ASVAHL system, the highly contaminated catalyst, containing also the impurities retained from the feed, is immediately eliminated. Thus, the feed and the hydrogen are further contacted with uncontaminated catalyst. In the Shell process, the catalyst that has retained the metals passes through the entire reaction volume before leaving the system. Despite the lack of comparative data, one may suppose that in identical conditions the performance of the ASVAHL process should be superior [3].

In many cases, the moving bed reactor is used as a first reaction step, followed by a fixed bed reactor (Figure 1.11). Thus, in the moving bed reactor the decomposition of the molecules with complex structures and the separation of the metals (Ni+V) takes place. Both are inherently accompanied by formation of coke deposits. Therefore, the moving bed reactor protects the fixed bed reactor system and significantly extends the length of the cycle.

The operational difficulties of such a reactor are related to the operations of introducing and removing of the catalyst into and out of the reactor, in which a high pressure and a hydrogen-rich atmosphere prevail.

In general, catalysts of spherical shape are used. Despite the fact that it has a lower catalytic activity, this shape has the advantage of easier circulation and a lesser attrition than other shapes. It must be mentioned that if attrition occurs in this reactor, the fines produced may be carried into the fixed bed reactor that follows and impact negatively the flow pattern through the bed.

The moving bed are used for feeds that are very rich in metals (500-700 ppm of Ni+V) [6].

Only a limited number of units of this type were operating worldwide as of 2002 [3].

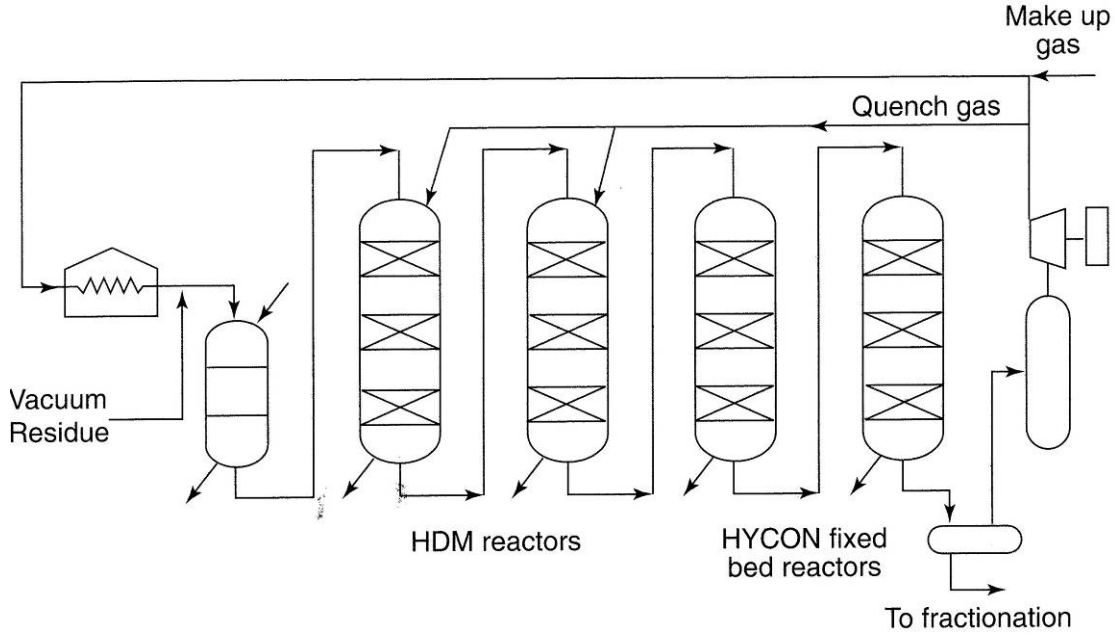

Figure 1.11 Hycon process flow scheme

Ebullating bed processes

In the ebullating bed process, hydrocarbon feed and H_2 are fed up-flow through a catalyst bed, expanding and backmixing the bed, minimizing bed plugging and pressure drop. The ebullated bed technology utilizes a three-phase system that is gas, liquid, and solid (catalyst). In this process, oil and catalyst is separated at the top of the reactor and oil is re-circulated to the bottom of the bed and mixed with the fresh feed. Fresh catalyst is added a daily basis on the top of the reactor and spent catalyst is withdrawn from the bottom of the reactor [7]. The ebullated bed process is carried out in reactors of the type described in Figure 1.12 [6].

The concominant presence in the reactor of the moving gas, solid, and liquid phases, in intimate contact, leads to difficult hydrodynamic conditions. Good liquid-solid mixing is performed by means of the recycling pump, while achieving adequate contact with the gas phase is much more complicated. Pressure has an important effect on the operation of the three-phase system [3].

There are two licensors concerning this process: H-Oil and L.C. Fining, with minimum differences in the design of the equipment. As per the end of 2002, a total of 11 ebullated bed units were in operation. Some of the units built earlier were either shut down or converted to hydrocracking operation [3].

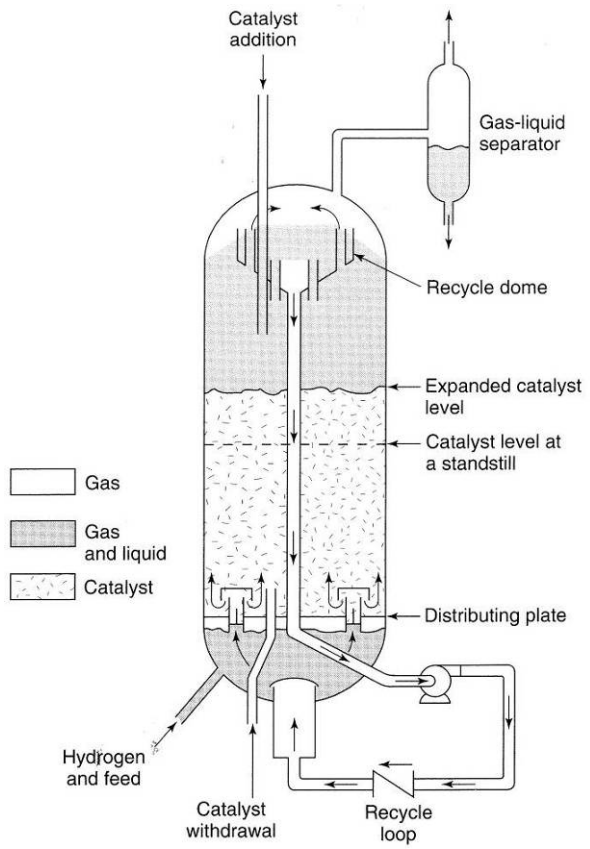

Figure 1.12 Ebullated bed reactor for residue hydrotreating

Entrained bed processes

Even more so than ebullating bed processes, slurry or entrained bed processes are designed to operate with residues having a high proportion of impurities, or even those containing wastes such as spent solvents and used plastic and tires. Some of these processes have reached the demonstration stage today: Veba's VCC, Petrocanada's Canmet and Exxon's Microcat [6]. Recently Eni's slurry technology (EST) process is moving towards the commercial proof at one of the Agip's refineries in Italy. Important modifications have been claimed by ENI for slurry processes (EST); the modifications mainly concern the possibility of obtaining high conversions while maintaining the stability and processability of the residues [8].

The reaction section (Figure 1.13) includes one or more reactors in-series where the feed, the recycle gas and the dispersed catalyst circulate in an upward stream. The linear velocities of the gas and the liquids must be high enough to entrain the catalyst and keep it from accumulating in the reactor.

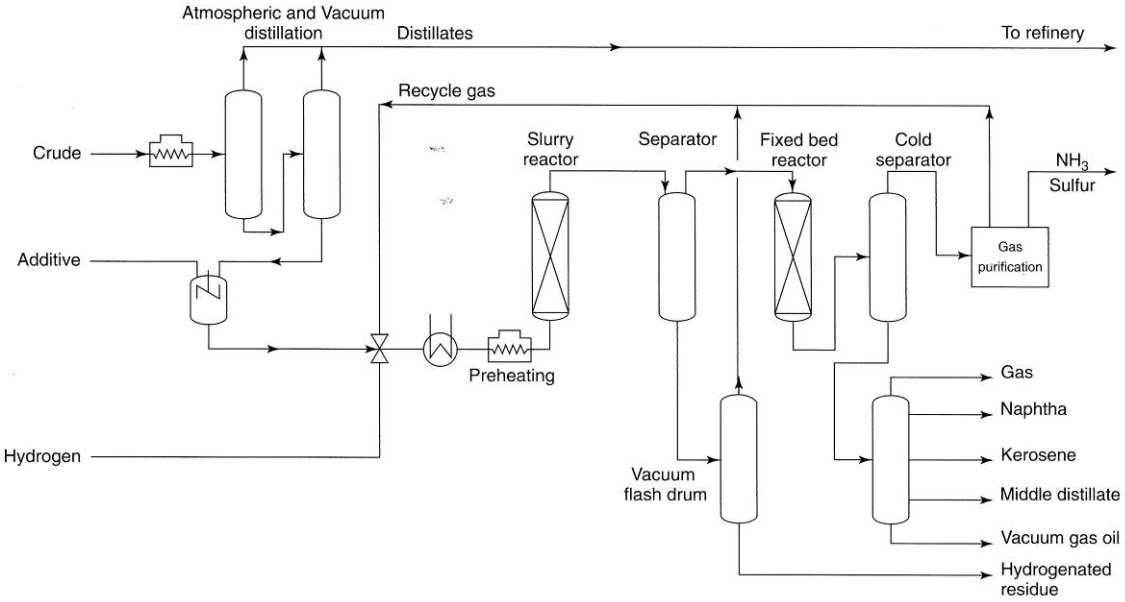

Figure 1.13 VCC process flow scheme

A process layout that is often proposed comprises a fixed bed reactor associated with a slurry reactor. The fixed bed reactor is designed to refine the light fraction produced by conversion in the slurry reactor.

The general operating conditions are similar to those for ebullating bed processes: high reaction temperatures and pressures, and residence times shorter than those for fixed or moving bed processes. Pressure losses are low and temperature profiles are isothermal in the reactor. Conversion to light products is very high (up to 90%).

However, slurry process operability is difficult. High reaction temperatures mean that coke is formed and agglomerated with the catalyst. The catalyst tends to accumulate in the reactor, which can in turn plug up the unit or equipment downstream. In general, in slurry

hydroprocessing a selected catalytic component is also dispersed in the feed to inhibit coke formation, which has been studied extensively for full and partial upgrading applications [9,10].

Advantages and drawbacks of the four types of process

Differences in process performance involve the ability to treat feeds that are more or less rich in impurities as well as the yields and quality of the products (Table 1.2).

Table 1.3 gives examples of product yields and quality from the different processes applied to a heavy Safaniya vacuum residue. The resulting products may need further hydrotreating steps to adjust their quality, especially in the case of ebullating and entrained bed processes.

Table 1.2 Comparison of the different processes

Type of process	Fixed bed	Moving bed	Ebullating bed	Entrained bed
Number of units (1993)	34	2	6	Demonstration
Maximum Ni + V content in feed (ppm wt)	120-500*	500-700	> 700	> 700
Tolerance for impurities	Low	Low	Average	High
Max. conversion of 550ºC+ (% wt)	60-70	60-70	80	90
Distillate quality	Good	Good	Good	Poor
Fuel oil stability	Yes	Yes	Borderline	No
Unit operability	Good	Difficult	Difficult	Difficult

* Swing reactor

When operating a fixed or moving bed type of process, wide-range gasoline is produced in small amounts (1 to 5% wt). Its naphtha fraction has a low octane number (around 60) and can serve as a catalytic reforming feed provided it undergoes pretreatment. The gas oil yield is higher (10-25% wt). Its sulfur content is often lower than 0.1% wt. Its cetane number hits a high of 42-45 and a further severe hydrotreating step is required to improve it. The same holds for its aromatics content (40 to 50% wt). The vacuum distillate is produced in significant amounts (20 to 35% wt). It is properly desulfurized (S = 0.25-0.5% wt). In contrast it has a high nitrogen content that is not favorable to using it as an FCC or hydrocracking feed.

Figure 1.14 shows the wide differences in the distillation curves for a Safaniya vaccum residue effluent according to the hydroconversion process applied to it.

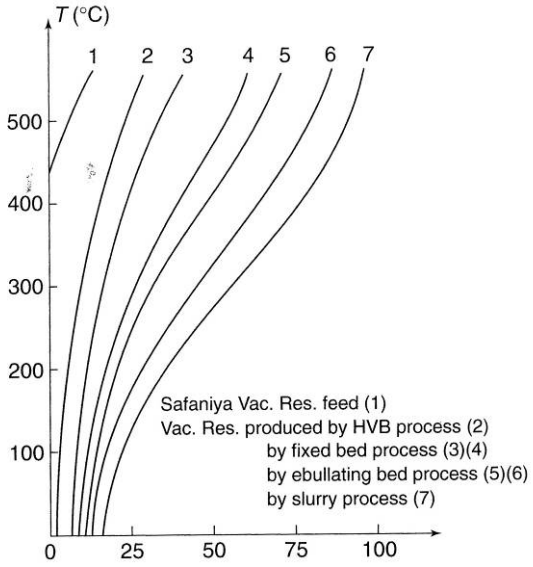

Figure 1.14 Hydroconversion of a vacuum residue: variation in product distillation curves according to the type of hydrotreating process

Table 1.3 Example of product yields and quality for the different processes

Type of process	Fixed/moving bed	Ebullating bed	Entrained bed
Gasoline:			
Yield/feed (% wt)	1-5	3-10	10-15
sp.gr.d_4^{15}	0.720-0.740	0.710-0.720	0.720
Sulfur (% wt)	< 0.01	0.01-0.2	< 0.06
Nitrogen (ppm)	< 30	< 50	200
P/N/A (% vol)	65/25/10	-	-
Gas oil:			
Yield/feed (% wt)	10-25	20-35	40-45
sp.gr.d_4^{15}	0.850-0.875	0.840-0.875	0.866
Sulfur (% wt)	< 0.05	< 0.1	0.7
Nitrogen (ppm)	< 500	< 1000	1800
Cetane number (% vol)	42-46	42-46	40
Aromatics (% wt)	40-50	-	40-50
Viscosity at 50ºC (mm^2/s)	2.5	-	3.5
Cloud point (ºC)	-15	-	-9
Vacuum distillate:			
Yield/feed (% wt)	20-35	35-45	20-25
sp.gr.d_4^{15}	0.925-0.935	0.930-0.940	1.010
Sulfur (% wt)	0.2-0.5	0.4-0.8	2.2
Nitrogen (% wt)	< 0.2	< 0.25	0.43
Viscosity at 100ºC (mm^2/s)	8-12	8-12	7
Conradson carbon (% wt)	< 0.5	< 1	< 2
Vacuum residue:			
Yield/feed (% wt)	35-60	20-40	5-20
sp.gr.d_4^{15}	0.98-1.010	1.010-1.050	1.16
Viscosity at 100ºC (mm^2/s)	150-1200	1000-2000	60 000
Sulfur (% wt)	0.5-1.0	1-2	2.7
Nitrogen (% wt)	< 0.4	< 0.5	< 1.1
Conradson carbon (% wt)	15-20	20-30	47
Ni + V (ppm)	10-40	50-100	90
Shell P-value stability	1.4-2.0	1.1-1.4	1.0

1.3. HDM and HDS catalysts deactivation

There are many causes that contribute to the catalyst deactivation in the catalytic processing of *resids* and heavy oils. Lots of authors have studied many of these causes but at the moment, there is not a complete agreement on a valid theory. Since the modeling of the deactivation process is needed, a literature review has been undertaken to understand what effects should be included in the model. To achieve this, it is important to understand the steps involved in the formation of coke and metals deposits and their influence on the catalyst activity.

1.3.1. Deactivation by coke

Catalyst deactivation by coke and metal deposits occurs simultaneously when metals are present in the feed. These deposits lay down on active sites in the catalyst contributing in this way to the overall deactivation, as well as the changes in the catalyst structure. It is not easy to distinguish quantitatively between the contributions of all these causes to deactivation. As shown in Figure 1.15, there is a difference between the deposition patterns of coke and metals [11]. Notice that coke rapidly deposits during the initial stages before attaining a steady-state (around 400-600h). Until the equilibrium is reached, catalysts used in hydrotreating of heavy petroleum fractions suffer a rapid coke build-up as a result of strong, initial adsorption of the polyaromatic fractions, including N-containing aromatic compounds, on the surface [12]. About one third of the pore volume of the fresh catalyst is filled during the initial stage on stream. At the same time, metals exhibit more or less linear deposition patterns with time. A similar observation was made by Marafi and Stanislaus [13] using a gas oil feed. Coke deposition was the main cause of the initial pore volume loss. The coke and metal buildup depend on the properties of the feed and hydroprocessing conditions. Netzel et al. [14] have shown that the structure of the catalyst can have a significant effect on the amount of deposited coke. Also, in the case of coke and metals, only a relative extent of deactivation could be estimated, as shown in the results of Table 1.4 published by Cable et al. [15]. These results suggest that when the fresh catalyst is compared with the aged-regenerated catalyst, metals appear to have a moderate effect on HDS activity, a very weak effect on hydrogenation activity and a weak effect on cracking activity. Comparing the aged catalyst with the aged-regenerated catalyst shows an additional effect on the HDS activity due to coke. Coke seems to have a strong effect on the hydrogenation. Metals have almost no effect on cracking but coke has a very strong effect on the cracking activity.

Table 1.4 Relative deactivation by metals and coke

Catalyst function	Relative effect	
	Metals	**Coke**
HDS	moderate	moderate
Hydrogenation	weak	strong
Cracking	weak	very strong

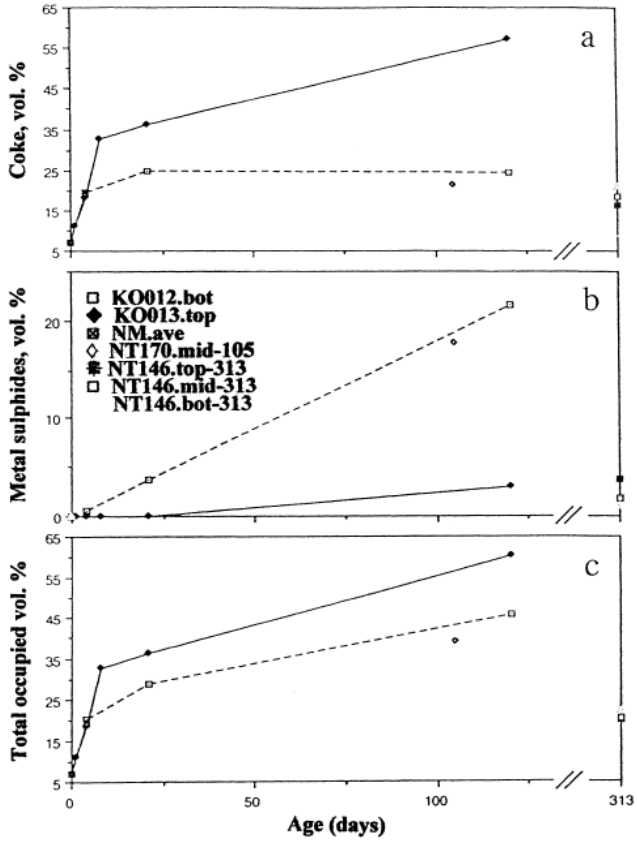

Figure 1.15 Evolution of (a) coke, (b) metals and (c) total occupied volume as a function of time on stream.

Origin and formation mechanism of coke

Coke on hydroprocessing catalysts is ubiquitous, i.e., coke is formed from virtually all hydroprocessing feeds employed. General trends which can be established from many studies on realistic feeds indicate that the coke build-up increases with the molecular weight and/or boiling range of the processed feed. However, among feeds having similar boiling range, the one with a high content of coke precursors, e.g., aromatics or heterocyclics, will require the most active catalyst to prevent coke formation.

The mechanism for the coke formation is not yet completely understood but it is common to consider that the formation of radicals by thermal decomposition of molecules initiate the polymerization and/or polyaddition reactions that produce the coke [16]. Coke forming reactions occur on the catalyst surface; therefore, the structure of the surface is important for controlling the extent of coking. Among hydrocarbon groups, the alkenes, aromatics and heterocyclics are most susceptible to coke formation. Their interaction with the surface is much stronger than that of saturated hydrocarbons. Therefore, they are more likely to convert to higher molecular weight species if sufficient active hydrogen is not available to prevent it.

Wiwel et al. have demonstrated that when the polynuclear aromatics (PNA) content in the feed increases, the amount of coke formed on the catalyst goes in the same direction [17].

Jong et al. showed that during hydroprocessing of a vacuum gas oil, the amount of coke decreased significantly by adding 0.2% of Mo to Al_2O_3, as the results in Figure 1.16 show [18]. However, if the Mo loading continues to increase, the amount of coke increases slightly. The authors assumed that to a certain extent MoS_2 can catalyze coke formation.

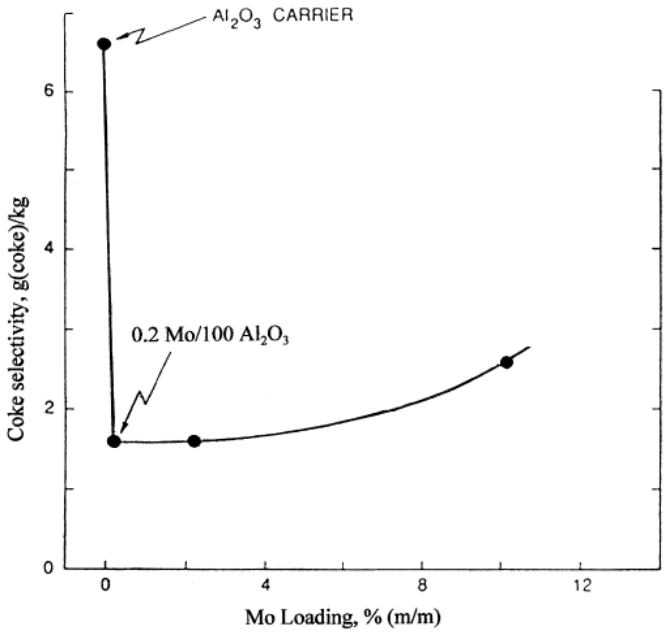

Figure 1.16 Effect of Mo loading on the coke selectivity and HDS activity (723K, 30 bar H_2)

Besides feed composition and catalyst properties, hydroprocessing conditions are also important for controlling the extent of coke formation. Of particular importance is the partial pressure of hydrogen, temperature and contact time. Hydrogen can convert coke precursors into stable products before they are converted to coke. However, the probability of this conversion decreases with increasing temperature. The results in Figure 1.17 suggest that there might be an optimal combination of catalyst properties and processing conditions, which ensures the best performance of the catalyst [19].

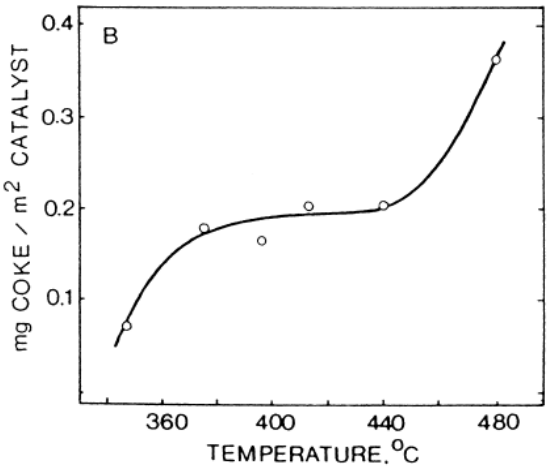

Figure 1.17 Effects of temperature on catalyst coke

It is believed that the flat region in Figure 1.17 can be expanded by increasing the partial pressure of hydrogen. This is supported by results for the initial coking published by Richardson et al., shown in Figure 1.18 [20], obtained at 430ºC.

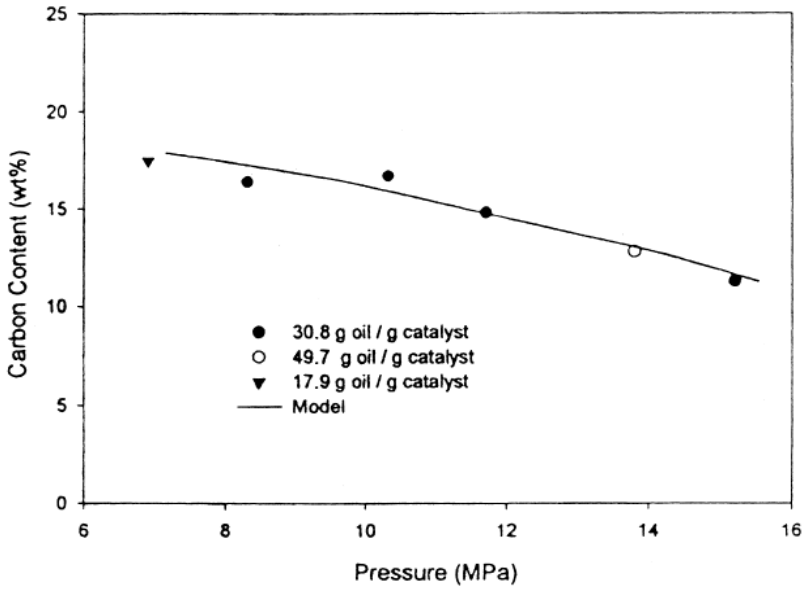

Figure 1.18 Carbon content of catalyst as function of H_2 pressure ($NiMo/Al_2O_3$, 703K)

As shown in Figure 1.19 [21], the effect of the partial pressure of hydrogen is even more pronounced on the steady-state level of coke.

Jong et al. showed that H_2/oil ratio also can influence coke formation. As seen in Figure 1.20, a distinct maximum in coke formation is observed at intermediate feed ratios [18].

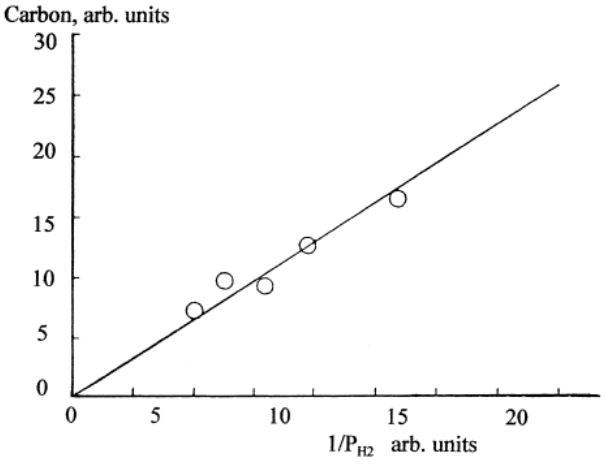

Figure 1.19 Steady-state level of carbon on catalyst as function of H_2 pressure

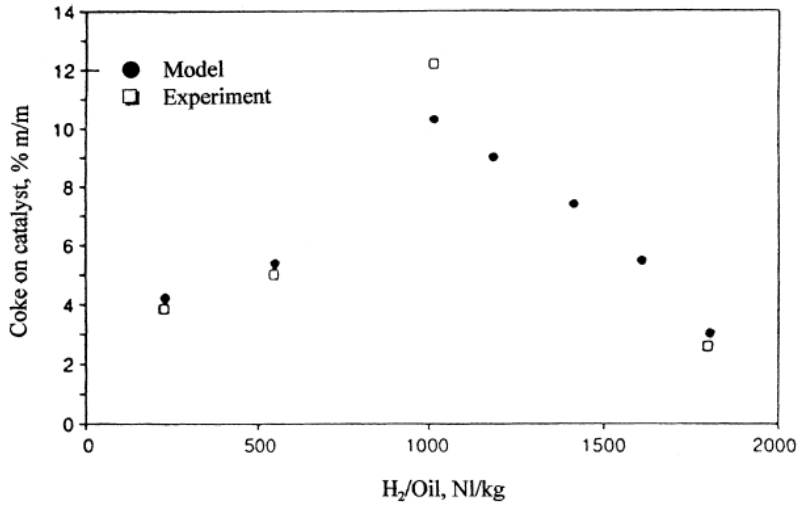

Figure 1.20 Effect of H_2/feed ratio on the coke content of catalyst (NiV/SiO_2, 723K, 30 bar H_2)

The mechanism shown in Figure 1.21 is based on the coupling of two naphthalene molecules via route 1b or two alkyl naphthalenes leading to coronene via route 1a. In the latter case, two additional rings can be formed via dehydrocyclization as depicted by dotted lines. Beguin and Setton [22] observed coupling of polynuclear aromatics (PNA) aided by various metals. Also, coupling was enhanced in the presence of a proton donating medium, such as a Brønsted acid [23]. In this case, the formation of the carbenium ions is predicted. It was established that such carbenium ions can combine with neutral PNA rings to yield larger structures [24]. The coupling capability was significantly diminished after the Brønsted acidity was destroyed by pretreating the support with basic species [25]. The involvement of carbenium ions was assumed in the mechanism proposed by Gates et al. [26] for coking of anthracene. Scaroni and Jenkins [27] assumed the participation of carbenium ions in a study of several model compounds in the presence of a $CoMo/Al_2O_3$ catalyst. These authors proposed that the carbenium ions were formed by electron transfer between aromatic and heteroatomic rings and the catalyst surface.

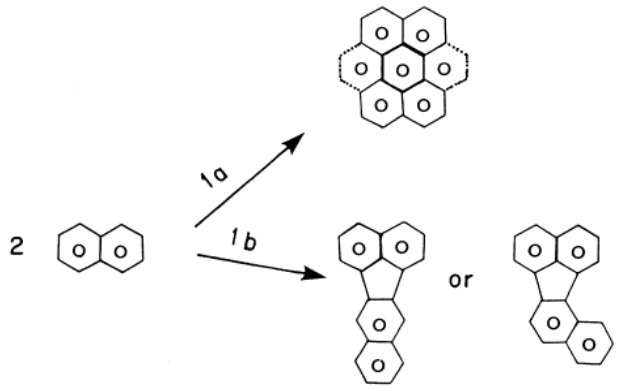

Figure 1.21 Tentative mechanism of coupling of naphthalene molecules

The involvement of free radicals in coke formation has been proposed by several authors [28,29]. The probability for such a mechanism increases with increasing temperature, which favors the formation of free radicals. An example of this mechanism, proposed by Lewis and Singer [28], is shown in Figure 1.22. A similar mechanism may be involved during coke formation from N-containing bases. In this case, two molecules adsorbed at neighboring Lewis acid sites may couple at temperatures favoring dehydrogenation of the heteroring. Once partially dehydrogenated, the heteroring may couple with an aromatic ring according to the mechanism in Figure 1.22. Absi-Halabi et al. [30] proposed the polymerization mechanism in Figure 1.23 to illustrate coke formation from both light and heavy hydrocarbons. Experimental support for this mechanism was provided by Nohara and Sakai [29] from coking studies of large aromatic structures with small molecules such as butadiene.

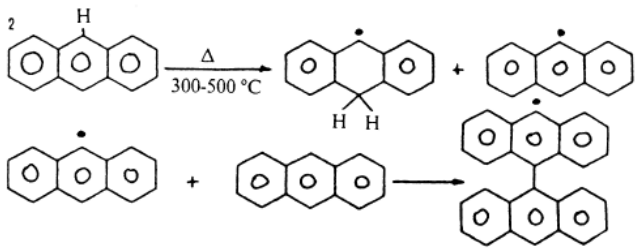

Figure 1.22 Free radical mechanism for formation of coke from anthracene

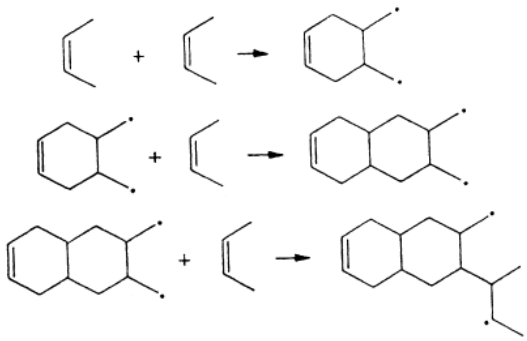

Figure 1.23 Mechanism of coke formation by polymerization

Effect of coke on catalyst activity

In hydroprocessing of residues, the decomposition of large asphaltene molecules speeds up the coke formation rate. This rapid coke formation in catalysts during the initial stages has a large effect in catalyst activity, covering up to 70% of active sites [31] and being responsible for more than 50% of total catalyst deactivation [12]. Besides this, coke deposits also reduce the catalyst porosity which implies a decrease in molecular diffusivity. This decrease diminishes the access of the reactants to the active sites and makes it more difficult for the products to exit, reducing the overall reaction rate.

1.3.2. Deactivation by metals

During hydroprocessing, part of the metals present in the feed will deposit on the catalyst surface and cause deactivation. The nature of the metals deposited depends on the origin of the feed. V and Ni are the predominant metals in petroleum crudes, heavy oils and oil shale-derived liquids, while Fe and Ti are the main metals in coal-derived liquids. Heavy oils derived from tar sands may contain V, Ni, Ti, Fe and small amounts of other metals, in addition to clay-like mineral matter. Alkalis can also be present if the feed is not completely dewatered. In some cases, alkalis are introduced during the separation of heavy oil from sands. Biofeeds, usually prepared by a thermal treatment of biomass, are the least contaminated by metals.

In summary of previous discussions, it is again emphasized that the deactivation by metals always occurs simultaneously along with that by coke. Deactivation by metals is irreversible. While the initial coke deposition is rapid before the pseudo-equilibrium level is reached, metal deposits continually increase with time [32]. The general trends in the formation of coke and metal deposits are shown in Figure 1.24 [21]. Then, during the entire period, metals deposition occurs on the catalyst, which has already lost a substantial portion of its original porosity and surface area [11]. This is generally true for petroleum-derived feeds and coal-derived feeds as well as other feeds.

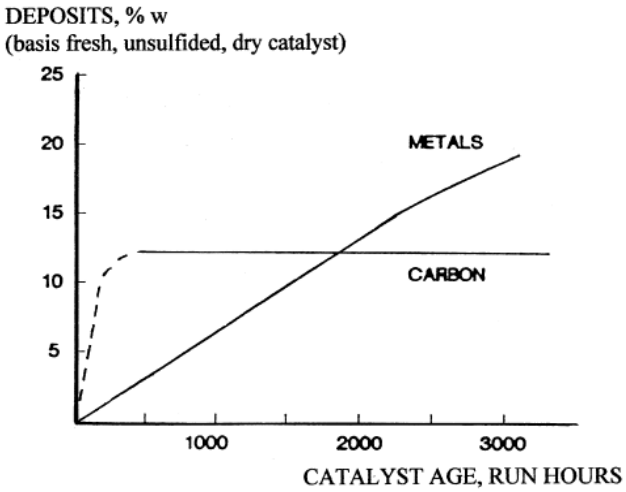

Figure 1.24 Metals and carbon deposits as function of catalyst age

In order to maintain the unit performance, the temperature is raised to offset deactivation (Figure 1.25 [33]). Hence, the deposition of metals affects the lifetime of the catalyst. Cross-sectional profiles show that some metals tend to deposit on the external surface of the catalyst particles, whereas others are more evenly distributed (Figure 1.26 [34]). This leads to diffusion limitations which affect access to the active sites in the particle interior. It is evident that coke and metals plug the pores and eventually may lead to a complete loss of the activity [35]. Jacobsen et al. [36] have suggested that metal sulfides gradually narrow the pores and thus slow down the diffusion of reactant molecules into the undeactivated interior of the catalyst particles. At the end of the run, the catalyst may still possess some activity. In other words, a complete loss of activity is generally not observed. End run occurs when either the temperature to maintain the activity is too high for reactor design or the loss of active sites by pore plugging is too large to maintain design activity by raising the temperature.

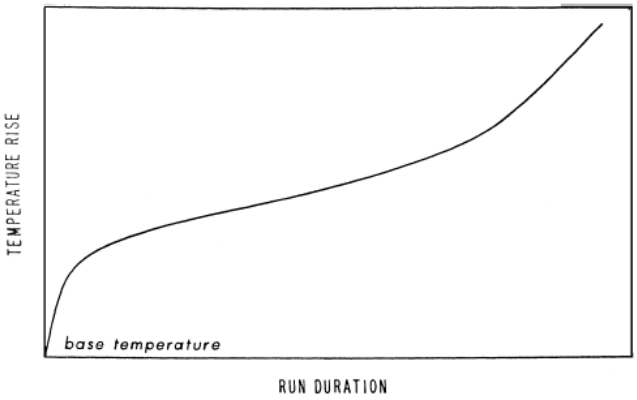

Figure 1.25 Typical S-shaped deactivation curve

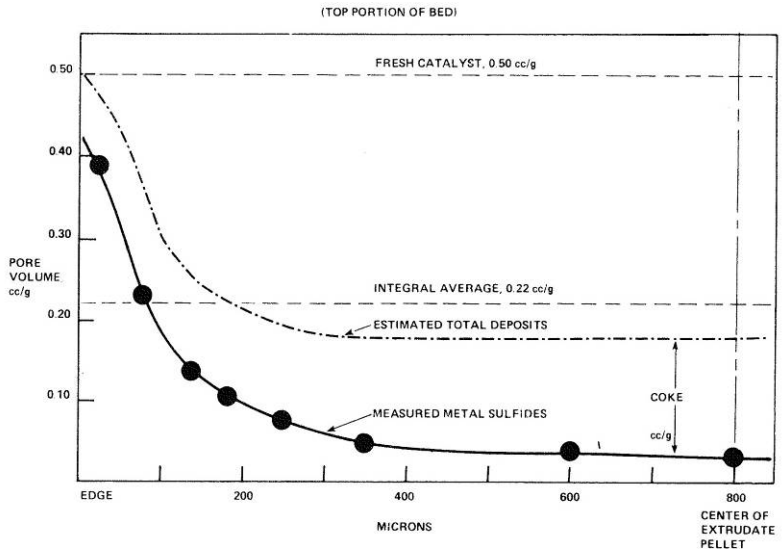

Figure 1.26 Effect of metal and coke deposits on pore volume (top portion of bed)

Mechanism of HDM

An ultimate result of the HDM of porphyrins and other metal containing compounds in the feed is the deposition of metals, predominantly as sulfides, on the catalyst surface and catalyst deactivation associated with it. Most of the efforts have been devoted to metal porphyrins. Because they are less stable than the other metal containing species, their HDM and the ultimate metal deposit formation will be faster. Understanding the HDM mechanism is essential to explain catalyst deactivation. Also, such knowledge may aid in the preparation of tailor-made catalysts to suit hydroprocessing of a particular feed. All evidence suggests that the presence of hydrogen and catalyst is prerequisite for the HDM of porphyrins to occur. Otherwise, their conversion will be very low.

The mechanism of HDM has been investigated using model compounds, as well as feedstocks containing metals of interest. Little information is available on the HDM mechanism of the non-porphyrin type V and Ni containing species, though their contribution to deactivation may be important. If this part of the V and Ni compounds is associated with the asphaltene sheets [21,37], their fate during hydroprocessing will depend on the conversion of the asphaltenes. Under hydroprocessing conditions, the metal porphyrin (M-P) is hydrogenated in the first step to chlorin, in which hydrogens are introduced into β positions of one of the pyrrole rings. The formation of the intermediate chlorin from V and Ni etioporphyrin was observed by Huang and Wei [38,39] in the presence of an oxidic $CoMo/Al_2O_3$ catalyst and high hydrogen partial pressure. Ware and Wei isolated a second (Ni-PH4) and a third intermediate (Ni-X) and included them in the overall HDM mechanism shown in Figure 1.27 [40].

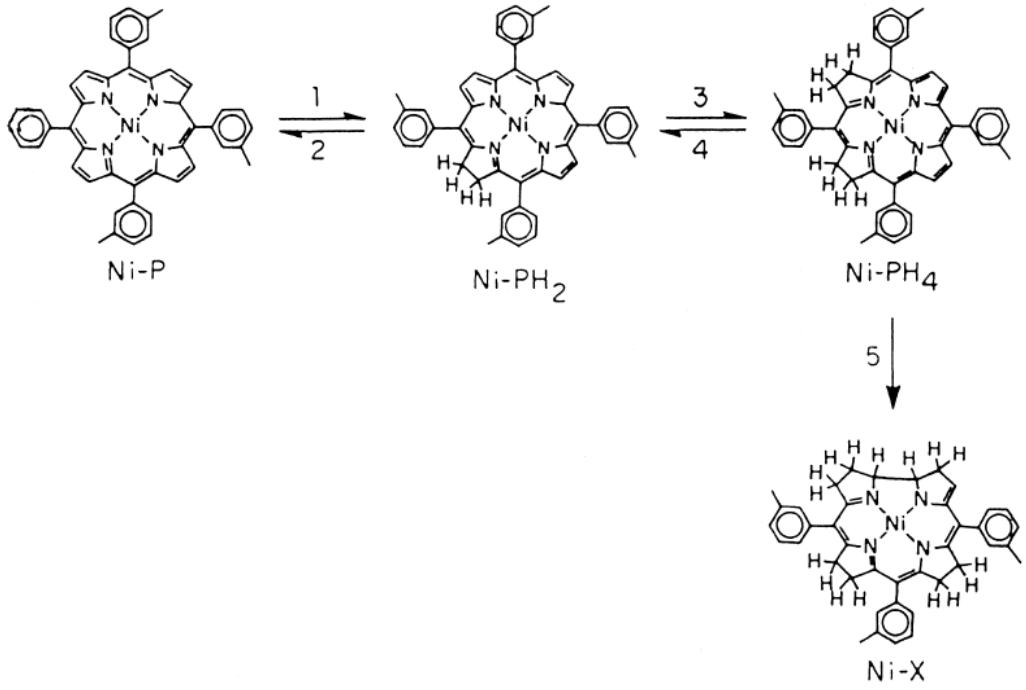

Figure 1.27 Tentative mechanism of HDM of Ni-porphyrin

As it was indicated earlier, the presence of catalyst is crucial for achieving the final fragmentation of the porphyrin molecule, which requires hydrogenolysis of C=N bonds. According to Weitcamp et al. [41], at lower temperatures, the main hydrocarbon products from the HDM of porphyrin would be predominantly dipyrroles, while at higher temperatures, the HDN of dipyrroles would lead to hydrocarbons and ammonia if a sufficient hydrogen pressure is maintained. Thus, at least a partial break up of the intermediates is required to release the metal, because the metal free porphyrin could not be detected in the liquid products [42]. Deposited metals will be rapidly sulfided by H_2S from the HDS reactions occurring simultaneously.

Perhaps the most detailed account of the mechanism of HDM of porphyrins was given by Janssens et al. [43]. From molecular modeling calculations and GCMS analysis of the HDM products, these authors were able to confirm the presence of the intermediates proposed by other researchers, as well as new intermediates not identified and/or proposed previously. The overall mechanism proposed by these authors is shown in Figure 1.28. In this case, M represents either Ni or V=O, as it was assumed that the different metal species should have little influence on the mechanism.

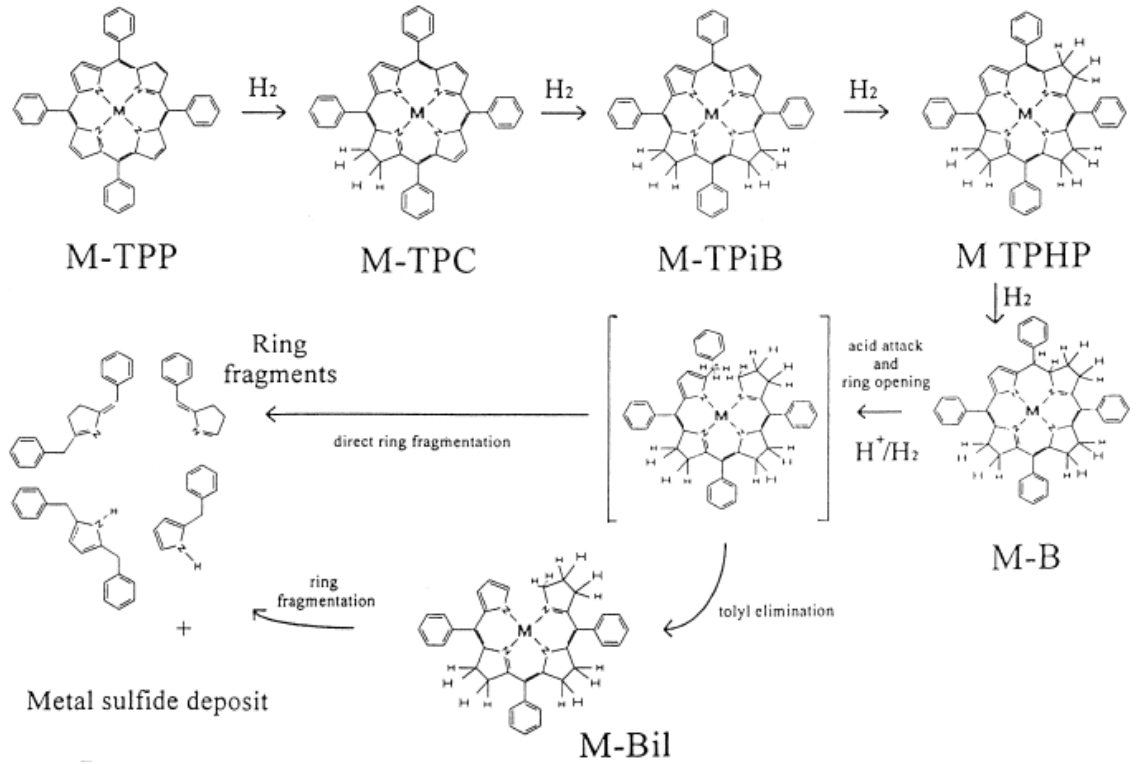

Figure 1.28 A complete reaction mechanism for HDM of metalloporphyrins; M = Ni or VO

The information on the HDM mechanism of nonporphyrin metal-containing species is limited because the structure of these species is much less identified than that of porphyrins. There are indications that the non-porphyrin type of the metal containing compounds may account for more metals than the porphyrins. More information on HDM of such structures would be desirable.

Effect of metals on catalyst activity

The deactivation curves of hydrotreatment catalysts typically show an initial period of rapid deactivation, which results in a quick raise of the temperature to maintain the activity, attributed to the establishment of an equilibrium coke loading on the catalyst surface, as shown in Figure 1.24 and Figure 1.25. This is followed by an intermediate deactivation period, characterized by a slow and almost constant deactivation rate, ascribed to increasing diffusional resistance as metal-sulfide deposits accumulate in the pores. Finally, there is a period of rapid deactivation attributed to pore plugging caused by the accumulation of metal deposits [44,45]. In spite of the fact that this mechanism of deactivation is widely accepted, Silbernagel and Riley concluded that metals are not the only reason for intermediate deactivation. In their experiments, they used a feed that was treated with hydrofluoric acid to reduce the V and Ni content. This feed let to about the same deactivation levels as the "whole" feed although the metals deposition level is approximately an order of magnitude lower. The role of metals in the deactivation mechanism was not completely understood.

1.3.3. Other effects

Besides the effect of the metals deposits and coke on deactivation, there are other effects that could be important to present.

Some authors refer that changes in catalyst structure could have an important impact in the catalyst activity. Indeed, although the carbonaceous and metallic depositions, which poison the active sites and lower the pore diffusion, have long been claimed to be the major cause of the catalyst deactivation, the aggregation of MoS_2 stacks was also claimed to be main cause of catalyst deactivation when the feed was almost free of the resid [46]. The stability of the active phase is essential for maintaining desirable lifetime of the catalyst. In this regard, temperature appears to be the most important parameter. Changes in catalyst structure are very slow at temperatures used during hydroprocessing operations. However, in some cases, the catalyst remains in operation for a long period of time, sometimes as much as several years. Although temperatures may be relatively low, prolonged exposure can lead to structural changes, which have a negative effect on the catalyst activity. These changes are for the most part irreversible, causing permanent loss of the activity. This may include segregation of the active phase, followed by the diffusion of active metals to the support and/or recrystallization. When metals are present in the feed, they can interact with the promoters in the active phase, in addition to the deactivating effects discussed earlier. The deactivation of $CoMo/Al_2O_3$ and $NiMo/Al_2O_3$ catalysts from upgrading of coal liquids was attributed to the gradual conversion of a more active type II Co(Ni)MoS phase into the type I Co/NiMoS phase [47]. The former consists of multilayer slabs of MoS_2 with Co/Ni at its edges, while type I phase consists predominantly of the monolayer slabs. The higher activity of the type II phase was attributed to the decreasing interaction between the support and MoS_2 in multilayer slabs compared with that between the

support and monolayer slabs. This increases the amount of edges in the MoS_2 crystallites, which are believed to be the active sites.

There are also in the feed contaminants that can decrease the activity such as nitrogen and oxygen. These contaminants could be irreversible absorbed in the catalyst active sites.

Although it has been proven that these effects also contribute to the catalyst deactivation, authors generally do not consider them in the modeling of the deactivation mechanism [48].

1.4. Modeling approaches to predict catalyst deactivation

The modeling of the deactivation on hydrotreating catalyst has been done by several authors using different approaches. In this section, some of the approaches will be described and referred.

The Shell RESIDS model was developed as a predictive tool for $CoMo/Al_2O_3$ or $NiMo/Al_2O_3$ petroleum residue hydro-conversion HDM/HDS catalysts [21,45,49]. The model was developed from a combination of scientific investigation, theory and experience. Initially, it includes a deactivation model for metals poisoning and pore-plugging but, for simplicity, the initial (rapid) build-up of coke was not taken into account in the model because it was assumed that coke reaches a stationary level. This implies that, when coke deposition becomes overruling, the model cannot be used. This situation may arise with a catalyst operating at too low hydrogen partial pressure [49]. This model appears to have been extended and improved through experience, to eventually cover all residue conversion processes [21]. It can predict the long-term performance of a single catalyst or multiple catalyst system using the initial activity for hydrotreating reactions (HDM, HDS, HDN, etc.), the coke deactivation parameter for each reaction, and the metals uptake capacity [50].

Oyekunle and Hughes developed a pore-plugging model to analyze catalyst deactivation by metal deposition, which prevents diffusion of large reactant molecules into the pores. They assumed a uniform pore structure and used a threshold value to the amount of metals deposited which plug the pore, and predicted the catalyst life as a function of the pore diameter. With the model they intended to demonstrate that an appropriate pore structure is required for achieving the desirable goals in HDM processes [51].

Another model proposed by Takatsuka, Wada and Inoue considers that the catalyst is deactivated in the early stages of the operation by coke deposition on the catalyst's active sites. The ultimate catalyst life is determined by pore mouth plugging depending on its metal capacity. The phenomena are mathematically described by losses of catalyst surface area and of effective diffusivity of the feedstock molecules in the catalyst pores by the deposition of metals and coke. The model parameters were collected through pilot plant tests with various types of catalysts and feedstocks [52].

A different approach has been taken by Janssens et al. at Delft University with Shell's support. The developed model predicts the deactivation on HDM catalysts and considers that restrictive intraparticle diffusion and the changing catalyst porous texture are the relevant

phenomena to describe this deactivation process. The changing catalyst porous texture during metal deposition has been successfully described by percolation concepts. Comparison of HDM catalyst deactivation simulations and experimental deposition profiles in catalyst pellets shows that metal deposition process can be reproduced [53].

A kinetic equation for HDS reactions considering that coke content is the only cause of deactivation has been developed by Corella, Adanez and Monzón. They considered a reversible formation of coke, to obtain a deactivation curve with a residual activity. To avoid mathematical complications, they considered only a monofunctional catalyst with homogenous surface and assumed that the main reaction is simple. The four-parameter kinetic equation obtained was successfully fitted to experimental data [54].

In spite of the fact that all the models referred above consider different approaches to describe the deactivation mechanism on hydrotreatment catalysts, all of them seem to successfully describe the deactivation phenomenon. This happens not necessarily because of all the considered effects are present in the deactivation mechanism but because most of these models have too many parameters that can be changed to fit the data.

2. The existing THERMIDOR code

THERMIDOR is an acronym for THERmal Monitoring for Isoperformance Demetallization of Oil Residua. The program, written in FORTRAN 77 language, was first conceived as a simulator for hydrotreating catalyst ageing. Today, it simulates the entire HYVAHL process along the time on stream, taking into account the complex associations of guard bed materials and catalysts, each with their particle size, activity, pore size and shape grading. Another of THERMIDOR's important features is the realistic representation of the two main catalyst deactivation mechanisms in residue hydroprocessing: coke lay-down and metal deposition. The model also clearly illustrates the synergy between dedicated HDM and HDS catalysts [55].

2.1. Feed representation

The feed in THERMIDOR is represented by a matrix of 8x6 subspecies [5]. The line entries of the matrix are the eight families of compounds, which are considered in the feed, and the column entries are the atoms from which they are formed. The grouping of the compounds is based on the SARA fractionation (Saturates, Aromatics, Resins and Asphaltenes). The (+) and (-) signs separate resins and aromatics with a boiling point of over 520°C from those with a boiling point lower than 520°C. The families and subspecies considered are indicated in Table 2.1 [55].

Table 2.1 Families and subspecies considered in THERMIDOR

Family	Sub-species						
	C	**H**	**S**	**N**	**O**	**V**	**Ni**
Asphaltenes	C-Asp	H-Asp	S-Asp	N-Asp	O-Asp	V-Asp	Ni-Asp
Resins $^{+}$	C-Res+	H-Res+	S-Res+	N-Res+	O-Res+	V-Res+	Ni-Res+
Resins $^{-}$	C-Res-	H-Res-	S-Res-	N-Res-	O-Res-	-	-
Aromatics $^{+}$	C-Aro+	H-Aro+	S-Aro+	N-Aro+	O-Aro+	-	-
Aromatics $^{-}$	C-Aro-	H-Aro-	S-Aro-	N-Aro-	O-Aro-	-	-
Saturates	C-Sat	H-Sat	S-Sat	N-Sat	O-Sat	-	-
Gas	C-Gas	H-Gas	S-Gas	N-Gas	O-Gas	-	-
Deposits	-	-	-	-	-	V-dep	Ni-dep

It is important to remind that the sub-species (C-Asp, H-Asp, etc.) in this representation have no individual chemical existence. Their use comes from the fact that is necessary to follow at the same time the transformations of the various families and the hydrotreating performances of the process. Developing a kinetic model for heavy oil processes is strongly hampered by the difficulty in obtaining a sufficiently detailed analysis of the reactants and products. Indeed, even cutting-edge analytical techniques only reveal part of the detailed composition of these mixtures. With a more abstract representation, such as the one used here, it becomes possible to create a lumped model for hydrocarbon conversion that also tracks their heteroatomic compositions, which vary due to different reaction rates for the various types of reactions (HDM, HDS, etc.) [55].

2.2. General equations

Since the goal of THERMIDOR is to simulate industrial operations, which are run in adiabatic large scale reactors, it is necessary to couple heat balances and mass balances so as to compute *T(z,t)*, the longitudinal temperature profile. A perfect piston flow was assumed for each trickle bed, which implies perfect radial mixing [56].

The reactor implemented in THERMIDOR consists in a multi-phase reactor divided in the following fractions: the volume filled with catalyst (V_{cat}), the volume between the catalyst grains (interstices) occupied with hydrocarbons (V_{HC}^{ext}) and the volume occupied by hydrogen (V_{H_2}). The hydrocarbons that diffuse into the catalyst grains occupy a volume defined as V_{HC}^{int}. Defining the average porosity of the catalyst (ε), the extra-granular void fraction (ϕ_{ext}) and the fraction of gas (Y), it is possible to correlate all the volumes using the following equations [57].

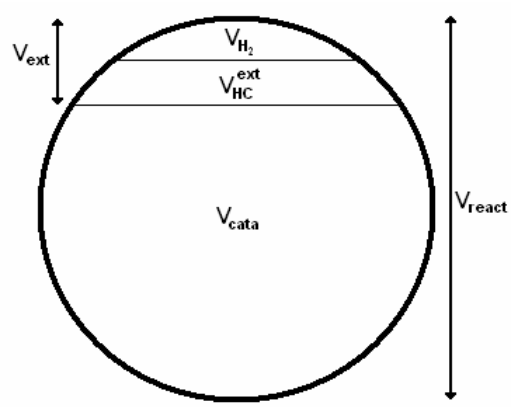

Figure 2.1 Schematic representation of a cut of the reactor

$$V_{ext} = V_{H_2} + V_{HC}^{ext} \quad (2.1)$$

$$V_{react} = V_{cat} + V_{ext} \quad (2.2)$$

$$V_{HC}^{\text{int}} = \varepsilon \cdot V_{cat} \quad (2.3)$$

$$Y = \frac{V_{H_2}}{V_{ext}} \quad (2.4)$$

$$\phi_{ext} = \frac{V_{ext}}{V_{react}} \quad (2.5)$$

$$\varepsilon = \frac{V_{HC}^{\text{int}}}{V_{cat}} \quad (2.6)$$

2.3. Mass balance

THERMIDOR has implemented two types of mass balances: a mass balance along the reactor and a mass balance over the catalyst grain [57].

2.3.1. Along the reactor

THERMIDOR simulates the fixed bed reactors by assuming that they behave like a plug-flow reactor in pseudo-stationary operation. Hence, the reactor can be divided into several volume elements on which differential mass balances can be written. The mass balance on a differential volume element is given by:

$$Q_L \cdot C_{L,X}(x) = Q_L \cdot C_{L,X}(x + dx) + r_X \cdot (1 - \phi_{ext}) \cdot S \cdot dx \quad (2.7)$$

Where Q_L is the feed volumetric flow, $C_{L,X}$ represents concentration of the species X in the feed, r_X the reaction rate for the species X and S the reactor section [57].

Making $dy = \frac{dx}{L}$ and $LHSV = \frac{Q_L}{S \cdot L}$, equation (2.8) is obtained.

$$LHSV \cdot \frac{dC_{L,X}}{dy} = -(1 - \phi_{ext}) \cdot r_X \tag{2.8}$$

Note that the reaction rate r_X is the average of reaction rates along the grain. Since equation (2.8) is a first-order differential equation, only one boundary condition is needed to solve it. The boundary condition chosen was the reactor inlet concentration [57].

2.3.2. Over the catalyst grain

The mass balance over the catalyst grain is very important since it provides the concentration profile for all the species inside the grain. This allows to determine the local reaction rate and with it the global reaction rate used in equation (2.8). With the species profiles it is also possible to observe the internal diffusional limitations and how they influence the different species. In THERMIDOR, the catalyst grains can be of two forms: cylindrical and spherical [57].

Cylindrical grain

The mass balance over a cylindrical grain section with *dr* width is written as follows:

$$2\pi L \cdot \left(r - \frac{dr}{2}\right) \cdot n\left(r - \frac{dr}{2}\right) - 2\pi L \cdot \left(r + \frac{dr}{2}\right) \cdot n\left(r + \frac{dr}{2}\right) + 2\pi L \cdot r \cdot dr \cdot r_X(r) = 0 \tag{2.9}$$

Where $n\left(r - \frac{dr}{2}\right)$ is given by:

$$n\left(r - \frac{dr}{2}\right) = -D_e \frac{\varepsilon\left(r - \frac{dr}{2}\right)}{\tau\left(r - \frac{dr}{2}\right)} \frac{C_X(r) - C_X(r - dr)}{dr} \tag{2.10}$$

If *dr* tends to zero, a second-order differential equation is obtained, where it is necessary to define two boundary conditions to solve it.

$$D_e \frac{\varepsilon(r)}{\tau(r)} \frac{d^2 C_X(r)}{dr} + r_X(r) = 0 \tag{2.11}$$

The boundary conditions chosen were:

$$\frac{dC_X(0)}{dr} = 0$$
$$C_X(R) = C_{X,ext}$$

Spherical grain

For a spherical grain section with *dr* width, the mass balance is written as follows:

$$4\pi \cdot \left(r - \frac{dr}{2}\right)^2 \cdot n\left(r - \frac{dr}{2}\right) - 4\pi \cdot \left(r + \frac{dr}{2}\right)^2 \cdot n\left(r + \frac{dr}{2}\right) + 4\pi \cdot r^2 dr \cdot r_X(r) = 0 \tag{2.12}$$

Where $n\left(r-\frac{dr}{2}\right)$ is given by equation (2.10) and the boundary conditions were the same.

2.4. Heat balance

The heat balance equation in THERMIDOR assumes a pseudo steady state, thermal equilibrium between solid, liquid and gas phases at any position *z* and any time *t*, and heat transfer solely by convection through the liquid. The following differential equation can be derived [56]:

$$\frac{dT(z,t)}{dz}=\frac{\left[1-\phi_{ext}(z)\right]\cdot\sum_{ij}N_{ijk}^{l}\left(r_k^g z,t\right)\Delta H_{ij}}{LHSV\left(C+F\right)} \tag{2.13}$$

With $\phi_{ext}(z)$ the extra-granular void fraction (assumed constant along each bed of catalyst), $N_{ijk}^{l}\left(r_k^g z,t\right)$ the fluxes of reactants consumed by each grain of catalyst *k* at the location *z* and time *t*, and ΔH_{ij} the heats of reactions (counted positive for an exothermic reaction). *C* is the local heat capacity, and *F* the local heat capacity flux [56]:

$$C=\phi_{ext}(z)\left[(1-Y)c_p^l d^l+Yc_p^g d^g\right]+(1-\phi_{ext})c_p^s d^s \tag{2.14}$$

$$F=c_p^l d^l+\frac{Q^g}{Q^l}c_p^g d^g \tag{2.15}$$

Where *Y* is the local fraction of gas in the extra-granular space, the *c* the specific heats and *d* the densities for liquid (*i* = *l*), gas (*i* = *g*) and solid (*i* = *s*) phases. c_p^i and d^i are assumed temperature dependant only for the liquid and gas phase. In other terms the composition of the liquid phase and the gas phases are assumed to vary only slightly along the reactors, since hydrotreating affects marginally the feedstock chemistry and the high linear velocity of gas tends to minimize composition gradients (mostly H_2S content) along the reactors. Q^g and Q^l are the flow rates of gas and liquid, assumed constant in reaction sections separated by quenches. For c_p^l the correlation provided by Perry et al. for hydrocarbon oils was used [58]:

$$c_p^l=\frac{\alpha^l}{\sqrt{d^l}}+\beta^l(T-288) \tag{2.16}$$

With α^l= 0.415 kCal.g^{-1}.K^{-1} and β^l= 9.10^{-4} kCal.g^{-1}.K^{-2}. For c_p^g, the formula for an ideal gas was used. The c_p^s and d_p^s are local since they depend on the amount of metal sulfides and coke laid down, and also as a consequence on the amount of liquid filled residual grain porosity at *z* and *t*. These quantities can be obtained by averaging *(r,z t)* dependant quantities furnished by the description at the grain scale. A linear dependency was assumed for c_p^s in the specific heats of metal sulfides, coke and fresh catalysts, themselves assumed to depend linearly on temperature [56].

In industrial residue desulfurization units, like in many hydroconversion units involving catalytic beds and reactors in series, temperatures are moderated by the use of “quenches”, that is to say devices where relatively cold hydrogen is injected and well mixed to the gas-liquid mixture collected at a bed or reactor outlet. The utility of quenches is two-fold: i) limit temperature elevation due to the heat released by the globally exothermal hydrotreating reactions, and ii) adjust the hydrogen partial pressure to compensate for the hydrogen consumed and for the amount of H_2S and hydrocarbon gases released at the previous stage. *T(z,t)* is therefore a saw teeth profile. If a multi-bed multi-reactor unit is to be simulated, it is quite important to correctly determine the inlet temperature T_{inlet}^{q+1} resulting from the quenching processes at quench *q*, following reactor *q*. This temperature is the positive solution of the parabolic equation which results from solving mass and heat balances around the quench [56]:

$$A_2\left(T_{inlet}^{q+1}\right)^2 + A_1\left(T_{inlet}^{q+1}\right) + A_0 = 0 \tag{2.17}$$

With coefficients:

$$A_2 = b^l d^l \tag{2.18}$$

$$A1 = \left[\frac{\alpha^l}{\sqrt{d^l}} - 288\beta^l\right] d^l + \left[G_{outlet}^q + G_{H_2}^q\right] d^g c_p^g \tag{2.19}$$

$$A_0 = -\left[d^l c_p^l \left(T_{outlet}^q\right) T_{outlet}^q + G_{outlet}^q d^g c_p^g T_{outlet}^q + G_{H_2}^q d^g c_p^g T_{H_2}^q\right] \tag{2.20}$$

In these equations, G_{outlet}^q and $G_{H_2}^q$ are the ratios of gas flow rates to the liquid flow rate, expressed in standard cubic meter per cubic meter, respectively of process gas at the outlet of reactor *q*, and fresh gas admitted at quench *q* [56].

2.5. Kinetic model

The kinetic scheme was established using Langmuir formalism. The corresponding kinetic equations consider the following hypotheses [5]:

- there is only one type of active site (hydrogenation and hydrogenolysis);
- there is only one adsorption constant for each species;
- the adsorption/desorption surface reactions are in equilibrium;
- the conversion reactions are irreversible and of order one with respect to the reactants;
- the reaction order with respect to hydrogen is zero because it is in large excess and at constant pressure. The hydrogen concentration is therefore integrated in the kinetic constants;
- the condensation reactions are negligible.

If |*L*| is the total number of sites and |*| the number of free sites, the following site balance can be derived:

$$|L| = |*| + |*\,Asp| + |*\,\mathrm{Re}\,s^{+}| + |*\,\mathrm{Re}\,s^{-}| + |*\,Aro^{+}| + |*\,Aro^{-}| + |*\,H_2S|$$

For asphaltenes, the adsorption constant is defined by:

$$K_{ads}^{Asp} = \frac{[*\,Asp]}{\left(\sum_X [X - Asp]\right)\cdot[*]}\text{, with } X \in C,H,S,N,O,V,Ni \qquad (2.21)$$

Taking as example the rate equation for subspecies *Res*$^-$, in a Langmuir case with adsorption of asphaltenes and H_2S, the equation (2.22) is obtained.

$$r_{\mathrm{Re}\,s^-} = \frac{\text{production term} - \text{consumption term}}{1 + K_{ads}^{Asp}\cdot[Asp] + K_{ads}^{H_2S}\cdot[H_2S]} \qquad (2.22)$$

The deposition of (Ni, V) sulfide particles inside the catalyst pore space is known to proceed through a nucleation and growth mechanism [59,60], with nucleation centers homogeneously distributed across the porous medium, and a radial distribution of sizes in correspondence with the average distribution measured by for instance a X-ray microprobe since these sizes are much smaller than the sampling volume. This distribution was represented as a homogenized local concentration of metals (Ni, V) in solid phase $C_m^s(r,z,t)$ with [56]:

$$\frac{dC_m^s(r,z,t)}{dt} = \frac{M_m}{d_g^0}\sum_j \rho_{mj}(r,z,t) \qquad (2.23)$$

Where M_m is the average molar mass of metals, d_g^0 the initial grain density of the catalyst (indexed by *k*, according to the interval of *z*) and the rate ρ_{mj} is expressed as mole of reactant per unit volume of catalyst and unit time.

Coke deposition is assumed to result from a reversible reaction of dehydrogenation of asphaltenic material, and its rate is first-order with respect to a driving force equal to the difference between actual $C_{coke}^s(r,z,t)$ and equilibrium $C_{coke}^{s\,*}(r,z,t)$ local coke concentrations in solid phase [56]:

$$\frac{dC_{coke}^s(r,z,t)}{dt} = k_{coke,k}(r,z,t)\cdot S_k(r,z,t)\cdot\exp\left(\frac{E_{coke,k}^{\pm}}{RT}\right)\cdot\left[C_{coke}^{s\,*}(r,z,t) - C_{coke}^s(r,z,t)\right] \qquad (2.24)$$

The coke forming equilibrated reaction can be schematized as:

Asphaltene (liquid fase) $\Leftrightarrow$ Coke (solid phase) + nH$_2$(gas phase) ΔG_{coke}^0

So that, following the law of mass action, the equilibrium local coke concentration can be expressed as:

$$C_{coke}^{s\,*}(r,z,t) = P_{H_2}^{-n}\exp\left(\frac{-\Delta G_{coke}^0}{RT}\right)C_{asp}(r,z,t) \qquad (2.25)$$

Where P_{H_2} is the hydrogen partial pressure in gas phase, and ΔG^0_{coke} characterizes the feedstock.

It is known that initial coke deposit strongly reduces the initial activities, while the poisoning is less marked as coke further accumulates [61]. To account for this non linear deactivation effect of coke, the model assumes the following relationship between local intrinsic rate constants and local coke concentrations [56]:

$$k_{ijk}(r,z,t) = k^0_{ijk}\left[1 + \frac{C^s_{coke}(r,z,t)}{C^{s\,*}_{coke}(r,z,t)}\right]^{-4} \tag{2.26}$$

2.6. Diffusivity model

Diffusion is controlled by the pore size, molecule size, total porosity, viscosity and temperature. Diffusion can be divided in three types, depending on pore size:

- Molecular diffusion, D_{mol}
- Knudsen diffusion, $D_{Knudsen}$
- Configurational diffusion

Molecular, or transport, diffusion occurs when the mean free path is relatively short compared to the pore size, and can be described by Stokes-Einstein's law as follows [4]:

$$D_{mol} = \frac{k_B \cdot T}{6 \cdot \pi \cdot \mu \cdot r} \tag{2.27}$$

Where r is the molecular radius, μ the viscosity and k_B is the Boltzmann's constant.

Knudsen diffusion occurs when the mean free path is relatively long compared to the pore size, so the molecules collide frequently with the pore wall. Knudsen diffusion is dominant for pores that range in diameter between 2 and 50 nm and can be estimated by equation (2.28).

$$D_{Knudsen} = \frac{4}{3} R_g \left(\frac{2}{\pi}\frac{RT}{MM_i}\right)^{0.5} \tag{2.28}$$

Where R_g is the molecular gyration radius and MM_i is the molecular weight of molecule i. R_g can be estimated by equation (2.29).

$$R_g = K \cdot MM^{1/3} \tag{2.29}$$

Configurational, or surface, diffusion is a pore diffusion type in which molecules adsorb on the surface of the pore and hop from one site to another through interactions between the surface and molecules. The three diffusion types are illustrated in Figure 2.2 [62].

The global effective diffusivity (D_e) is calculated by Bosanquet's equation, equation (2.30), that considers molecular and Knudsen diffusivities as two serial resistances.

$$\frac{1}{D_e} = \frac{1}{D_{mol}} + \frac{1}{D_{Knudsen}} \tag{2.30}$$

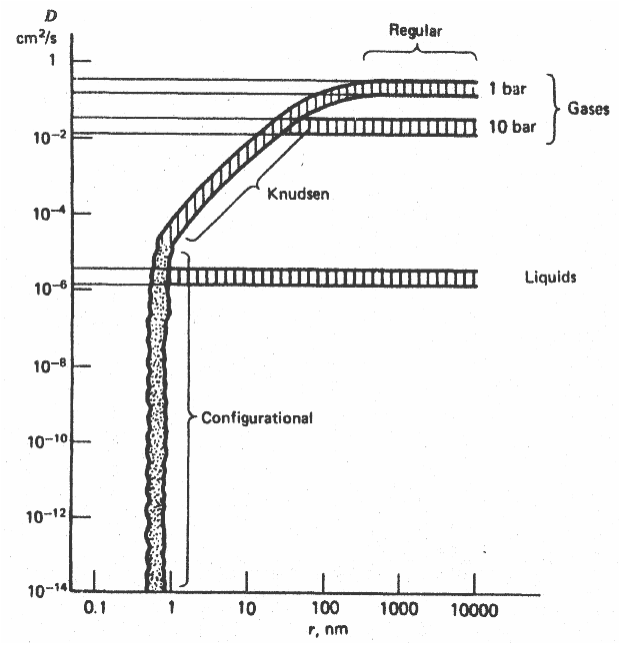

Figure 2.2 Diffusivity and size of aperture (pore); the classical regions of regular and Knudsen and the new regime of configurational diffusion.

The problem of this approach is that Bosanquet's equation does not take into account the configurational diffusion, which tends to zero. To overcome this limitation, the global effective diffusivity is also estimated by Spry and Sawyer's equation, equation (2.31) [63].

$$D_e = D_{mol} \cdot (1-\lambda)^4 \tag{2.31}$$

Where λ is defined as the ratio between molecular gyration radius and the average pore size.

The two equations for estimating global effective diffusivity are implemented in THERMIDOR where only the smaller of the two is considered:

$$D_e = \min\left(D_e^{Bosanquet}, D_e^{Spry,Sawyer}\right)$$

Finally, the global effective diffusivity is corrected with a factor that is the ratio between porosity and tortuosity:

$$D_e = \frac{\varepsilon(r,z,t)}{\tau(r,z,t)} \min\left(D_e^{Bosanquet}, D_e^{Spry,Sawyer}\right) \tag{2.32}$$

2.7. Catalyst representation

To represent the structure of the catalyst, the Random Spheres Model (RSM), Random Needles Model (RNM) and Random Coins Model (RCM) were used [64,65].

In the RSM, spheres of radius *b* and volumic density n^s are placed at random in space, and allowed to overlap. The RCM is derived from the RSM by cutting off from each sphere the parts outside two parallel planes each placed at a distance e from the sphere center and oriented at random. The RNM is derived from the RSM by keeping from each sphere the part

inside a cylinder of radius *e*, the main axis which passes through the sphere center and is oriented at random. For the three types of media, with α the aspect ratio *b/e*, the general results for the porosity ε and the surface area Σ are [66]:

$$\varepsilon = \exp\left[-\left(4\pi/3\right) n^s \beta \left(b/\alpha\right)^3 \right] \tag{2.33}$$

$$\Sigma = 4\pi \cdot n^s \cdot \xi \cdot \left(b/\alpha\right)^2 \varepsilon \tag{2.34}$$

Where β and ξ are shape factors depending solely on α. The parameters α, β and ξ are equal to 1 in the RSM.

For random coins:

$$\beta_{coin} = 1 + 3 \cdot \int_1^{\alpha} r^2 \cdot \ln\left(\frac{r}{r-1} \right) \cdot dr \tag{2.35}$$

$$\xi_{coin} = \alpha + \frac{1}{2}\left(\alpha^2 - 1\right) \tag{2.36}$$

For random needles:

$$\beta_{needle} = 1 + 3 \cdot \int_1^{\alpha} r^2 \cdot \ln\left(\frac{r}{\sqrt{r^2 - 1}} \right) \cdot dr \tag{2.37}$$

$$\xi_{needle} = \alpha^2 + \left(1 - \alpha\right) \cdot \sqrt{\alpha^2 - 1} \tag{2.38}$$

Moreover, a good estimate of the corresponding equivalent pore diameter is given by the formula:

$$r^{pores} = 4\varepsilon/\Sigma \tag{2.39}$$

These three models are suitable to represent the fresh catalysts as random porous media, but moreover, they are also very convenient to account for the catalyst ageing resulting from the nucleation and homothetic growth of solid deposits (metal sulfides and coke) inside the porosity. Indeed, the aged catalyst may be represented by the superposition of 3 random media according to Figure 2.3: the fresh catalyst, the metal sulfides deposit and the coke deposit. With the representation, it is straightforward to derive exact relationships relating the residual porosity, surface area, coke volume and metal sulfide deposit volume to the dimensions and aspect ratios of the constitutive elementary particles for each random distribution. With indices F, M and C, respectively, for the fresh porous medium, the porous medium formed by the spatial distribution of metal sulfides particles, and the porous medium formed by the spatial distribution of coke particles, equation (2.40) was written for the catalyst porosity:

$$\varepsilon_k\left(r,z,t\right) = \left[\varepsilon_{kF} - V_{kM}\left(r,z,t\right) - V_{kC}\left(r,z,t\right)\right] \tag{2.40}$$

Where V_{kM} and V_{kC} are the local volume fractions of metal sulfides and coke accumulated at time *t*. Besides, one has:

$$\varepsilon_k(r,z,t) = \exp\left[-\left(\frac{4\pi}{3}\right)\left(n^s_{kF}\beta_{kF}\left(\frac{b_{kF}}{\alpha_{kF}}\right)^3 + n^s_{kM}\beta_{kM}\left(\frac{b_{kM}}{\alpha_{kM}}\right)^3 + n^s_{kC}\beta_{kC}\left(\frac{b_{kC}}{\alpha_{kC}}\right)^3\right)\right] \quad (2.41)$$

The probabilities P_{ki} that a point belongs to a solid particle if the distributions of fresh catalyst, metal sulfides and coke are separated in space, are equal to (1-ε_{ki}), with i = F,M, C:

$$P_{ki}(r,z,t) = 1 - \exp\left[-\left(\frac{4\pi}{3}\right)n^s_{ki}\beta_{ki}\left(\frac{b_{ki}(r,z,t)}{\alpha_{ki}}\right)^3\right] \quad (2.42)$$

Considering that the fresh catalyst pre-exists to deposits, and that a deposit is either coke or metal sulfides, by the proper combination of independent probabilities the following relationships were obtained:

$$V_{kM} = P_{kM} - P_{kF}P_{kM} - \frac{1}{2}(P_{kM}P_{kC}) + \frac{1}{2}(P_{kF}P_{kM}P_{ks}) \quad (2.43)$$

$$V_{kC} = P_{kC} - P_{kF}P_{kC} - \frac{1}{2}(P_{kM}P_{kC}) + \frac{1}{2}(P_{kF}P_{kM}P_{kC}) \quad (2.44)$$

$V_{kM}(r,z,t)$ and $V_{kC}(r,z,t)$ are directly proportional to the concentrations in solid phase $C^s_m(r,z,t)$ and $C^s_{coke}(r,z,t)$, respectively, determined by equations (2.23) and (2.24). The unknown $b_{ki}(r,z,t)$ (i = M, C) are therefore determined as solutions of the system (2.42)-(2.44), allowing to determine local residual surface areas and pore sizes, for which exact expressions were derived in a similar way as for (2.43) and (2.44).

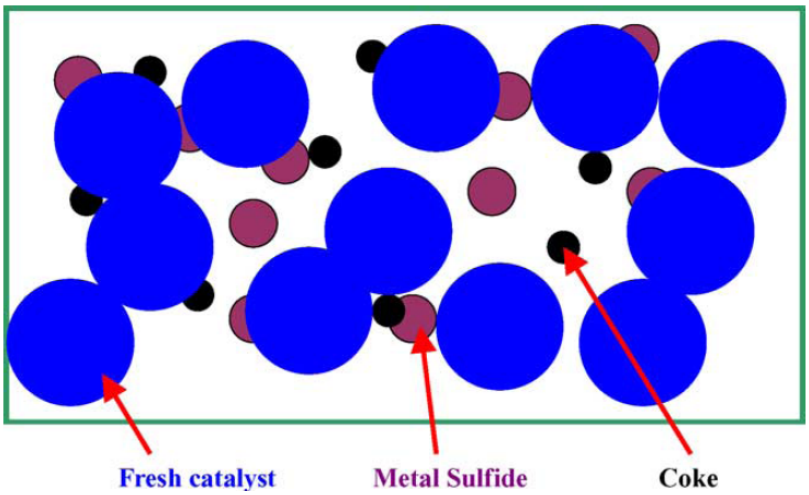

Figure 2.3 Schematic representation of an aged catalyst as superposition of three random porous media: fresh solid + metal sulfides deposit + coke

THERMIDOR has been designed to represent the broadest possible family of hydrotreating catalysts, including monomodal, bimodal, and last but not least, the “chestnut bur” proprietary HDM catalyst [67].

In the general case, the presence of macropores is accounted for by considering the solid as made of randomly seed macrodomains (spheres, coins or needles but usually spheres), i.e. of typical size of the order of a few microns, leaving void interstices figuring the macropores.

These macrodomains embed random seeds of nano-particles (again, spheres, needles or coins, but coins are the most suited for representing the platelets of gamma alumina almost exclusively used to manufacture standard hydrotreating catalysts). The texture of a fresh macroporous catalyst can then be determined by 6 parameters at most: b_{Fi}, α_{Fi}, n_{Fi}^{s} where the index i = 1 or 2 now stands for macropores or mesopores. The shapes of objects (spheres, needles, or coins) and their aspect ratios α_{Fi} need to be decided: for that, electron microscopy studies of the real fresh catalysts and a good knowledge of the manufacturing process may be helpful. The remaining four parameters can be determined from measured textural properties of the real catalyst: macropore and mesopore volumes and average macropore radii can be determined for instance from mercury porosimetry data and specific area by the BET method. A check of consistency can then be provided by the comparison of predicted (from equation (2.38)) and measured (by mercury porosimetry) average mesopore radii. THERMIDOR includes identification routines so that experimental textural data can be input directly. Of course, in the case of monomodal catalysts, it suffices to identify 2 parameters, e.g. total pore volume and surface area, after the aspect ratio has been chosen [56].

The “chestnut bur” catalysts receive a special treatment as described by Toulhoat et al. [56]: the spherical macro-domains of radius b_{Fmacro} are now the “burs” themselves. For each of these domains the radial organization of acicular alumina platelets is approximated by considering that at any fractional radius $x=b/b_{Fmacro}$ inside the sphere, the cross-section of these platelets by the corresponding spherical envelope forms a bi-dimensional random needle model (2D RNM), as represented on Figure 2.5. The average number of acicular platelets per spherical macrodomain being fixed, the areal density of 2D needles is now decreasing with increasing fractional radius. In this case, the identification strategy starts by an estimation of the chestnut bur average radius b_{Fmacro}, using for instance SEM micrographs as presented on Figure 2.4.

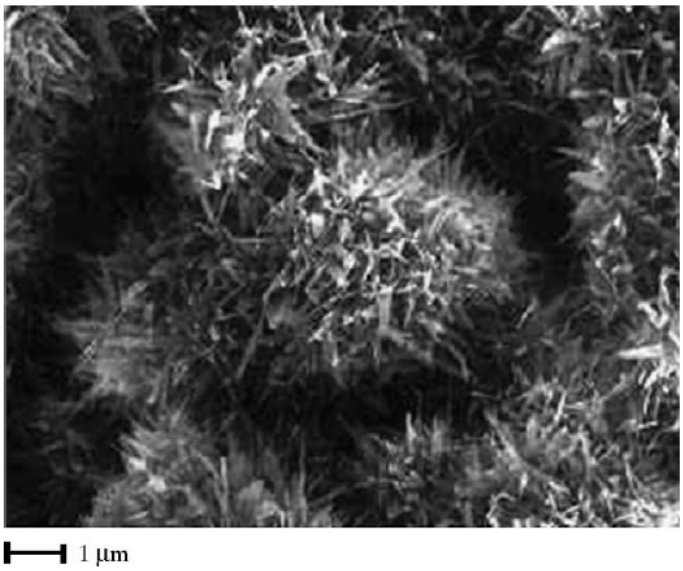

Figure 2.4 Scanning electron microscopy picture of the ‘‘chestnut bur’’ porous structure characteristic of the HDM catalyst A.

In view of their particular manufacturing process [67] it was assumed that the burs do not interpenetrate. The effective number of burs per unit volume n_{Fmacro}^{eff} is then evaluated according to:

$$n_{Fmacro}^{eff} = \frac{1-\varepsilon_{Fmacro}}{\frac{4\pi}{3} b_{Fmacro}^{3}} \tag{2.45}$$

Where ε_{Fmacro} is the experimental macropore volume determined by mercury porosimetry.

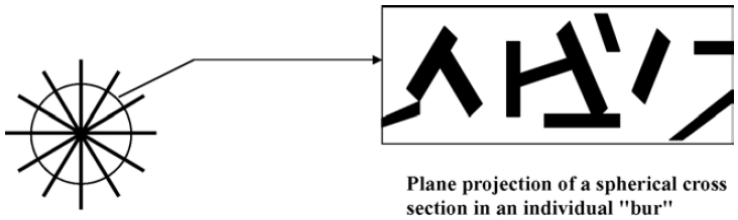

Figure 2.5 Schematic representation of burs in the ‘‘chestnut bur’’ multimodal catalyst: inside a spherical bur, a cross-section of the radially oriented acicular alumina platelets by any concentric spherical envelope forms a bi-dimensional random needle model (2D RNM)

The complement to the experimental total pore volume, ε_{Fmeso}, is assigned to mesopores, and the volume of platelets per single chestnut bur is now:

$$V_{platelets} = \left[\frac{4}{3}\pi \cdot b_{Fmacro}^{3} - \frac{\varepsilon_{Fmeso}}{n_{Fmacro}^{eff}} \right] \tag{2.46}$$

The total area developed by acicular platelets per single chestnut bur is simply:

$$S_{platelets} = \frac{S_{Ftotal}}{n_{Fmacro}^{eff}} \tag{2.47}$$

In the 2D RNM, the specific area ε_{2D} and specific perimeter Σ_{2D} have expressions analogous to 3D equations (2.33) and (2.34) but in 2D. With the aspect ratio α_{Fmeso} of 2D needles estimated for instance from TEM micrographs, the remaining unknowns are the number of platelets per bur n_{Fmeso}^{s} and the half-length of a 2D needle b_{Fmeso}. They will be identified thanks to the following integrals, making use of the results of equations (2.46) and (2.47):

$$V_{platelets} = 4\pi \int_{0}^{b_{Fmacro}} \left[1 - \exp\left(\frac{-C_1}{x^2} \right) \right] x^2 \cdot dx \tag{2.48}$$

$$S_{platelets} = C_2 \int_{0}^{b_{Fmacro}} \exp\left(\frac{-C_1}{x^2} \right) \cdot dx \tag{2.49}$$

Where C_1 and C_2 are constants defined by:

$$C_1 = \frac{1}{4} n_{Fmeso}^{s} \beta_{2DRN} \left(\frac{b_{Fmeso}}{\alpha_{Fmeso}} \right)^2 \tag{2.50}$$

$$C_2 = 2\pi n^s_{Fmeso}\xi_{2DRN}\left(\frac{b_{Fmeso}}{\alpha_{Fmeso}}\right) \tag{2.51}$$

And the shape factors for 2D RNM are:

$$\beta_{2DRN} = 1 - \int_1^{\alpha_{Fmeso}} 2x\ln\left[1 - \frac{2}{\pi}\arccos\left(\frac{\sqrt{x^2-1}}{x}\right)\right]\cdot dx \tag{2.52}$$

$$\xi_{2DRN} = \frac{2}{\pi}\left[\sqrt{\alpha^2_{Fmeso}-1} + \alpha_{Fmeso}\arcsin\left(\frac{1}{\alpha_{Fmeso}}\right)\right] \tag{2.53}$$

In practice, C_1 is deduced from (2.48) by numerical inversion (Newton method), then C_2 is determined from (2.49), and the unknowns come out as solutions of the system formed by equations (2.50) and (2.51). Lastly, the average mesopore radius r_{Fmeso} is determined by averaging the whole radius $r_{2DRN}(x)$ along the radius of one bur, with:

$$r_{2DRN}(x) = \frac{4x^2}{n^s_{Fmeso}b_{Fmeso}\xi_{2DRN}} \tag{2.54}$$

$$r_{Fmeso} = \frac{3}{2\pi\cdot r^3_{Fmacro}}\int_0^{r_{Fmacro}} 4\pi\cdot r_{2DRN}(x)\cdot x^2\cdot dx \tag{2.55}$$

Finally:

$$r_{Fmeso} = \frac{24\cdot r^2_{Fmacro}}{5n^s_{Fmeso}b_{Fmeso}\xi_{2DRN}} \tag{2.56}$$

For this particular chestnut bur geometry, the nucleation and growth of metal sulfides and coke particles are treated similarly as for the other less complex RSM, RCM or RNM geometries, and one arrives at equations similar to (2.40)-(2.44) for the local residual pore volume, surface area and mesopore radius.

Another crucial feature in THERMIDOR is the introduction of a percolation threshold for the residual local pore space, below which it becomes locally discontinuous, and mass transfer is interrupted [56]. In principle, this threshold depends on the radius of gyration of molecules transported, since bigger molecules explore only a subset of the pore space accessible to smaller molecules. As coke and metal sulfides are laid down, the local pore space and mesopore radius decrease. Mass transfer may be discontinued for a molecular species of given radius of gyration, either when the residual pore space becomes locally lower than the percolation threshold for the considered medium, or when the local pore radius becomes smaller than the radius of gyration times some coefficient. Both conditions are tested locally at every time step in THERMIDOR, so as to determine where and when occlusion pores occur for each reactant considered in the simulation. For instance, in the case of a strong radial concentration gradient determined by significant diffusional limitations in a particular type of catalyst pellet, pore mouth plugging will occur early in the life of this catalyst, first selectively for the larger reactants, then completely when shutdown occurs also for diffusion of the smallest.

2.8. Deactivation model

To take into account the catalyst deactivation due to coke and metals deposition, it is possible to use equations empirical deactivation functions of coke or metals deposits and have parameters which allow to model the deactivation curve [68]. The original version of THERMIDOR used equation (2.57) [4]. This equation has two parameters.

$$a_i(r) = \frac{1}{(1 + \alpha_i C_{Coke}(r))^n} \tag{2.57}$$

Where α_i is a coefficient for every subspecies (C, H, S, etc.), $C_{coke}(r)$ is the coke concentration in the catalyst grain and n is a parameter which allow to modulate the shape of the deactivation curve.

The value used for parameter n is 4, chosen according to Toulhoat et al. [56]. Although the main effects responsible for the catalyst deactivation are coke and metals deposition (see chapter 1.3), in equation (2.57) only the coke has been considered. Finally, the combination of equations (2.22) and (2.57) results in the equation below:

$$r_i(r) = \underbrace{\frac{\text{production term} - \text{consumpion term}}{1 + K_{ads}^{Asp} \cdot [Asp](r) + K_{ads}^{H_2S} \cdot [H_2S](r)}}_{\text{reaction rate}} \cdot \underbrace{\frac{1}{(1 + \alpha_i C_{Coke}(r))^4}}_{a_i(r)} \tag{2.58}$$

With this equation, the reaction rate will decrease only as a result of coke deposition.

3. Modifications in THERMIDOR code

Now that the concepts of the THERMIDOR code have been explained (Chapter 2), the modifications introduced in the code will be explained.

Since the main objective of this work was to improve the deactivation mechanism implemented in THERMIDOR, it was necessary to understand the existing code to realize what modifications could be imported.

3.1. Deactivation equation

As can be seen in Figure 1.25, the temperature is raised to compensate for the deactivation of catalyst and to maintain the unit performances. Comparing the shape of the curve with Figure 1.24, it is easy to understand that the deactivation equation will need to include the coke and metals deposits to reflect the initial and rapid temperature increase due to coke, and then the gradual and almost constant increase caused by metals. For this reason, the effect of metals deposits was added to equation (2.57) which resulted in:

$$a_i(r) = \frac{1}{(1+\alpha_i C_{Coke}(r))^n} \cdot \frac{1}{(1+\beta_i C_{Metals}(r))^m} \tag{3.1}$$

Where α_i and β_i are coefficients for every subspecies (C, H, S, etc.), $C_{coke}(r)$ and $C_{Metals}(r)$ are respectively the coke and metals concentration in the catalyst grain and *n* and *m* are parameters which allow to modulate the shape of the deactivation curve.

Although this is a valid approach and permits to obtain the desired results, it lacks from physical reality. Beside this, the equation has four parameters to manipulate and since there are not much deactivation data available, there are too many possibilities to the parameters values. To overcome this problem, and since THERMIDOR has implemented a very advanced model to describe the catalyst grains and the deposition of coke and metals on them (see chapter 2.7), it is wise to use this possibility in the deactivation equation. According to this, the reduction in surface area due to coke and metals was re-introduced in equation (3.1) and resulted in:

$$a_i(r) = \frac{SS(C_{Coke}, C_{Metals})}{SS_0} \cdot \frac{1}{(1+\alpha_i C_{Coke}(r))^n} \cdot \frac{1}{(1+\beta_i C_{Metals}(r))^m} \tag{3.2}$$

Where $SS(C_{Coke}, C_{Metals})$ is the catalyst surface area available and depends on the amounts of coke and metals deposited, SS_0 is the surface area of the fresh catalyst. Only the remaining alumina surface is considered. The surface area coming from the deposited Ni and V were considered to have no activity even though experimental data shows that some activity comes from these deposited metals sulfides.

This new equation predicts well the deactivation even with α_i and β_i equal to zero, as it will be seen in chapter 4.1.1.

Since the parameters of the kinetic model were not obtained on a fresh catalyst but on a stabilized catalyst, it was decided to multiply the equation (3.2) by a parameter, a_0, to correct the initial activity of the catalyst. Equation (3.3) was implemented in THERMIDOR.

$$a_i(r) = a_0 \cdot \frac{SS(C_{Coke}, C_{Metals})}{SS_0} \cdot \frac{1}{(1+\alpha_i C_{Coke}(r))^n} \cdot \frac{1}{(1+\beta_i C_{Metals}(r))^m} \qquad (3.3)$$

3.2. Coke increases along the reactor

Experimental data show that in hydrotreatment processes, the coke increases along the reactor. To reproduce this observation in THERMIDOR, the coke formation has been only associated to asphaltenes and aromatics minus (< 520 ºC). The association to these last ones was made just because they are the only spheres that increase along the reactor. With this approach, since the mass fraction of asphaltenes is inferior to the mass fraction of aromatic minus, the kinetic constant for coke formed by aromatics minus need to be an order of magnitude higher when compared to the kinetic constant of asphaltenes. Moreover, it was considered that neither the resins plus and minus, aromatics plus and saturates produce coke [4]. These hypotheses do not have any reality as it is known that the coke build-up increases with the molecular weight and/or boiling range of the processed feed.

Some authors believed that coke is produced by precipitation of large molecular hydrocarbons such as asphaltenes when their solubility in oil is lowered [30,69]. An increase in the conversion of vacuum residues increases the aromaticity of the asphaltenes and decreases the aromaticity of the maltenes* [70]. Consequently, the solubility of the asphaltenes in the maltenes decreases. Absi-Halabi et al. propose that absorption of asphaltenes on the acidic sites of an alumina support is a major cause of the initial rapid coke deactivation, while a decrease in asphaltene solubility causes the following steady coke build-up [30]. This explains that the amount of coke increases from the entrance to the exit of the reactors as asphaltenes solubility decreases and that an increase in the residue conversion increases the amount of coke at the reactor exit [31]. Based on this information, a new function was added in THERMIDOR, which reflects the variation of aromaticity of asphaltenes and maltenes in coke formation, overcoming the lack of reality of the previous approach.

$$\Delta_{\text{aromaticy}}(L) = \left(\frac{\frac{[H]_{maltenes}(L)}{[H]_{asphaltenes}(L)}}{\frac{[H]_{maltenes}(\text{inlet})}{[H]_{asphaltenes}(\text{inlet})}} \right)^n \qquad (3.4)$$

Where $[H]_X$ is the hydrogen content of compound *X*, *n* is the parameter to model the aromaticy variation effect, *L* represents a generic position in the reactor bed and *inlet* corresponds to the reactor entrance.

---

* Maltenes are the sum of the entire feed compounds without asphaltenes.

As maltenes and asphaltenes become respectively less and more aromatic along the reactor, this results in an increase of hydrogen content for maltenes increases, while the hydrogen content of asphaltenes decreases. In this way, if *n* is positive, $\Delta_{\text{aromaticy}}(L)$ will always be bigger then 1 and increases along the reactor.

As the coking tendency increases when the aromaticity difference between asphaltenes and maltenes increases, the rate constants for the coking reactions were multiplied by the aromaticity function given in equation (3.4). Since the coking reactions are equilibrated reactions, this means that the equilibrium constant is now a function of temperature and of the aromaticity of asphaltenes.

3.3. Other modifications to the code

With the modifications implemented in the code, it was necessary to tune some parameters of the model. Similarly, the way that THERMIDOR saves the simulations results was changed, because it was important to save some profiles during the simulation to see their evolution along the time and not only at the end of the simulation as was done before. Moreover, new profiles were added to the save routines such as metals and coke profiles in the grain.

3.4. Creation of Excel macros

To make the analysis and comparison of the results easier task, several Excel macros were created. A complete description of the objective of all the macros is given below:

- **ETUDEXX_COK**: Draw the evolution of the coke along the time in the grain, for the first and last rector section;
- **ETUDEXX_HYT**: Obtain the hydrotreatment profiles along the reactor and time;
- **ETUDEXX_MET**: Represent the development of the metals deposits in the grain, for the first and last rector section, along the time;
- **PROFILcoke**: Draw the evolution of the coke along the time in a section of the rector;
- **PROFILFractions**: Acquire the profiles for the families of compounds along the reactor;
- **PROFILgrain**: Obtain the profiles of the families of compounds in the grain, for a given reactor section;
- **PROFILmetaux**: Draw the evolution of the metals deposits along the time in a section of the rector;
- **PROFILsulfur**: Represent the development of the sulfur fraction in the families of compounds along the reactor;
- **VARIATIONTEMP**: Obtain the temperature profile of the reactor along the time.

4. Results

After the modifications had been implemented, it was necessary to tune the new parameters in the model. Thus, the description of this tuning will be shown and a comparison will be made with the previous version of THERMIDOR [4] to demonstrate the effects of the modifications.

4.1. Tuning the parameters

All the parameters were tuned to the same operating conditions that were:

- Space velocity 0.3 h^{-1}
- Total pressure 150 bar
- Sulfur fraction in the products of 0.5 wt% S

The reactor inlet temperature is automatically adjusted by the code to reach the desired sulfur content in the total liquid effluent.

4.1.1. Deactivation equation

According to equation (3.3), the new parameters, a_0, α_i and β_i, that respectively represent the initial activity and the effect of coke and metals in deactivation of the catalyst, need to be tuned.

Initial activity

The objective of the initial activity parameter is to adjust the start temperature to an expected value. If a_0 take the value 1, then the initial temperature was be near 480ºC. This value is not acceptable for the chosen conditions since a value close to 370ºC was expected. To tune the parameter, a sensitivity analysis was made and the results are presented in Figure 4.1.

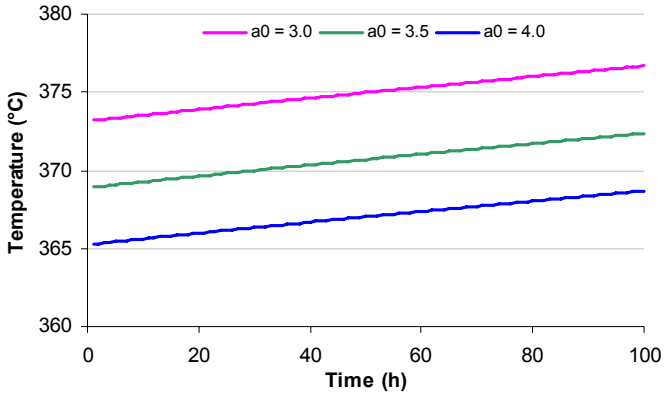

Figure 4.1 Sensitive analysis to the parameter a_0

The temperature profiles in Figure 4.1 show that the value of 3.5 is a good value for the initial activity, since this also corresponds to literature data [31] that shows that after the initial period about 70% of the active sites is covered by coke.

Heuristic parameters, α and β

With the initial temperature corrected, it is important to understand the effect of the deactivation functions on the deactivation curve. The obtained results are illustrated in Figure 4.2 and Figure 4.3. It is important to note that deactivation curve (given by the increase of temperature) is divided in three zones (see Figure 1.25). The first zone corresponds to the one where temperature increases rapidly and is caused by the rapid coke deposition. In the second, the increase of temperature is almost constant and is caused by the gradual deposition of metals. Finally, when the catalyst pores start to plug, the temperature needs to be rapidly increased again to maintain a constant performance.

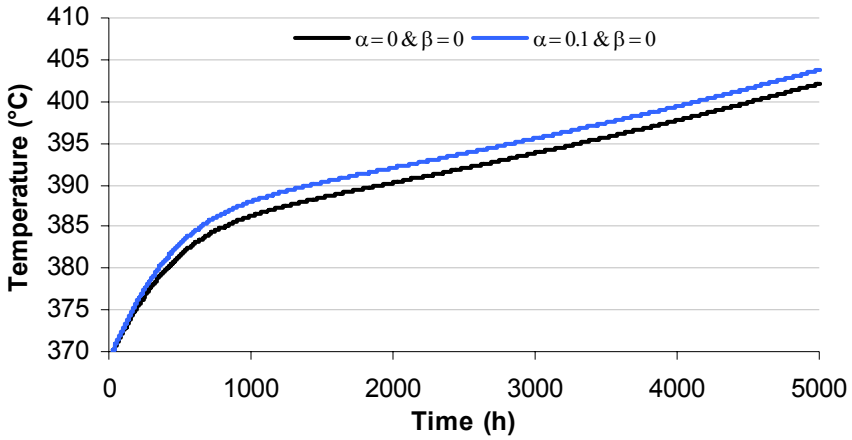

Figure 4.2 Sensitivity analysis to the empirical parameter α

In the first zone, the one that correspond to the rapid deactivation by coke, the effect of the parameter α is evident since it increases the initial deactivation effect but does not affect the second zone, where the coke level is almost constant.

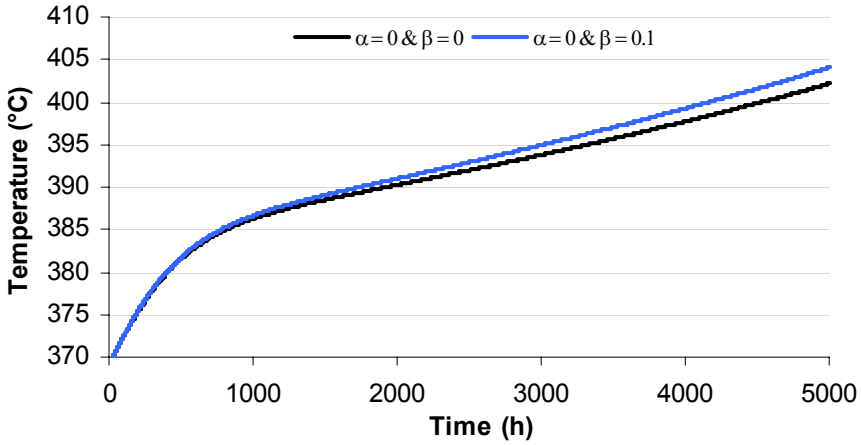

Figure 4.3 Sensitivity analysis to the empirical parameter β

In the second zone, for the operating conditions considered, a slope of about 3ºC/month was expected. As can be seen in Figure 4.3, even with the both parameters equal to zero, the slope is acceptable (≈3.4ºC/month). For this reason, the empirical deactivation functions were not used in the subsequent simulations.

4.1.2. Rapid initial deactivation

As described in chapter 1.3.1, coke has an important role in the first hours since it builds up rapidly and covers a large fraction of the active sites. For this reason, it is essential to adjust the coke content at equilibrium and the rate at which it reaches this state.

Coke equilibrium constant

According to experimental data from IFP laboratories (see chapter 7.1), the coke at equilibrium is near 10% of the fresh catalyst mass. This way, a sensitivity analysis was performed in the equilibrium constant parameter to find an acceptable value. The results are illustrated in Figure 4.4.

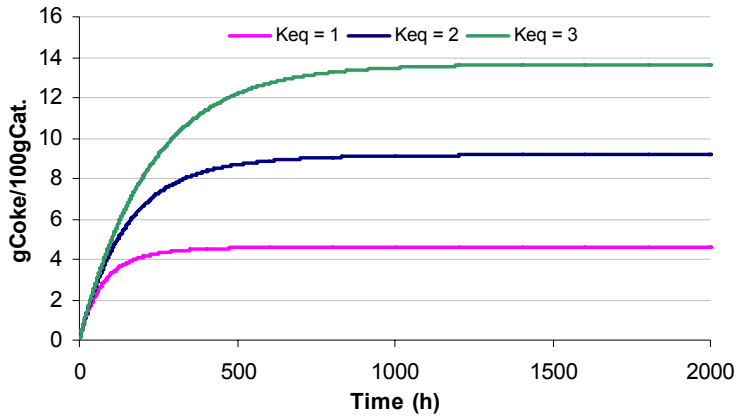

Figure 4.4 Sensitivity analysis to the coke equilibrium constant, K_{eq}

From Figure 4.4 it is perceptible that a value for K_{eq} near 2 is satisfactory.

Coke kinetic constants

Now that the amount of coke at equilibrium is adjusted, it is crucial to define the coke formation rate by varying the corresponding kinetic parameters. As mentioned before, in the previous version of THERMIDOR, coke was only formed from asphaltenes and aromatics$^-$. These values were considered to be in contradictive with the literature. In Table 4.1 three new groups of kinetic parameters were proposed and the results are shown in Figure 4.5.

Table 4.1 Kinetic constants considered in sensitive analysis for coke formation rate

	Previous	Group 1	Group 2	Group 3
Asp → Coke	0.001	0.008	0.004	0.002
Res$^+$ → Coke	0	0.006	0.003	0.002
Res$^-$ → Coke	0	0.006	0.003	0.002
Aro$^+$ → Coke	0	0.006	0.003	0.002
Aro$^-$ → Coke	0.01	0.006	0.003	0.002
Sat → Coke	0	0.004	0.002	0.001

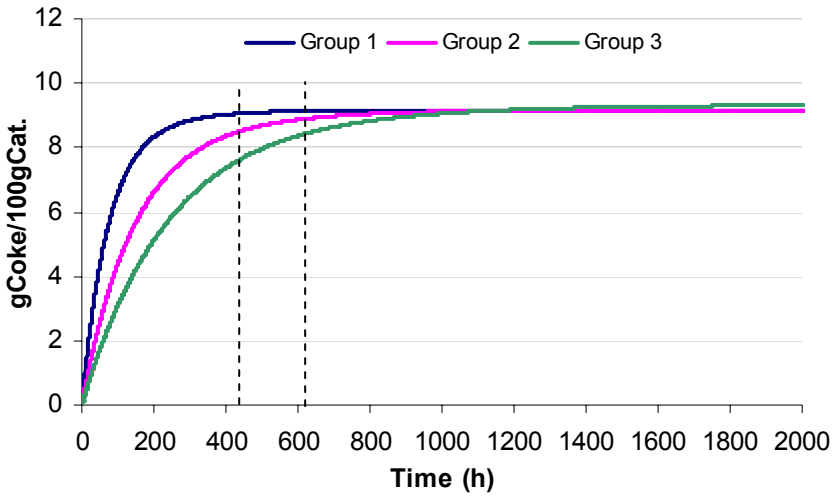

Figure 4.5 Sensitivity analysis of coke formation rate

In agreement with some authors [11] which say that coke reaches the equilibrium near 400-600h (see chapter 1.3.1), it can be seen in the Figure 4.5 that in this period, the parameters of Group 2 agree more.

4.1.3. Aromaticy effect on coke deposits

As described in chapter 3.2, the variation of aromaticy along the reactor influences the coke formation. The parameter which models the aromaticy variation effect was adjusted according to the variation observed in experimental data from IFP laboratories (see chapter 7.1, Table 7.1). The obtained results are shown in Figure 4.6.

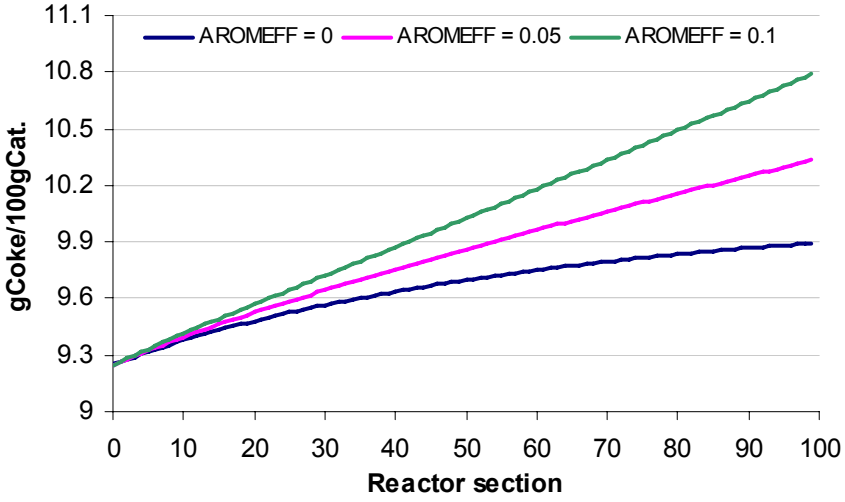

Figure 4.6 Variation of aromaticy parameter and its influence on coke deposition along the reactor

Since the experimentally observed variation between the entrance and the exit of the reactor is around 20%, the value chosen for the parameter which models the influence of aromaticy on coke deposition is 0.1.

4.1.4. Percolation threshold

The percolation threshold is the limiting porosity at which the compounds do not diffuse further in the catalyst. This limit represents the moment that the grain of catalyst is no longer active. The percolation threshold typically has a value between 0.2 and 0.3. This means that this limit defines the start of the third zone of the deactivation curve, as can be seen in Figure 4.7.

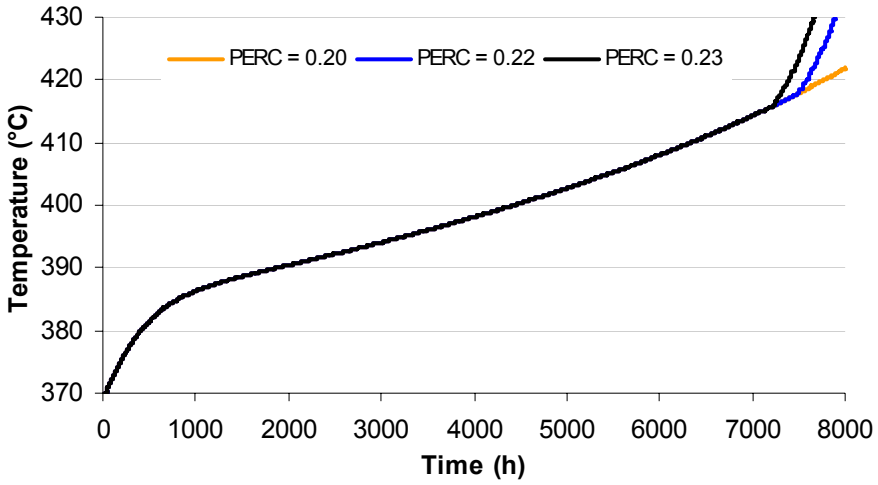

Figure 4.7 Sensitivity analysis to the percolation limit and its influence in the deactivation curve

Since the catalyst should be operated over a one year run, approximately 8000h, the value chosen for the percolation limit is 0.22.

4.1.5. Comparison with previous THERMIDOR version

Now that all the new parameters added to the deactivation mechanism are tuned and the existing coking parameters readjusted, a comparison was made between the new deactivation curve and the one from the previous THERMIDOR version [4] at the same operating conditions. Thus is illustrated in Figure 4.8.

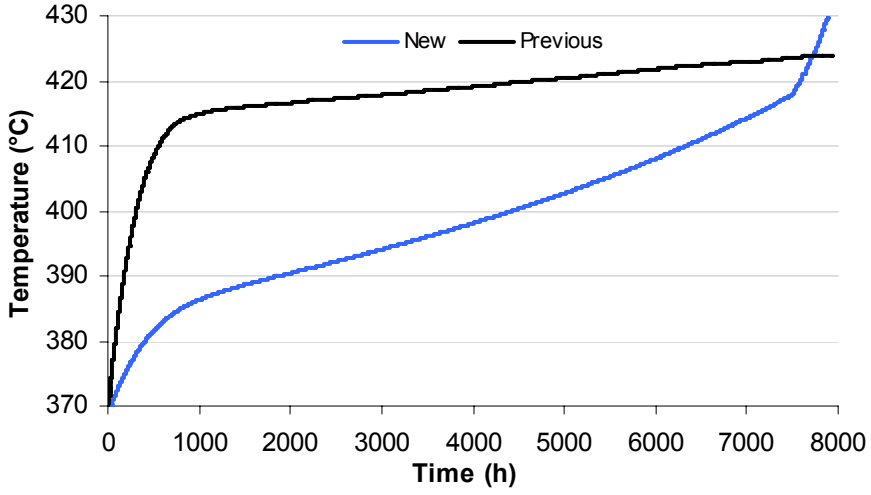

Figure 4.8 Comparison between the new deactivation curve and the previous one

By comparison of the new deactivation curve obtained with the one presented in Figure 1.25, it is evident that the new curve, in opposition with the previous, has all three stages well represented even without the use of empirical deactivation functions.

4.2. Results for a complete run of an HDS reactor in isothermal mode

Since the model already obtains good results, a 12 month run simulation in isothermal mode was made to review all the results obtained such like the profiles of coke and metals along the reactor and into the grain for different reactor sections.

4.2.1. Grain profiles

To understand the evolution of the coke and metals deposits in the grain during the run (simulation), their profiles will be presented along the time.

Families of compounds

Before showing the coke and metals profiles, it is important to understand the profiles of the families of compounds into the grain and their variation along the reactor, which are represented in Figure 4.9 and Figure 4.10.

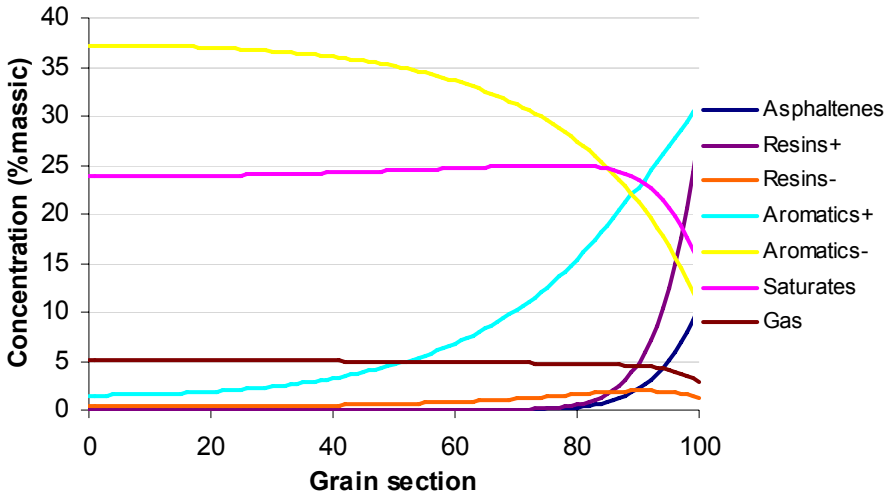

Figure 4.9 Profiles of the families of compounds in the grain for the first reactor section

As can be seen in the above figure, the size of the molecules influences a lot their concentration in the grain. The diffusion of the biggest molecules (asphaltenes and resins) is very limited and they do not reach the center of the grain. Otherwise, as the lighter molecules (gas, saturates) are formed inside the grain, their concentrations are higher in the center that at the surface of the grain.

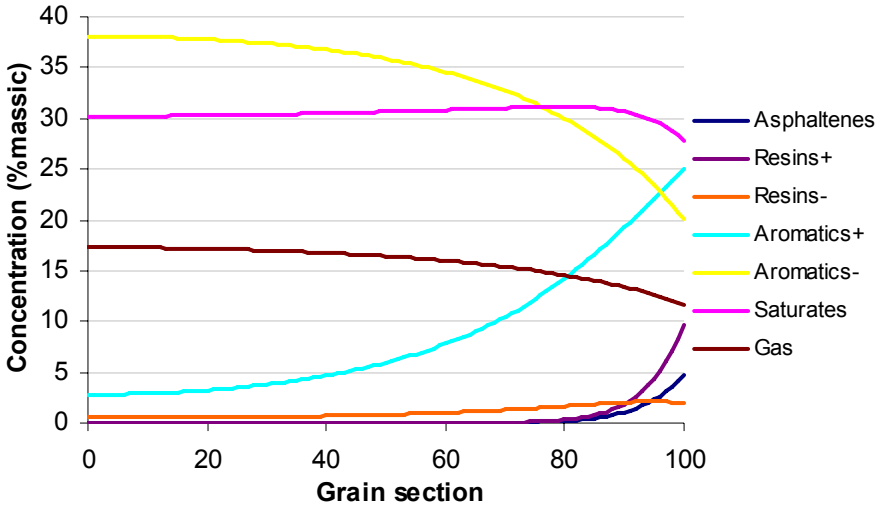

Figure 4.10 Profiles of the families of compounds in the grain for the last reactor section

From the comparison between Figure 4.9 and Figure 4.10 it is observed that, at the exit of the reactor, the asphaltenes and resins penetrate less into the grain since their concentrations decrease along the reactor, a result of the asphaltenes and resins conversion along the reactor bed.

Coke

The evolution of the coke intraparticle coke profile along the time is presented in Figure 4.11 and Figure 4.12 for the first and final section of the reactor, respectively.

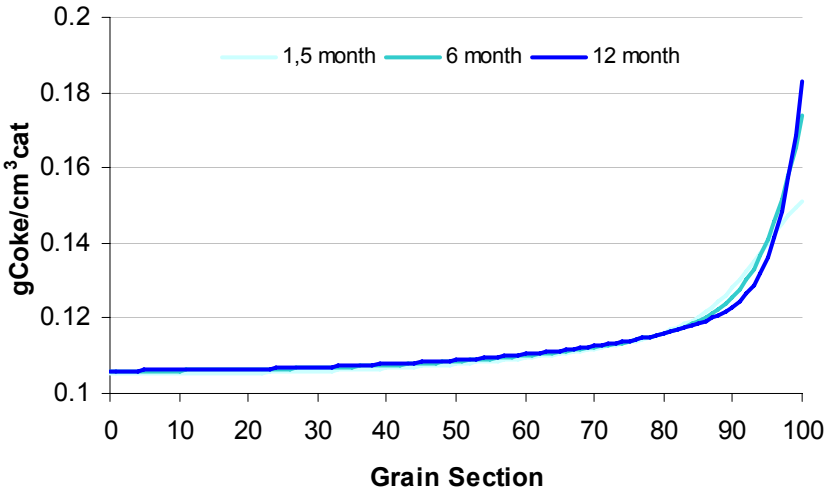

Figure 4.11 Grain profile for coke in the first section of the reactor along the run time

Comparing Figure 4.11 with Figure 4.12, it can be seen that the coke content in the grain is lower in the entrance of the reactor than at the exit. This is due to the effect of the aromaticy variation across the catalyst bed, as already explained in chapter 3.2. Other important observation is the bigger accumulation of coke near the grain surface in the front of the reactor which happens because the kinetic parameter for the coke formation from asphaltenes is the

highest (see Table 4.1). Since asphaltenes do not penetrate far in the grain and since they decrease along the reactor, the accumulation of coke near the surface is not so pronounced in the final reactor section.

In Figure 4.11 is also possible to observe that coke gradually becomes more concentrated near the surface. This happens because the asphaltenes and resins penetrate less into the grain along the time (as will be seen below) and since coke is at equilibrium, its profile follows their shape.

It also can be seen in both figures that along the time, the coke in the grain increases due to the temperature raise.

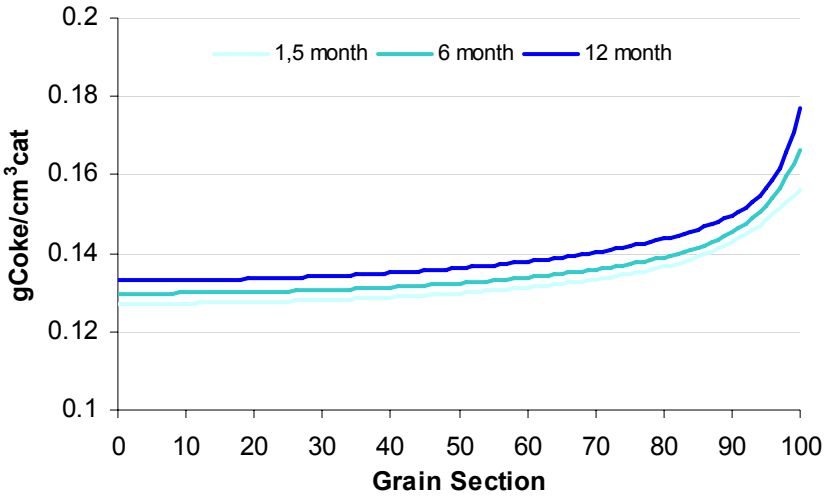

Figure 4.12 Grain profile for coke in the final section of the reactor along the run time

Metals

The metals are only present in the asphaltenes and resins^{+} (see Table 2.1), and since it is evident in Figure 4.9 and Figure 4.10 that they do not penetrate deeply into the grain, it is obvious that metals will have similar profiles, as shown in Figure 4.13 and Figure 4.14. These profiles correspond well to results shown by many authors and illustrated in Figure 1.26.

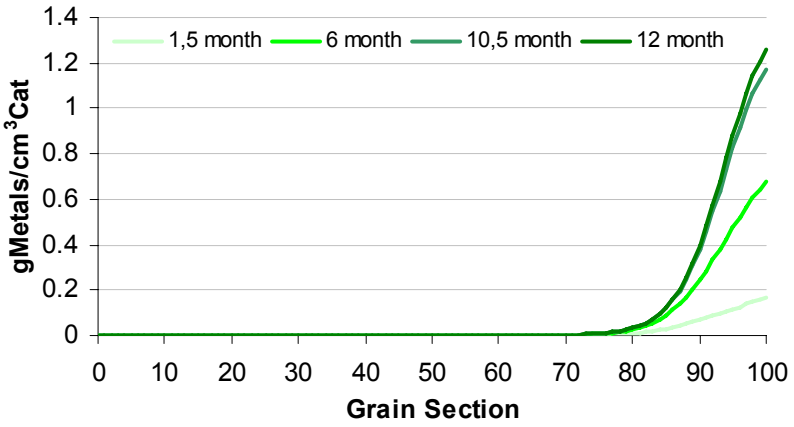

Figure 4.13 Grain profile for metals in the first section of the reactor along the run time

In Figure 4.13 the evolution of metals deposition along the time is significant near the surface of the catalyst grain. It also can be observed that plugging of the grain occurs between 10th and 12th, resulting in a slight variation in metals deposits over the last two months. On the other hand, near the exit of the reactor, Figure 4.14, the metals content is much lower (near an half) and there is no grain plugging.

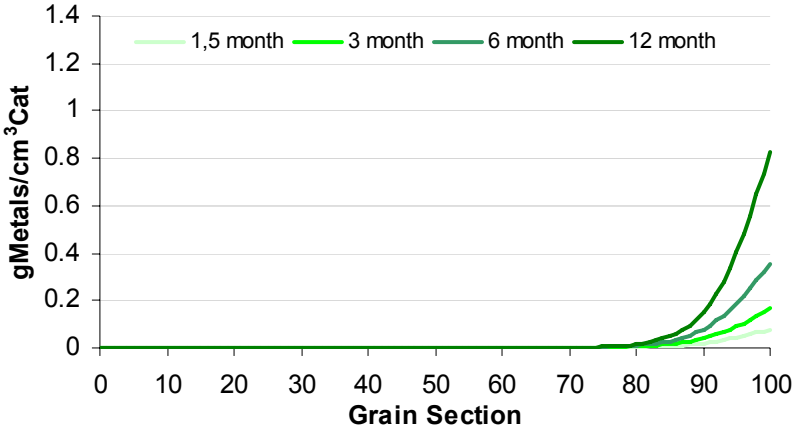

Figure 4.14 Grain profile for metals in the final section of the reactor along the run time

Total deposits

The *Total deposits* were calculated as the sum of coke and metals deposits. The obtained results for the first reactor section after a 12 month run, illustrated in Figure 4.15, are similar to the ones obtained by Beuther et al. [34] (see Figure 1.26) and confirm that when grain plugging occurs, its interior remains active, but inaccessible.

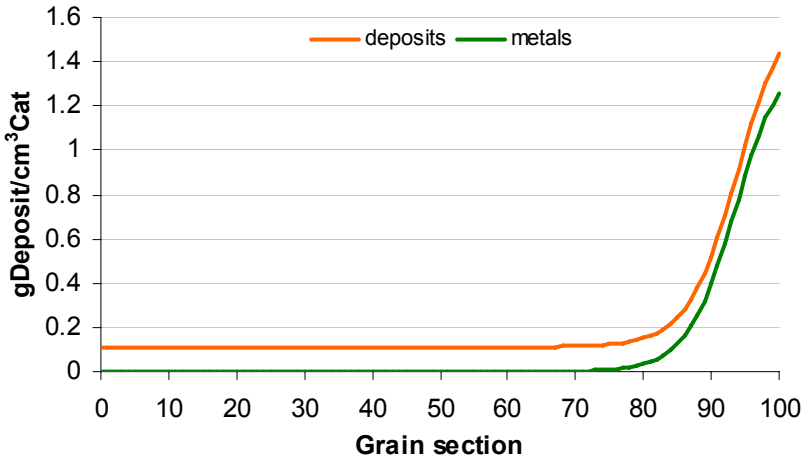

Figure 4.15 Representation of total deposits in the catalyst grain in the first reactor section for a 12 month simulation (plugged grain)

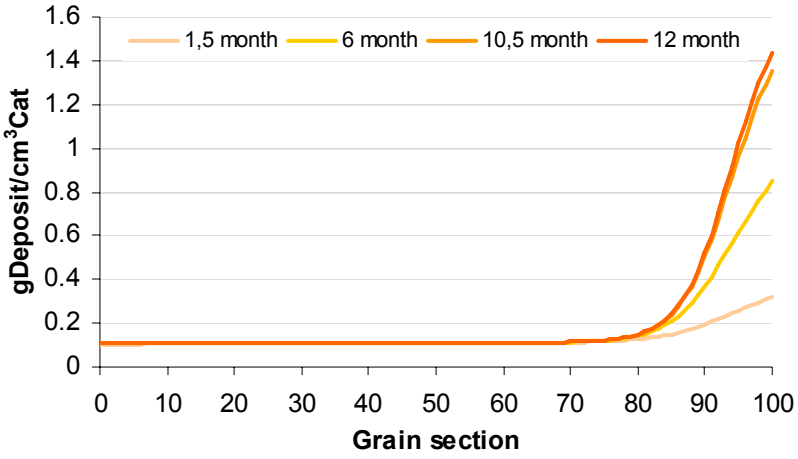

Figure 4.16 Evolution of deposit along the time in a grain on the first reactor section

Figure 4.16 shows the evolution of the deposits in the grains of the first reactor section. These deposits accumulation near the grain surface creates an extra resistance which significantly decreases the diffusion of the biggest molecules like resins and asphaltenes. This results in a smaller penetration into the grain, as shown in Figure 4.17.

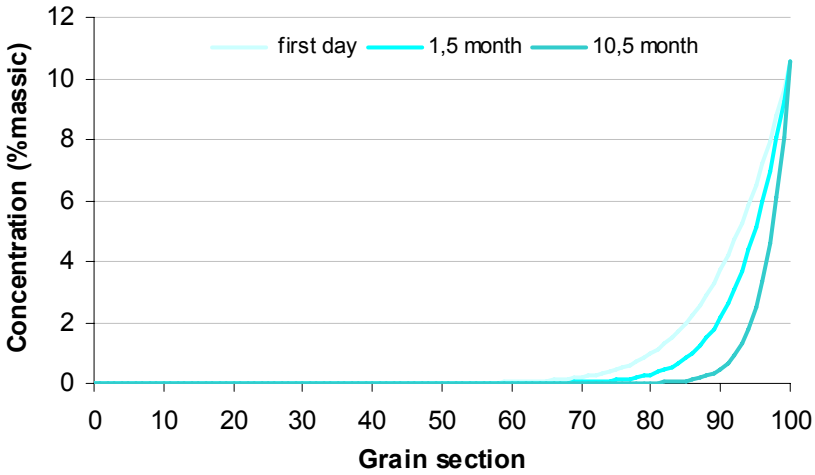

Figure 4.17 Decrease of the asphaltenes diffusion into the catalyst grain along the run

4.2.2. Reactor profiles

Now that the grain profiles are understood, the reactor profiles for coke, metals and the families of compounds will now be shown.

Families of compounds

The profiles of the families of compounds after 10.5 month of run, before the start of the percolation, are shown in Figure 4.18. It is possible to see that the lighter compounds such as gas, saturates and aromatics^{-} increase along the reactor by opposition to the heavier compounds (asphaltenes, resins^{+} and aromatics^{+}) which decrease.

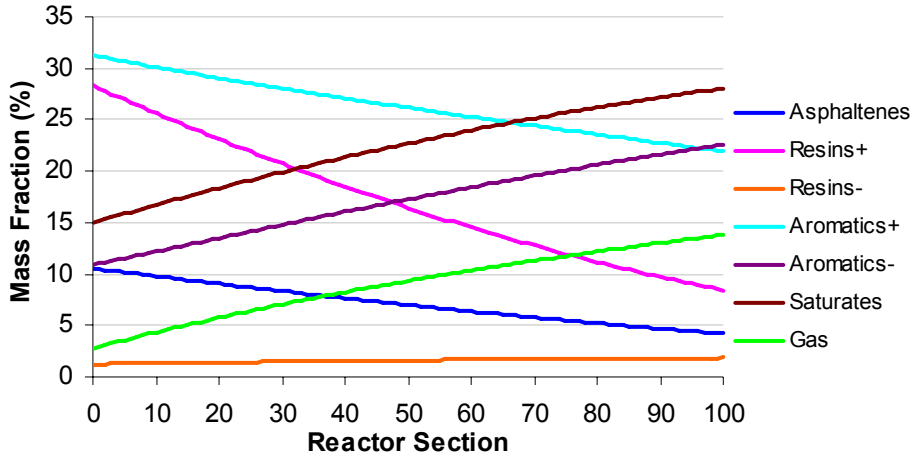

Figure 4.18 Profiles of the families of compounds along the reactor for a 10.5 month simulation (before percolation)

When pore plugging starts, the first sections of the reactor begin to die and the temperature increased to compensate the loss of catalyst which results in steeper profiles as shown in Figure 4.19. Notice that at the end of the run approximately 20% of the catalyst bed is no longer active.

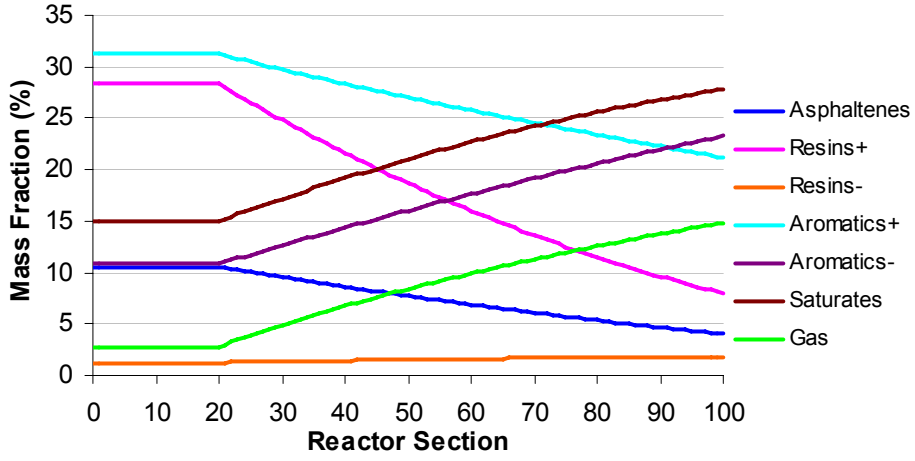

Figure 4.19 Profiles of the families of compounds along the reactor for a 12 month simulation (after the start of percolation)

Coke

The coke increases rapidly in the first month of the run and becomes approximately steady until the end, as can be seen in Figure 4.20. The simulation profile corresponds well to the literature and is corroborated by Figure 1.24, which is a result from Shell's studies in hydroprocessing.

In the 20th reactor section, illustrated in Figure 4.20, the coke content suddenly decreases after about 7500h due to the start of percolation in the first reactor sections. This is due to the

fact that the conversion of the asphaltenes at this section starts to decrease. Hence, the aromaticy effect parameter approaches to 1 resulting in a decrease of the coke equilibrium constant. Therefore, when percolation starts, the coke content in the sections after to the percolated ones decreases.

Comparing the sections represented in the figure below, the increase of the coke content along the reactor is noticeable and the coke content is maximum at the final section.

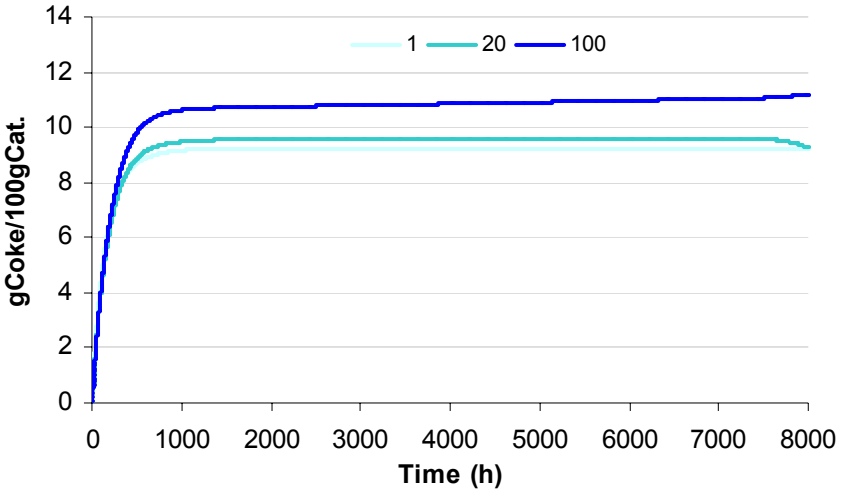

Figure 4.20 Various coke profiles along the run time for different reactor sections

In Figure 4.21 the effects described above can easily be seen: the percolation effect in the first reactor sections and the coke build-up along the reactor. It is also evident in this figure that coke increases along the time due to the temperature raise to maintain the reactor performance.

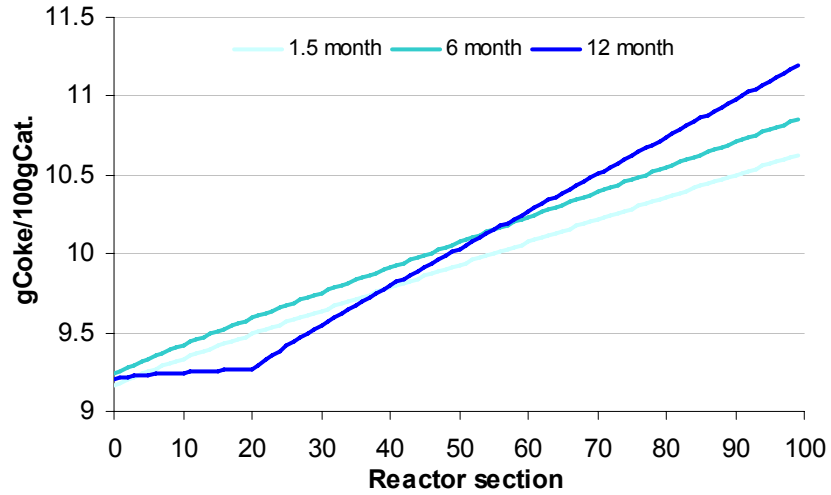

Figure 4.21 Various coke profiles along the reactor for different run times

Metals

According to Figure 1.24, the metals content should increase fairly linear with time. In the THERMIDOR simulation the same happens, with the particularity that near the 11th month (7300h), pore plugging occurs in the first section of the reactor and begin to extend to the following sections, as shown in Figure 4.22.

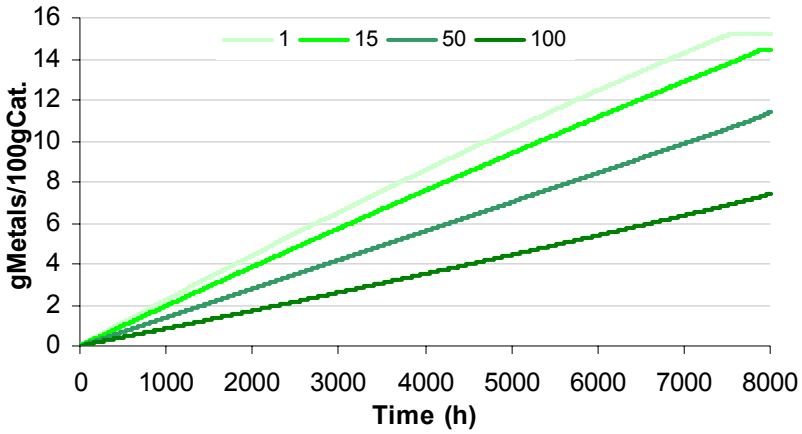

Figure 4.22 Various metals profiles along the run time for different reactor sections

From Figure 4.23, it can be seen that the metals profiles for different times of simulation decrease along the reactor as expected. The slope of this decrease depends on the catalyst, feed characteristics and operating conditions. Comparing the experimental data available (see chapter 7.1, Table 7.1) with the obtained results, it is perceptible that they have similar trends.

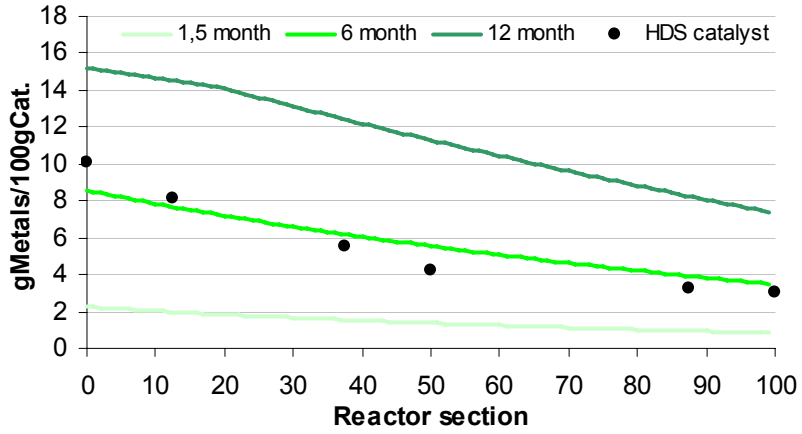

Figure 4.23 Various metals profiles along the reactor for different run times

Total deposits

In the first months of run, the deposits are almost constant along the reactor. This is because coke increases along the reactor but the metals go in the opposite direction as represented in Figure 4.24.

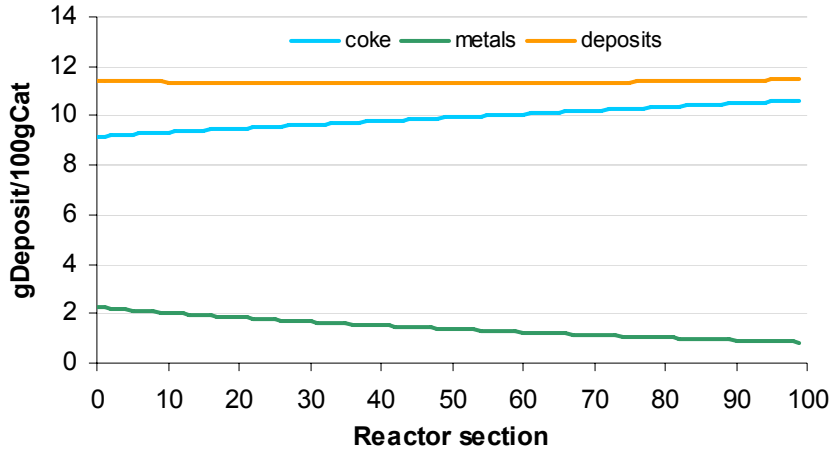

Figure 4.24 Representation of the deposits along the reactor for a 1.5 month run

During the run, coke remains almost constant but the metals begin to accumulate mostly in the entrance of the reactor which creates the steeper profiles presented in Figure 4.25. At the end of the run, the initial part of the reactor (20%) is dead but the rest is still active. Despite this, the run must be stopped because the temperature needed to maintain the performance is too high (over 430ºC).

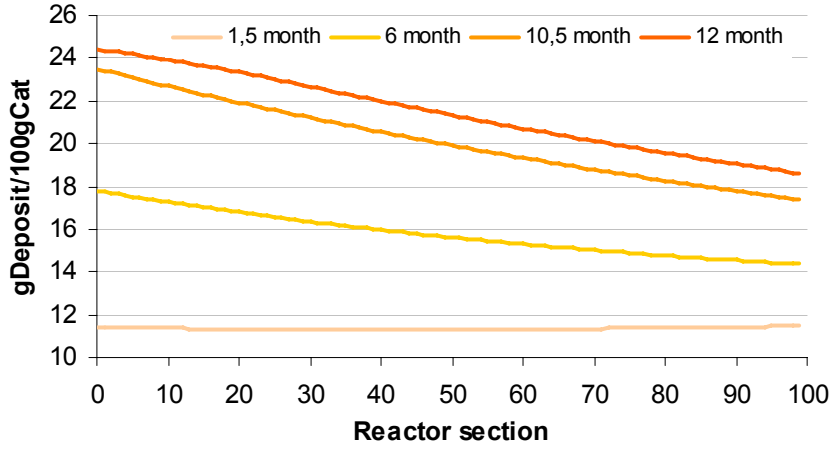

Figure 4.25 Variation of the deposits content in the reactor along the time

Hydrotreatment

The aim of ARDS units is to get near 95% of conversion for HDM and near 90% for HDS. This is obtained with a reactor filled with two sections of catalyst, the first one with a HDM catalyst and the second with a HDS catalyst, as shown in Figure 1.8. In the present simulation, as only HDS catalyst was used in the reactor, the results will be somewhat different. It is clear from Figure 4.26 that HDS reaches the objective but HDM does not. At the end of the run, with near 20% of the catalyst dead, the HDS performance was maintained by the temperature increase but the rest of hydrotreatment reactions changed. These changes are due to the differences between the activation energies of the reactions.

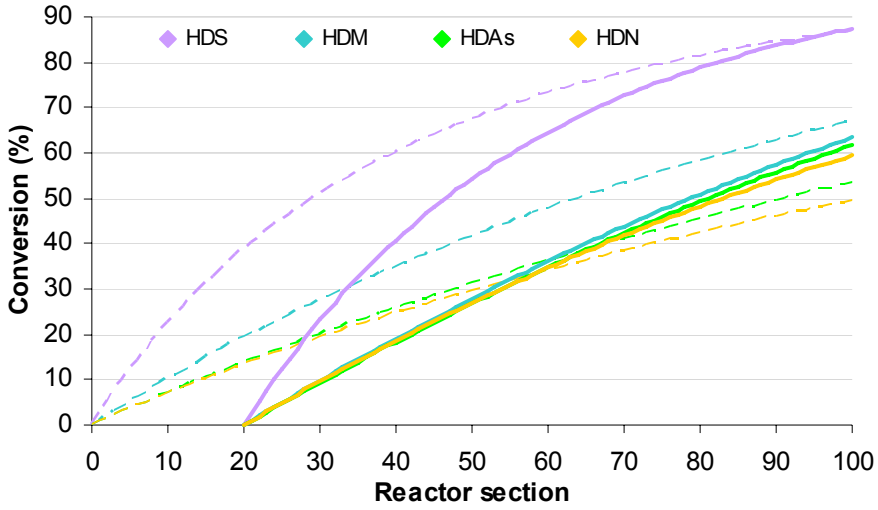

Figure 4.26 Variation in HDS, HDM, HDAs and HDN along the reactor bed. The dashed and full lines respectively correspond to the profiles at the beginning and at the end of a 12 month run

In Figure 4.27 the variations of the hydrotreatment reactions during the run are more perceptible. The biggest changes occur at the start and at the end of the run because it is at this moments that the temperature rises more, initially due to the rapid coke build-up and finally due to the start of the percolation.

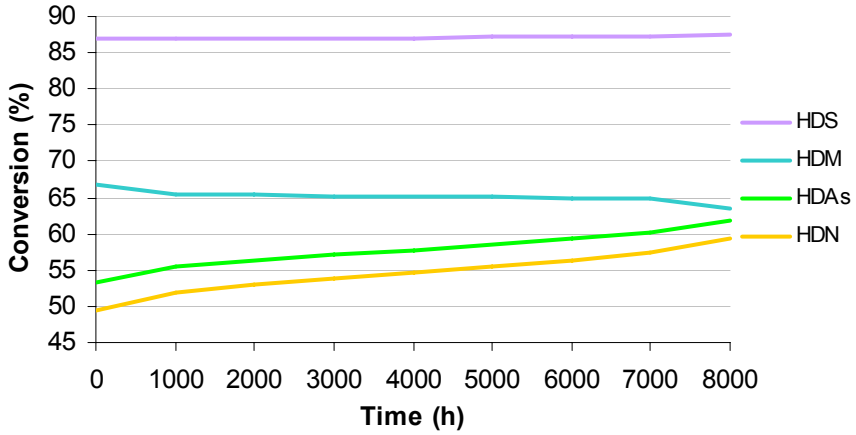

Figure 4.27 Variation in HDS, HDM, HDAs and HDN performances along the time

Since the objective chosen was to maintain a constant the HDS performance, as easily seen in the previous figure, the evolution of sulfur content in the various families of compounds was also followed and illustrated in Figure 4.28. The lighter species such like aromatics and resins$^-$ are almost completely desulfurized (the sulfur content becomes much lower than 0.5wt %). The heavier compounds as asphaltenes and resins$^+$ are only partially desulfurized and remain with a sulfur content higher than 1wt %. They are effectively the most difficult to desulfurize. Moreover, their desulfurization is reduced along the run time.

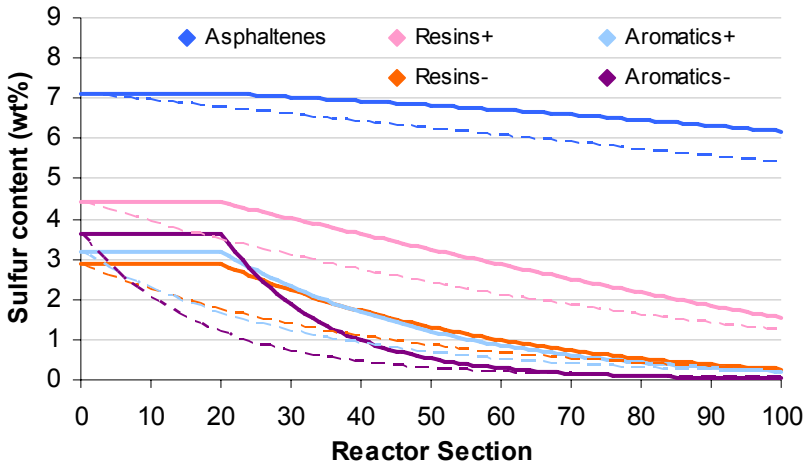

Figure 4.28 Evolution of the sulfur content in the families of compounds along the reactor. The dashed and full lines respectively correspond to the profiles at the beginning and at the end of a 12 month run

4.3. Results for a complete run of an HDS reactor in adiabatic mode

To understand the effect of a reactor temperature gradient on hydrotreatment reactions, a 12 month adiabatic simulation with the same feed, same catalyst and at the same operating conditions was made and compared to the one in isothermal mode.

4.3.1. Temperature profiles

The only difference between the adiabatic and the isothermal simulation is the temperature profiles inside the reactor, shown in Figure 4.29 and Figure 4.30. Their influence will be discussed.

Across the reactor bed

As can be seen in the first graph the temperature increases fairly linearly by approximately 40ºC from the entrance to the exit of the reactor. This increase is due to the heat released by the hydrotreating reactions which are globally exothermal. Figure 4.29 also illustrates that the isothermal temperature is equal to the weight average bed temperature

(WABT), which corresponds closely to the temperature in the middle of the reactor in adiabatic mode. This is no longer true however during the 12th month. This exception happens because in isothermal mode, after the 11th month, the reactor bed starts to percolate and in adiabatic mode there is no percolation observed, as will be seen later.

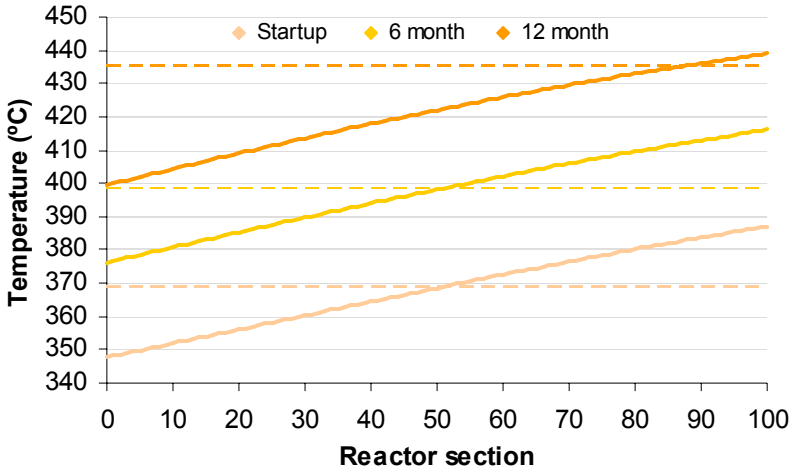

Figure 4.29 Temperature profiles along the reactor for different run times. The dashed and full lines respectively correspond to the profiles of isothermal and adiabatic modes

Along the simulation time

From Figure 4.30, it is observed that the average temperature for the adiabatic run is almost equal to the isothermal temperature. One significant difference is that for the adiabatic run, there is no catalyst percolation. This occurrence will be explained later with the study of the coke and metals deposits.

Note that the temperature profile in the middle section of the reactor is not shown because is similar to the average profile. This result is due to an almost linear profile inside the reactor, as Figure 4.29 illustrates.

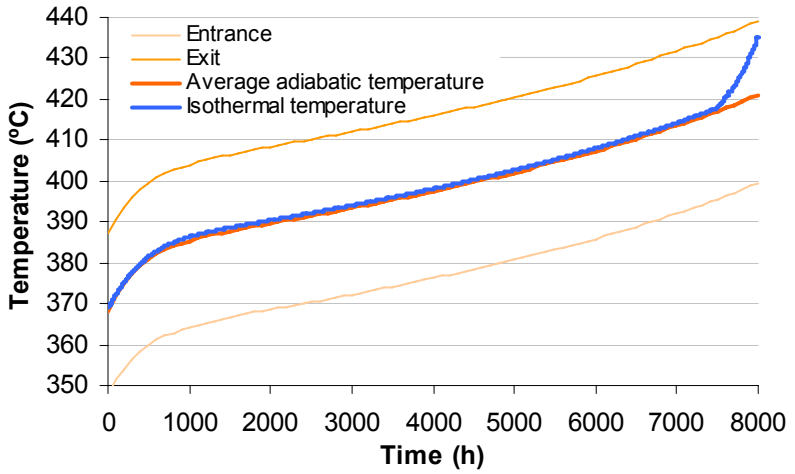

Figure 4.30 Temperature profiles for the isothermal and adiabatic mode

4.3.2. Grain profiles

Since the grain profiles are very similar, only a few of them will be shown.

Families of compounds

The profiles obtained in adiabatic mode are similar to those obtained in isothermal mode. For this reason, and since all the conclusions are equal, they are presented in chapter 7.2.1.

Coke

For the coke build-up, there are some differences between the isothermal and adiabatic mode. Comparing Figure 4.11 with Figure 4.31, which correspond to the reactor entrance, it is seen that the main difference is the coke content near the grain surface for 1.5 months. This may be justified because in adiabatic mode the inlet temperature is about 20ºC lower than in isothermal mode. Hence, the kinetic parameters will be lower too. For this reason, the time required to reach the equilibrium is higher, as will be seen further.

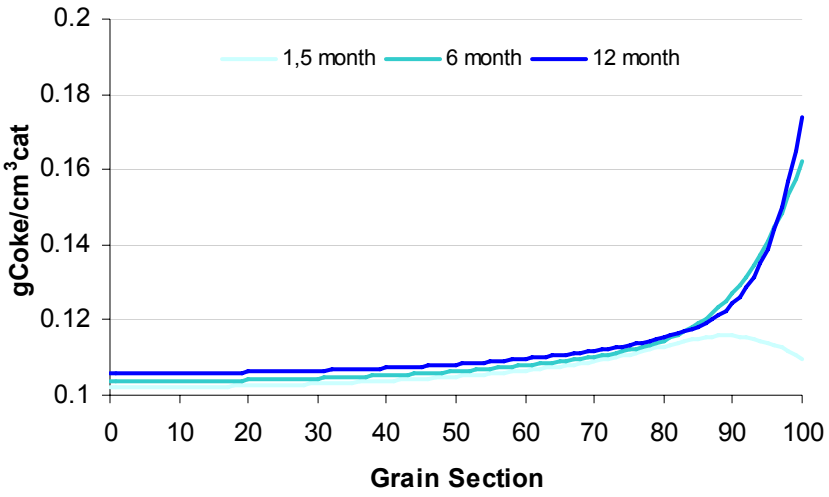

Figure 4.31 Grain profile for coke in the first section of the reactor along the run time for adiabatic mode

In contrast, unlike the reactor entrance, the main difference observed in the reactor exit between isothermal and adiabatic mode is at the last month of simulation. This difference is due to the absence of percolation in adiabatic mode which does not require to raise the temperature at the end of the run and which results in a lower coke production. Hence, by comparison of Figure 4.12 with Figure 4.32, the lower coke content in the adiabatic mode is noticeable for the 12^{th} month.

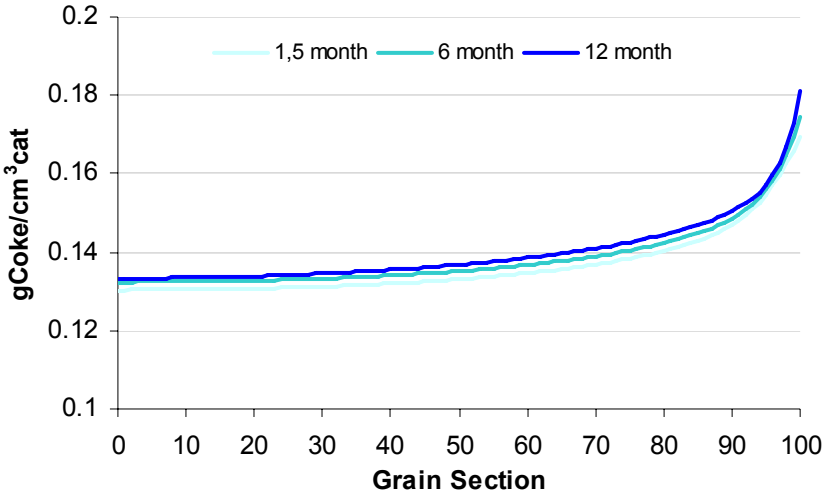

Figure 4.32 Grain profile for coke in the final section of the reactor along the run time for adiabatic mode

Metals

Metals deposition profiles inside the grain are the profiles that have changed most. Comparing the profiles obtained in isothermal mode (Figure 4.13 and Figure 4.14) with the ones obtained in adiabatic mode (Figure 4.33 and Figure 4.34), it is perceived that the metals content near the grain surface is lower at the entrance but higher at the exit for the adiabatic mode. Another curious observation in adiabatic mode is that the metal content near the surface is higher for the outlet than for the inlet although the total content in the grain remains higher at the entrance. This happens because the temperature is higher at the exit which increases the kinetic parameters but since the asphaltenes and resins concentrations are lower, they do not penetrate as much into the grain as at the reactor inlet.

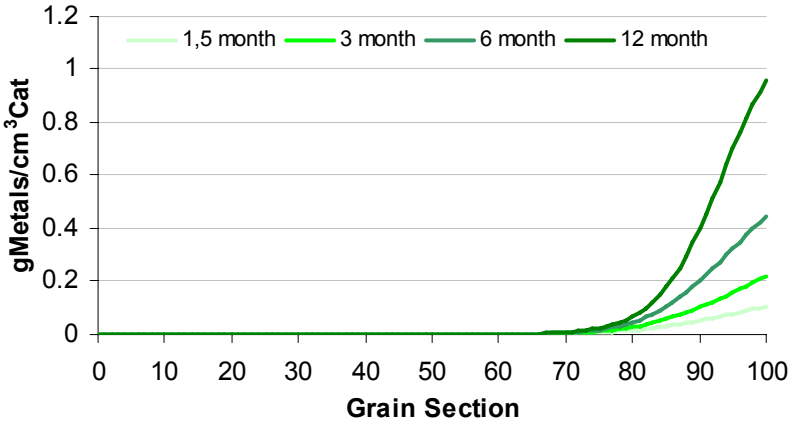

Figure 4.33 Grain profile for metals in the first section of the reactor along the run time in adiabatic mode

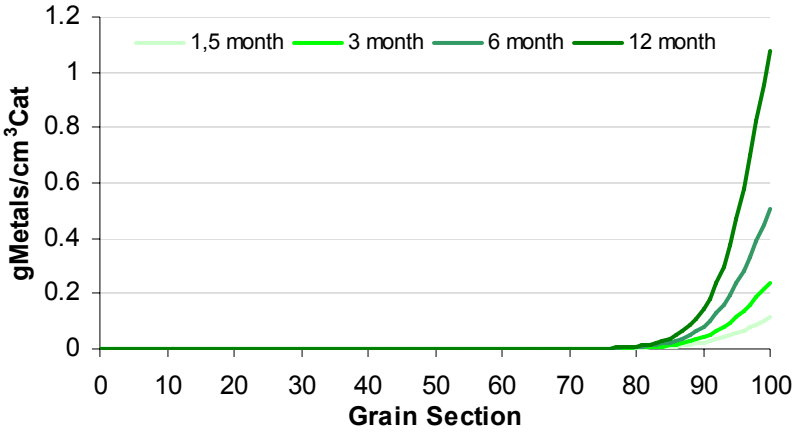

Figure 4.34 Grain profile for metals for the last reactor section along the run time in adiabatic mode

Total Deposits

The total deposits profiles confirm the conclusions obtained by the comparison between the profiles of coke and metals for isothermal and adiabatic mode. As concluded, the major differences between this two operation modes reside in the metals deposition profiles which are reflected in the accumulation of deposits near the surface. Hence, in the adiabatic run, the content of deposits near the surface is lower at the entrance (Figure 4.35) and higher at the exit (Figure 4.36) when compared with the isothermal simulation. On the other hand, in the grain center, the results are similar, as already observed by comparison of the coke profiles. It should be noted however that the total amount of deposits remains higher at the inlet than at the outlet of the reactor.

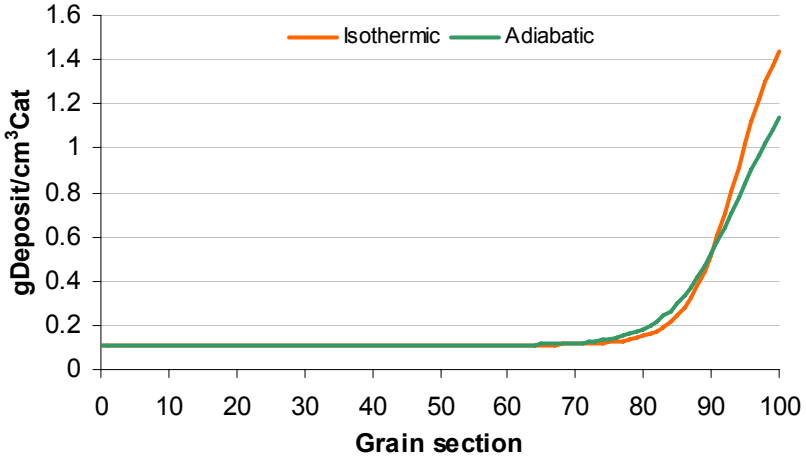

Figure 4.35 Representation of the total deposits inside the catalyst grain for the reactor entrance at the end of 12 months run in adiabatic or isothermal modes

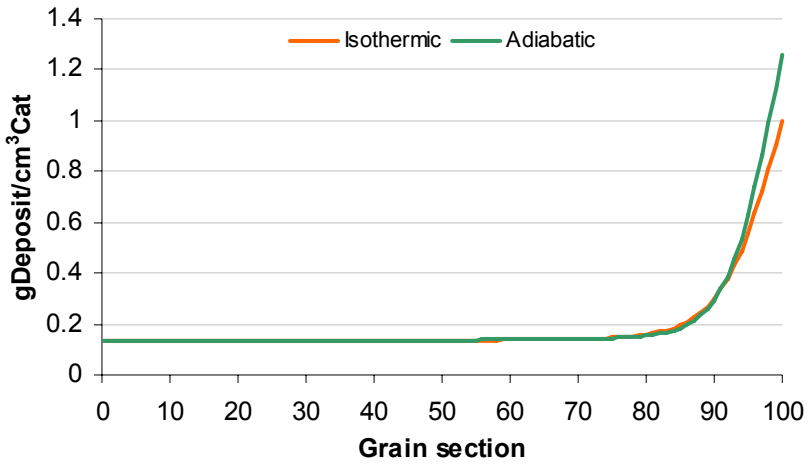

Figure 4.36 Representation of the total deposits inside the catalyst grain for the reactor exit at the end of 12 months run in adiabatic or isothermal modes

4.3.3. Reactor profiles

Since some reactor profiles obtained in adiabatic mode are similar to those obtained in isothermal mode, they are only shown in the appendices' chapter.

Families of compounds

The profiles obtained in adiabatic mode are similar to those obtained in isothermal mode. For this reason, and since all the conclusions are equal, they are in the appendices' chapter 7.2.1.

Coke

Temperature has a big influence on coke formation since it changes the kinetic and equilibrium constants. For this motive, the time that a given section of the reactor takes to reach the equilibrium, decreases along the reactor. This happens because with the temperature increase, the kinetic parameters also increase. This reduction in time to reach the equilibrium is illustrated in Figure 4.37.

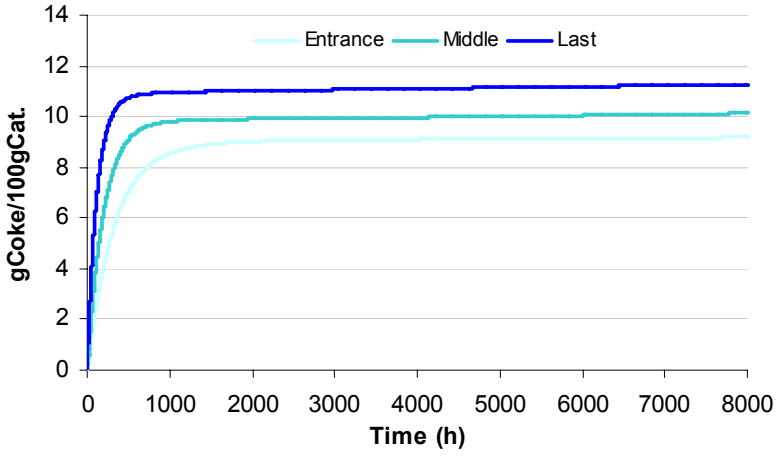

Figure 4.37 Various coke profiles along the time to the adiabatic run for different reactor sections

Since the coke profile along the reactor is similar to the one obtained in isothermal mode, its illustration is shown in chapter 7.2.2.

Metals

As already discussed, in adiabatic mode the metals deposits are more balanced along the reactor. The main consequence of this result is that the front of the reactor did not percolate during the 8000h simulation, as is evident in Figure 4.38.

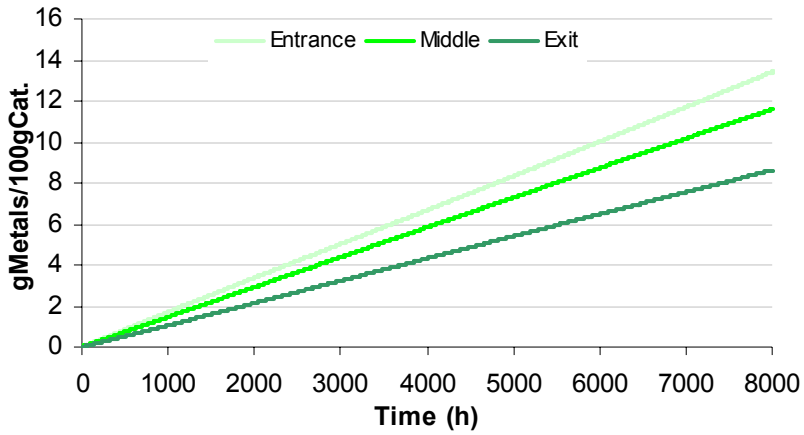

Figure 4.38 Various metals profiles along the run time for different reactor sections

The metals profiles along the reactor are less steep than the ones obtained in isothermal mode but this result has already been discussed. Therefore, these profiles are illustrated in chapter 7.2.2.

Total deposits

As already mentioned, one of the most unexpected results in the adiabatic mode is that percolation does not occurs. From the Figure 4.39, this fact is easily understood since the deposits are more balanced along the reactor and not so concentrated in the inlet. This happens because the temperature gradient increases along the reactor which is also reflected in the kinetic parameters.

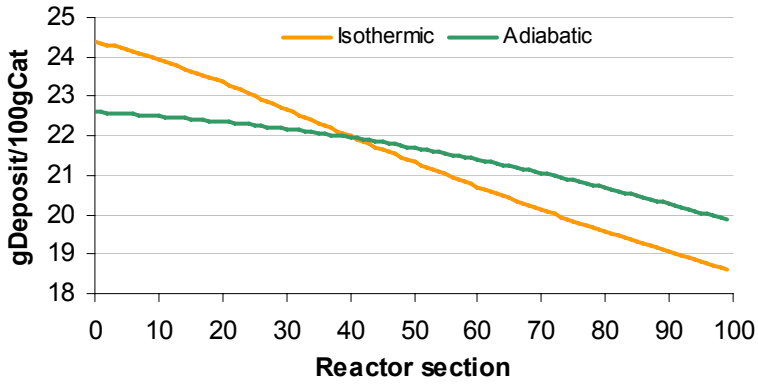

Figure 4.39 Comparison between the deposits profile in isothermal and adiabatic mode for a 12 months run

Contrarily to what happens in isothermal mode, the evolution of the deposits inside the reactor during the simulation does not have always the same trend. In the first month, the deposits content increases along the reactor since the coke is the first one to build-up and it increases through the reactor. As time passes, the metal deposits begin to accumulate preferentially near the inlet. Hence, after the middle of the run time, the deposits profile is already descendent, as can be seen in Figure 4.40.

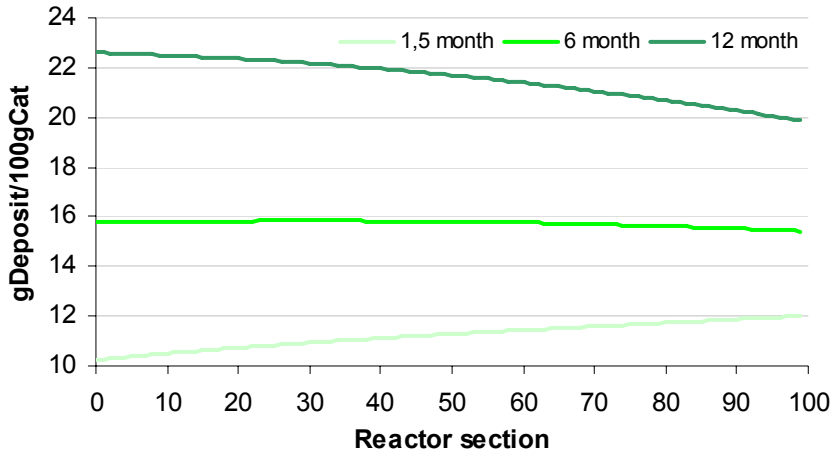

Figure 4.40 Evolution over the time of the deposits profile along the reactor for an adiabatic run

Hydrotreatment

Since the temperature profile inside the reactor is not constant in the adiabatic mode, its effect on the hydrotreatment profiles will be shown in the following figures.

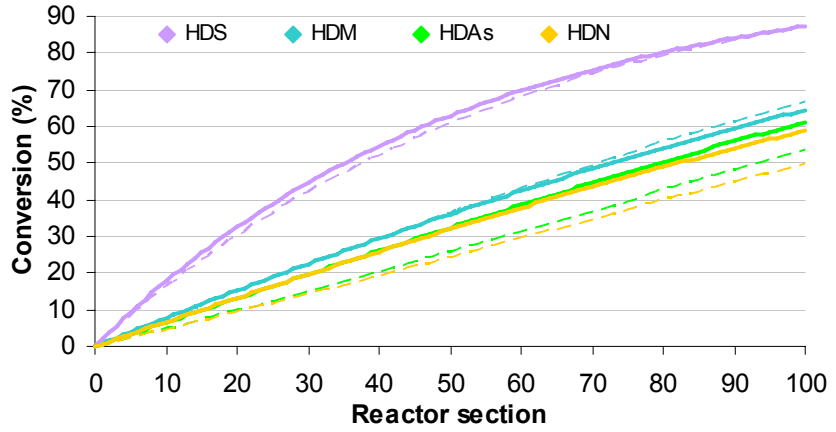

Figure 4.41 Variation in HDS, HDM, HDAs and HDN along the reactor bed. The dashed and full lines respectively correspond to the profiles at the begin and the end of a 12 month run

Comparing Figure 4.26 and Figure 4.41, the main difference between them is that in the adiabatic operation there is no percolation at the end of the run, as already discussed.

As happens in Figure 4.26, Figure 4.41 also shows that the extent of the hydrotreatment reactions changes. This is due to the differences in activation energies of each one of them.

If the hydrotreatment profiles of the two operating modes are compared, as illustrated in Figure 4.42, it is noticeable that in adiabatic mode (full lines), all the profiles are below the isothermal ones, only reaching the same performance at the outlet. This is because in adiabatic conditions, the inlet reactor temperature is lower (see Figure 4.29) which results in lower kinetic constants. Advancing in the reactor bed, temperature starts to increase and therefore all the kinetic parameters. In both simulations, the kinetic parameters are equal near the middle of the bed. At the end, they are higher than in isothermal mode.

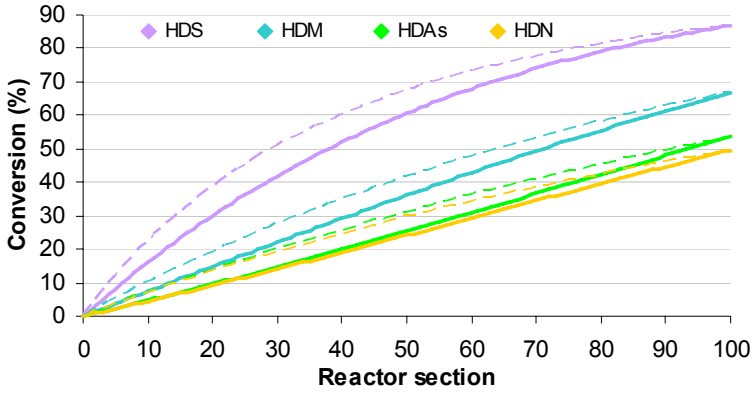

Figure 4.42 Variation in HDS, HDM, HDAs and HDN along the reactor bed. The dashed and full lines respectively correspond to the initial profiles of isothermal and adiabatic modes

Since the HDS performance in the adiabatic run was maintained, the profiles of the sulfur contained in the families of compounds are similar to those obtained in isothermal mode presented in Figure 4.28 except the fact that at the end of the run the reactor bed is not percolated. Hence, they are illustrated only in chapter 7.2.3.

4.4. Simulation of an industrial hydrotreatment unit

Industrial hydrotreatment units have two sections using different catalysts, the HDM and the HDS section. In the fixed bed HYVAHL process, the first section (HDM) can include 3 reactors where the first 2 work as swing reactors. The second section (HDS) may include also 3 reactors. Industrially, the catalyst of the swing reactors in HDM section is completely replaced every 2 months because of the bed plugging in between the catalyst particles. Hence, the pressure drop over the first reactor becomes too high and the catalyst needs to be replaced.

In THERMIDOR, a simulation was made with 6 reactors, 3 in every section. The catalyst used in HDM section is a “chestnut bur” catalyst, while the HDS catalyst is a monomodal catalyst.

Since THERMIDOR does not account for coke deposition in the void space between the catalyst particles, the swing operation of the two first reactors will not be accounted for in the simulation.

The results obtained are presented in the following subchapters.

4.4.1. Temperature profiles

Figure 4.43 illustrates the temperature profiles along the reactors. Between every reactor there is a hydrogen quench which causes the temperature to drop. The evolution of the percolation in each reactor can also be clearly noticed (temperature does not change). In our simulation, the catalyst in the HDM section is completely dead after 1.5 months. This result is not normal and the causes will be discussed below.

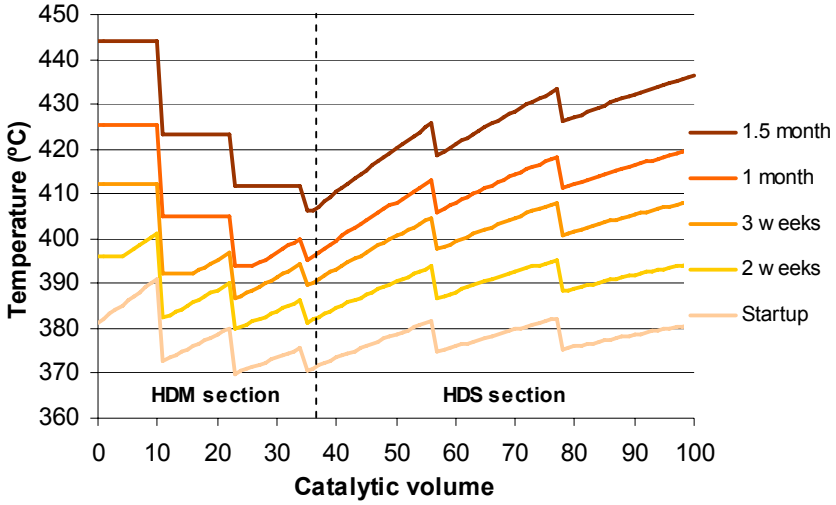

Figure 4.43 Evolution of the temperature profiles along the reactors during the simulation time

4.4.2. Hydrotreatment profiles

Comparing the typical hydrotreatment profiles (HDM and HDS) presented in Figure 1.8 with the startup profiles from Figure 4.44, illustrates the good agreement between the simulation and the experimentally observed profiles. This means that THERMIDOR has the ability to simulate a complete hydrotreatment industrial unit. As can be seen from the Figure 4.44, at the end of the run, the catalyst in the HDM section has become completely inactive strongly reducing the HDM performance of the unit.

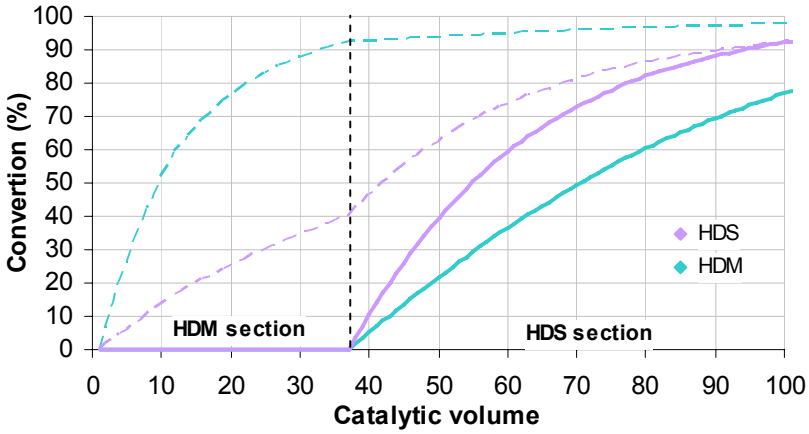

Figure 4.44 Variations in HDM and HDS as function of the advancement in the catalytic volume. The dashed and full lines respectively correspond to the profiles at the begin and the end of a 3 month run

4.4.3. Grain profiles

The grain profiles will be shown in the following section. A comparison between the HDM and the HDS catalyst will be made.

Families of compounds

Figure 4.45 shows that, by comparison with Figure 4.9, the asphaltenes and resins penetrate more into the grain for the HDM catalyst. Although this penetration seems to be higher, an even more deep diffusion was expected. This may reveal a problem in the choice of the diffusion coefficients, in the coding of the diffusion mechanism or in the representation of HDM catalyst in THERMIDOR.

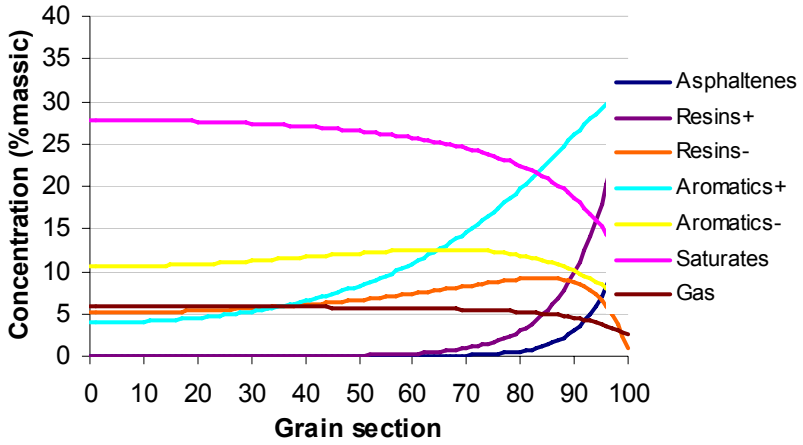

Figure 4.45 Profiles of the families of compounds in the first slice of the HDM section

Coke

From the comparison between Figure 4.46 and Figure 4.11, it is concluded that the coke accumulates more in the center of the grain in the HDM catalyst. This happens because the heaviest species such like asphaltenes and resins penetrate deeper into the catalyst particle.

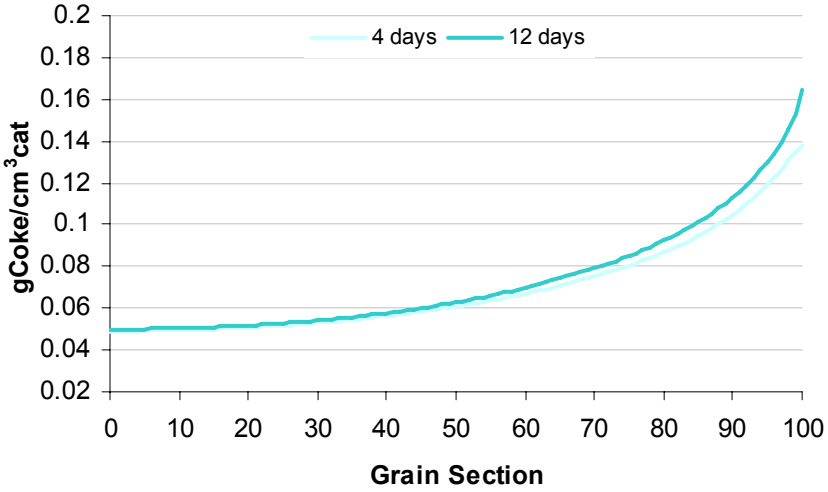

Figure 4.46 Coke's grain profile for the first slice of the HDM section

Metals

Although in the HDM catalyst the heavier species like asphaltenes and resins penetrate more deeply into the catalyst grain, from the comparison of Figure 4.47 with Figure 4.13 it is concluded that for the HDM catalyst the metals accumulate closer to the outer surface of the grain. This should not be happening because the objective of the HDM catalyst is to permit the access of the heavier compounds to the center, which results in an increase of the capacity to retain metals. This demonstrates that the HDM catalyst is not well implemented in THERMIDOR, with either the diffusion or the reaction being under or overestimated. The simulation of the HDM section therefore needs improvements.

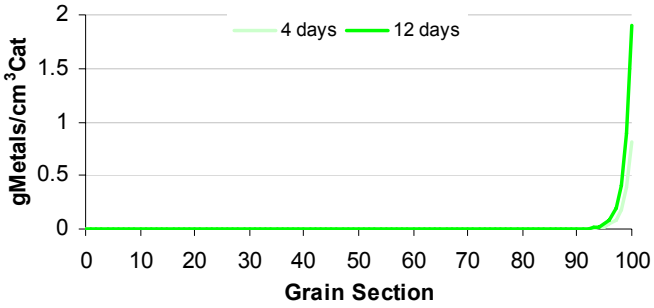

Figure 4.47 Metals' grain profile for the first slice of the HDM section

4.4.4. Reactor profiles

After showing the grain profiles and identifying some limitations of THERMIDOR, the profiles for coke, metals and the families of compounds along the catalytic volume will now be shown.

Families of compounds

The HDM catalyst favors the disaggregation of the heavier compounds such like asphaltenes and resins into lighter ones. This happens because it contains a high macro and mesoporosity (see Figure 1.6). As can be seen in Figure 4.48, the difference between the two types of catalyst is not as evident as expected. Future developments in the HDM catalyst will therefore probably be needed.

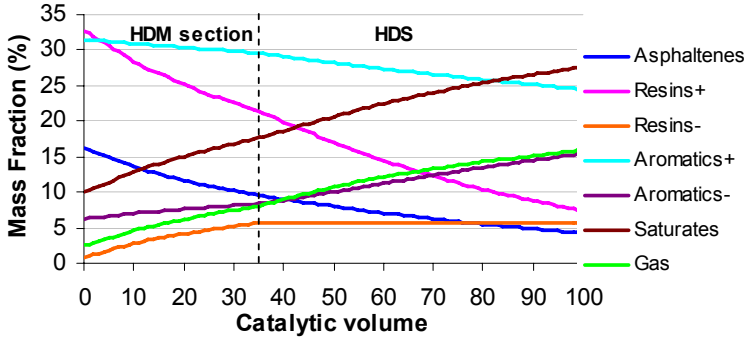

Figure 4.48 Profiles of the families of compounds along the catalytic volume at the startup of the hydrotreatment unit

Coke

As can be seen from Figure 4.49, the equilibrium coke content is higher for the entrance of the HDS section than for the HDM, although the temperature in the HDM entrance is higher. This may be due to the aromaticy effect (see chapter 3.2) that will be higher for the HDS entrance, or to the early percolation (<200h) of the HDM section.

It can be also observed in this figure that the equilibrium is more rapidly reached in the HDM than in the HDS catalyst. This is probably due to the deeper penetration of heavy products in the HDM catalyst, since the coking parameters have been kept the same for both catalysts.

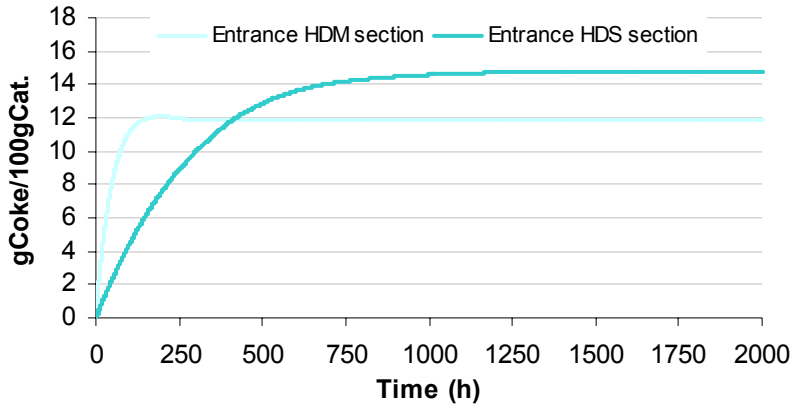

Figure 4.49 Coke profiles along the time for the entrance of the HDM and HDS reactor sections

The coke content along the catalytic volume is illustrated in Figure 4.50. The big difference between the HDM and HDS section is due to the time needed to reach the equilibrium in each section, as well illustrated in Figure 4.49. If a closer look is made into the HDM reactor section, it is visible that the tendency of the coke gradient changes with time evolution. This happens because the percolation of the HDM catalyst already begins at the 10th day. This event changes the aromaticy effect and reduces the equilibrium constant in the sections after to the percolated ones, reducing also the coke content.

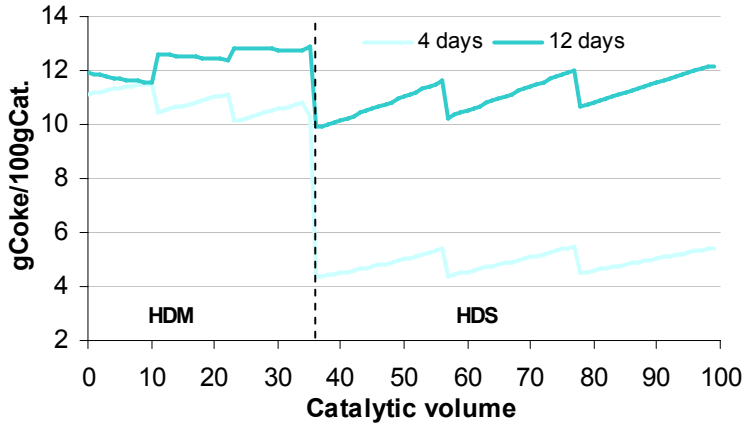

Figure 4.50 Coke profiles along the catalytic volume for different simulation times

Metals

The main objective of the HDM section is to reduce the metals content in the feed, protecting the HDS catalyst from metal deactivation. As shown in Figure 4.51, near the 250 hours (approximately 10 days) the first slice of the HDM section became plugged and the metals content in the HDS section starts to increase. As already referred, the HDM catalyst activity is probably not well defined in THERMIDOR since it should retain near 100 wt% of his weight of metals, while the simulations show that the catalyst percolates after 10 wt% of metals deposition.

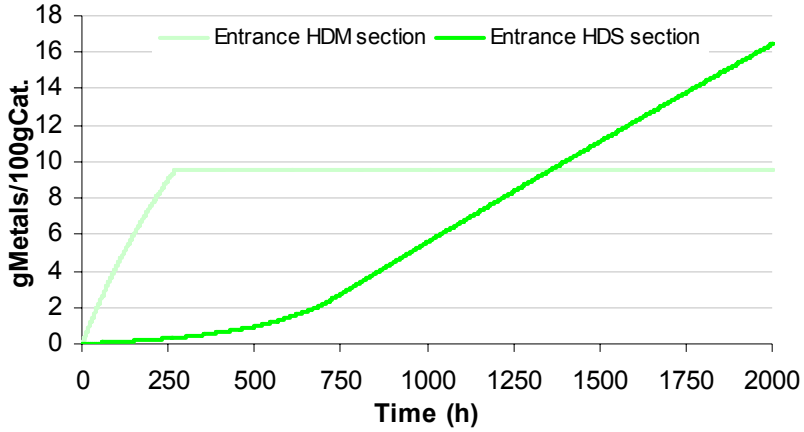

Figure 4.51 Metals profiles along the time for the entrance of the HDM and HDS reactor sections

From the analysis of Figure 4.52, it is again evident that the HDM catalyst is not well defined since the HDS catalyst is able to retain more metals (after 3 months) before percolating. In spite of this, the metal deposition profiles before the 12th day (before percolation starts) seem correct.

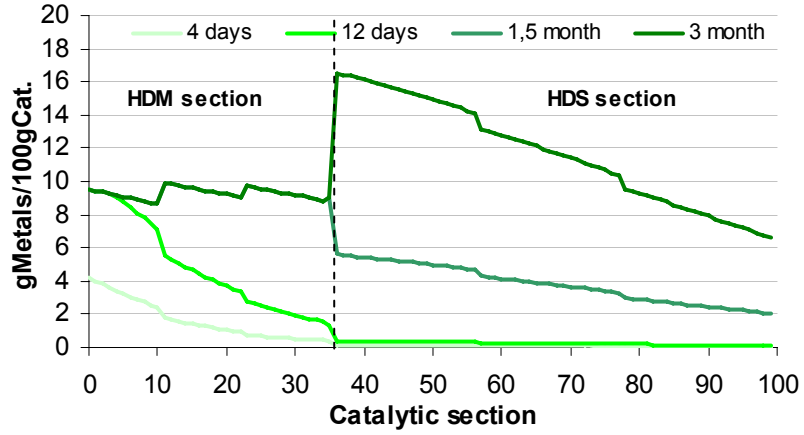

Figure 4.52 Metals profiles along the catalytic volume for different simulation times

5. Conclusions and perspectives

The objective of the present traineeship was to improve the process model by accounting for catalyst deactivation through coke laydown and metals deposition.

In agreement with the obtained results, it is now possible to say that the representation of the deactivation process is satisfactory for the HDS catalyst. The deactivation equation implemented contains a physical part predicted by the model, the surface area reduction, and an empirical deactivation term. Since the results are acceptable only using the physical part, the empirical deactivation functions have not been used.

To take into account the increase of coke along the reactor, an "aromaticy" effect was implemented in the code. This effect reflects the variation of the asphaltenes and maltenes aromaticity across the reactor bed. The implementation of this effect has enabled the possibility to adjust the variation of coke along the reactor. When the catalyst starts to plug however, the aromaticity effect decreases resulting in a decline of the equilibrium coke. This result does not have any experimental validation at this moment. Hence, this effect could also be implemented in a different way.

Finally, after the modifications were implemented and some parameters tuned, the deactivation curve obtained was much more realistic than that of the previous version.

THERMIDOR also demonstrates well the existing difficulties to desulfurize the heaviest compounds such like asphaltenes and resins.

For the two modes of simulation in THERMIDOR, adiabatic and isothermal, it was concluded that in adiabatic mode the catalyst lasts longer. This is due to a more balanced deposition of the metals along the bed.

A simulation of an industrial hydrotreatment unit was also carried out. This simulation has demonstrated that THERMIDOR has the ability to simulate a complete industrial unit which includes the HDM and HDS sections. Although the hydrotreatment profiles obtained at startup were acceptable, the diffusion of the heaviest molecules into the HDM catalyst is not well described since they only penetrate a little deeper into the grain than for the HDS catalyst. Another problem with the HDM catalyst is the metals deposition. They accumulate for too much near the exterior surface. This results in a total retention capacity of about 10 wt%, which is lower than that of the HDS catalyst. Thus, future developments for the catalyst in the HDM section will be needed.

6. References

[1] LE PAGE, J.F.; CHATILA, S.G.; DAVIDSON, M., *Resid and Heavy Oil Processing*, Éditions TECHNIP, Paris, 1992

[2] GARY, J.H.; HANDWERK, G.E.; KAISER, M.J., *Petroleum Refining, Technology and Economics*, Fifth Edition, Taylor & Francis Group, 2007

[3] RASEEV, Serge, *Thermal and Catalytic Processes in Petroleum Refining*, Marcel Dekker, Inc., New York, 2003

[4] BEECKMANS, J.L., *Modélisation de la Désactivation des Catalyseurs utilisés dans l'hydrotraitement des résidus lourds*, Institut Français du Pétrole, 2006

[5] PINHEIRO, A.F.N, *Modeling of a fixed bed residue conversion process*, Traineeship Report, Institut Français du Pétrole, 2005

[6] LEPRINCE, P., *Petroleum Refining - Conversion Processes*, Editions TECHNIP, Paris, 2001

[7] RANA, M.S.; SÁMANO, V.; ANCHEYTA, J.; DIAZ, J.A.I., A review of recent advances on process technologies for upgrading of heavy oils and residua, Fuel, 86, pg. 1216-1231, 2007

[8] MYERS, R.D.; MACLEOD, J.B.; GHOSH, M.; CHAKRABARTY, T., Exxon Research and Engineering Co. Producing Pipelinable Bitumen, US Patent 6,096,192, 2000

[9] KANEKO, T.; TAZAWA, K.; OKUYAMA, N.; TAMURA, M.; SHIMASAKI, K., Fuel, 79, pg. 263, 2000

[10] SASAKI, M.; SONG, C.; PLUMMER, M.A., Fuel, 79, pg. 295,2000

[11] FONSECA, A.; ZEUTHEN, P.; Nagy, J.B., Fuel, 75, pg. 1363, 1996

[12] ZEUTHEN, P.; BARTHOLDY, Jesper et al., *Formation of coke on hydrotreating catalysts and its effect on activity*, Catalyst Deactivation, Vol.88, pg. 199-206, 1994

[13] MARAFI, M. ; STANISLAUS, A., Applied Catalysis, 159, pg. 259, 1997

[14] NETZEL, D.A. et al., Fuel, 75, pg. 1397, 1996

[15] CABLE, T.L.; MASSOTH, F.E.; THOMAS, M.G., Fuel Processing Technology, 4, pg. 265, 1981

[16] FURIMSKY, Edward; MASSOTH, Franklin E., *Deactivation of hydroprocessing catalysts*, Catalysis Today, 52, pg. 381-495, Elsevier, 1999

[17] WIWEL, P.;ZEUTHEN, P.;JACOBSEN, A.C., Catalyst Deactivation, pg. 257, 1991

[18] JONG, K.P.; REINALDA, D.; EMEIS, C.A., Catalyst Deactivation, pg. 155, 1994

[19] TERNAN, M.; FURIMSKY, E.; PARSONS, B.I., Fuel Processing Technology, 2, pg. 45, 1979

[20] RICHARDSON, S.M.; NAGAISHI, H.; GRAY, M.R., Industrial & Engineering Chemistry Research, 35, pg. 3940, 1996

[21] OELDERIK, J.M.; SIE, S.T.; BODE, D., *Progress in the catalysis of the upgrading of petroleum residue. A review of 25 years of R&D on Shell's residue hydroconversion technology*, Applied. Catalysis, 47, pg. 1-24, 1989

[22] BEGUIN, F. ; SETTON, R, Carbon, 10, pg. 539, 1972

[23] KOVACIC, P.; OZIOMEK, J., Journal of Organic Chemistry, 29, pg. 100, 1964

[24] MEOT-NER, M., Journal of Physical Chemistry, 88, pg. 2724, 1980

[25] FLOCKART, B.D.; SESAY, I.M.; PINK, R.C., Journal Chem. Soc. Chem. Comm., 10, pg. 439, 1980

[26] GATES, B.C.; KATZER, J.R.; SCHIT, G.C.A., Chemistry of Catalytic Processes, McGraw Hill, New York, 1979.

[27] SCARONI, A.W.; JENKINS, R.G., Am. Chem. Soc. Div. Petrol. Chem. (Preprints), 30, pg. 544, 1985

[28] LEWIS, I.C.; SINGER, L.S., Am. Chem. Soc. Div. Petrol. Chem. (Preprints), 31, pg. 834, 1986

[29] NOHARA, D.; SAKAI, T., Industrial & Engineering Chemistry Research, 31, pg. 14, 1992

[30] ABSI-HALABI, M.; STANISLAUS, A.; TRIM, D.L., Applied Catalysis, 72, pg. 193-215, 1991

[31] KOYAMA, H.; NAGAI, E.; KUMAGAI, H., *Catalyst deactivation in commercial residue hydrodesulfurization*, Preprints, International Symposium on Deactivation and Testing of Hydrocarbon Conversion Catalysts, Div. Pet. Chem., 210th Nat. Mtg. ACS, Chicago, 1995

[32] MYERS, T.E.; LE, F.S.; MYERS, B.L.; FLEISCH, T.H.; ZAJAC, G.E., AIChE Symposium Series 273, vol. 85, pg. 32, 1989

[33] TAMM, P.W.; HARNSBERGER, H.P.; BRIDGE, A.G., Industrial Engineering Chemistry Process Design and Development, 20, pg. 262, 1981

[34] BEUTHER, H.; LARSON, O.A.; PERROTTA, A.J., *The mechanism of coke formation on catalysts*, Catalyst Deactivation, pg. 271, 1980

[35] NEWSON, E.; Industrial Engineering Chemistry Process Design and Development, 14, pg. 27, 1975

[36] JACOBSEN, A.C.; COOPER, B.H.; HANNERUP, P.N., 12th Petrol World Congress, volume 4, pg. 97, 1987

[37] MITCHELL, P.C.H.; Catalysis Today, 7, pg. 439, 1990

[38] HUANG, C.-W; WEI, J., Industrial Engineering Chemistry Process Design and Development, 19, pg. 250, 1980

[39] HUANG, C.-W; WEI, J., Industrial Engineering Chemistry Process Design and Development, 19, pg. 257, 1980

[40] WARE, R.A.; WEI, J., Journal of Catalysis, 93, pg. 100, 1985

[41] WEITKAMP, J.; GERHARDT, W.; SCHOLL, D., Proc. 8th International Congress on Catalysis, vol. II, pg. 269, 1984

[42] HUNG, C.W., Ph.D Thesis, MIT, Cambridge, MA, 1979

[43] JANSSENS, J.P.; ELST, G.; SCHRIKKEMA, E.G.; VAN LANGEVELD, A.D.; SIE, S.T.; MOULIJN, J.A., Recl. Trav. Chim. Pays Bas, 115, pg. 465, 1996

[44] REYES, L.; ZERPA, C.; KRASUK, J. H., *Catalyst deactivation in HDM of heavy deasphalted oils*, Catalyst Deactivation, pg. 85, 1994

[45] SIE, S.T., *Catalyst deactivation by poisoning and pore plugging in petroleum processing*, Catalyst Deactivation, pg. 545, 1980

[46] YOKOYAMA, Y.; ISHIKAWA, N.; NAKANISHI, K.; SATOH, K.; NISHIJIMA, A.; SHIMADA, H.; MATSUBAYASHI, N.; NOMURA, M., *Deactivation of Co-Mo/Al2O3 hydrodesulfurization catalysts during a one-year commercial run*, Catalysis Today, 29, pg. 216-266, 1996

[47] VAN DORN, J.; MOULIJN, J.A.; DJEGA-MARIADASSOU, G., Applied Catalysis, 63, pg. 77, 1990

[48] SILBERNAGEL, B.G.; RILEY, K.L., *Heavy feed hydroprocessing deactivation: The chemistry and impact of vanadium deposits*, Catalyst Deactivation, pg. 313, 1980

[49] DAUTZENBERG, F.M.; KLINKEN, J.; PRONK, K.M.A.; SIE, S.T.; WIJFFELS, J.B., *Catalyst deactivation through pore-mouth plugging during residue desulfurization*, 5th International Symposium on reactor engineering, ACS Symp. Ser. 65, pg. 254-267, 1978

[50] BIRTILL, J.J.; BERGER, R., *Industrial catalyst decay - Part I: Review of test methods and Part II: Literature review, gaps and need*, EUROKIN, 2004

[51] OYEKUNLE, L.; HUGHES, R., *Catalyst deactivation during hydrodemetallization*, Industrial & Engineering Chemistry Research, 26, pg. 1945-1950, 1987

[52] TAKATSUKA, T.; WADA, Y.; Inoue, S., *A catalyst deactivation model for residual oil hydrodesulfurization and application to deep hydrodesulfurization of diesel fuel*, Deactivation and Testing of Hydrocarbon-Processing Catalysts, ACS Symp., 634, Chapter 30, pg. 414-427, 1996

[53] JANSSENS, J.P.; LANGEVELD, A.D.; SIE, S.T.; MOULIJN, J.A., *Catalyst deactivation in hydrodemetallization*, Deactivation and Testing of Hydrocarbon-Processing Catalysts, ACS Symp., 634, Chapter 18, pg. 238-252, 1996

[54] CORELLA, J.; ADANEZ, J.; MONZÓN, A., *Some intrinsic kinetic equations and deactivation mechanism leading to deactivation curves with a residual activity*, Industrial & Engineering Chemistry Research, 27, pg. 375-381, 1988

[55] GONÇALVES, N., Modeling of a fixed bed hydrotreating reactor, Traineeship Report, Institut Français du Pétrole, 2006

[56] TOULHOAT, H.; HUBEDINE, D.; RAYBAUD, P.; GUILLAUME, D.; KRESSMANN, S., *THERMIDOR: A new model for combined simulation of operations and optimization of catalysts in residues hydroprocessing units*, Catalysis Today, 109, pg. 135-153, 2005

[57] HUBEDINE, D.; RAYBAUD, P.; TOULHOAT, H., *Un code de simulation du vieillissement des catalyseurs associés dans une unité d'hydrotraitement de résidus*, Master's thesis, ENSIC, 1999

[58] PERRY, J.H., *Chemical Engineer's Handbook*, Fourth Edition, Mc Graw-Hill, New York, 1963

[59] TOULHOAT, H.; SZYMANSKI, R.; PLUMAIL, J.C., Catal. Today, 7, pg.531, 1990

[60] SMITH, B.; WEI, J., J. Catal., 132, pg. 21, 1991

[61] GUALDA, G.; KASZTELAN, S., J. Catal., 161, pg.319, 1996

[62] FROMENT, G.F.; BISCHOFF, K.B., Chemical Reactor Analysis and Design, 2nd edition, Wiley, 1977

[63] SPRY, J.; SAWYER, W., Paper presented at 68th annual aiche meeting, Los Angeles, 1975

[64] WEISSBERG, H.J., J. Appl. Phys., 34 (9), pg. 2636,1963

[65] EEKELEN, H.A.M., J. Catal., 29, pg. 75, 1973

[66] MACÉ, O.; WEI, J., Ind. Eng. Chem. Res., 30, pg. 909, 1991

[67] TOULHOAT, H.; JACQUIN, Y.; DUPIN, T., US Patent 4,499,203, 1985

[68] DEVOLDERE, K.R. ; FROMENT, G., *Coke formation and gasification in the catalytic dehydrogenation of ethylbenzene*, Industrial & Engineering Chemistry Research, 38, pg. 2626-2633, 1999

[69] WIEHE, I.A., Industrial & Engineering Chemistry Research, 32, pg. 2447, 1993

[70] TAKATSUKA, T.; WADA, Y.; HIROHAMA, S.; FUKUI, Y., Journal of Chemical Engineering of Japan, 22, pg. 298, 1986

7. Appendices

7.1. Experimental data for coke and metals deposition

Table 7.1 list the experimental data for coke and metals deposits for a 7700h HDS run with a demetallized vacuum residue feed*.

Table 7.1 Experimental data for coke and metals deposition on a HDS catalyst after a 7700h run with a demetalized vacuum residue feed

Ref. IFP	E10360U1	E10360U2	E10360U4	E10360U5	E10360U8	E10360U9
Reactor position	0 (entrance)	12.5	37.5	50	87.5	100 (exit)
Ni+V (wt %)	10.1	8.1	5.5	4.2	3.2	3.0
Coke (wt %)	10.5	9.4	10.8	11.7	13.8	12.6

7.2. Some adiabatic profiles

7.2.1. Families of compounds

Grain profiles

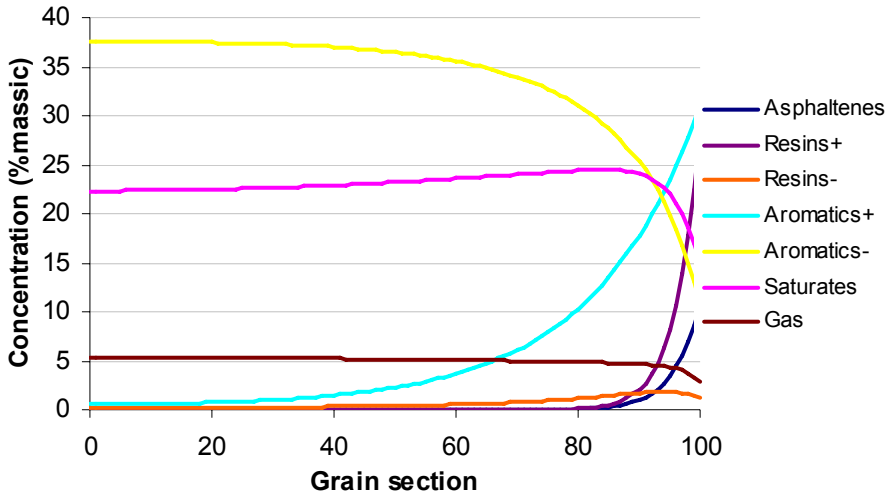

Figure 7.1 Profiles of the families of compounds in the grain for the first reactor section

* IFPTechnical note RH10 – VH/mcr – nº74

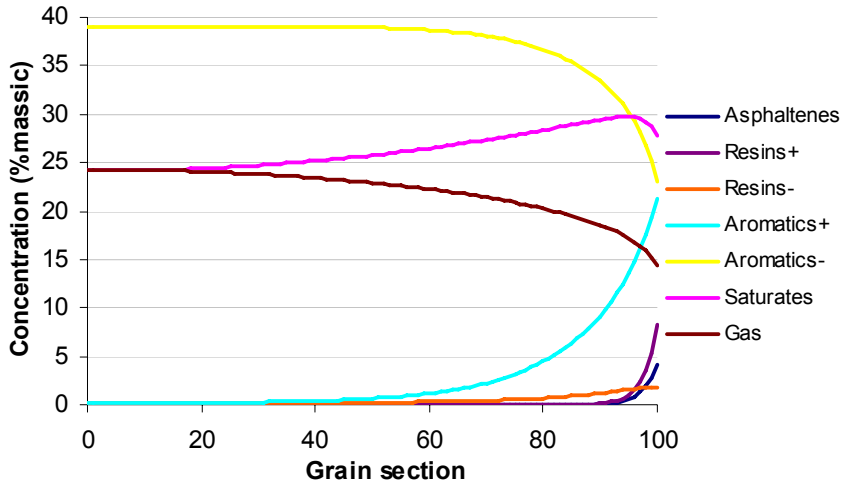

Figure 7.2 Profiles of the families of compounds in the grain for the last reactor section

Reactor profiles

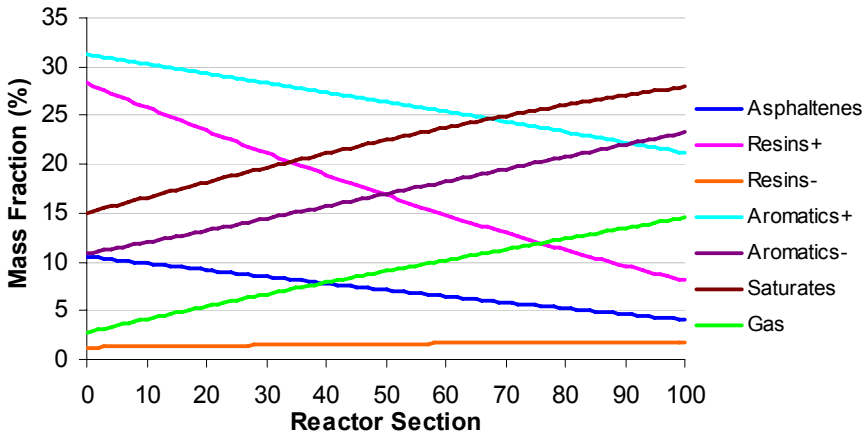

Figure 7.3 Profiles of the families of compounds along the reactor for a 12 month simulation

7.2.2. Coke and metals deposits along the reactor

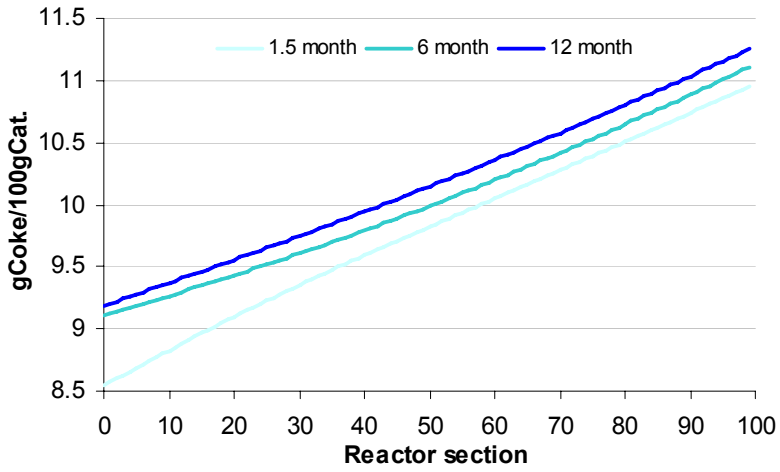

Figure 7.4 Various coke profiles along the reactor for different run times

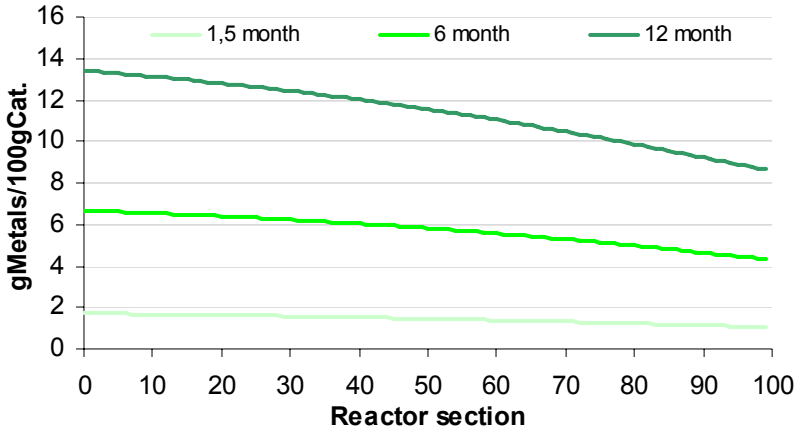

Figure 7.5 Various metals profiles along the reactor for different run times

7.2.3. Hydrotreatment profiles

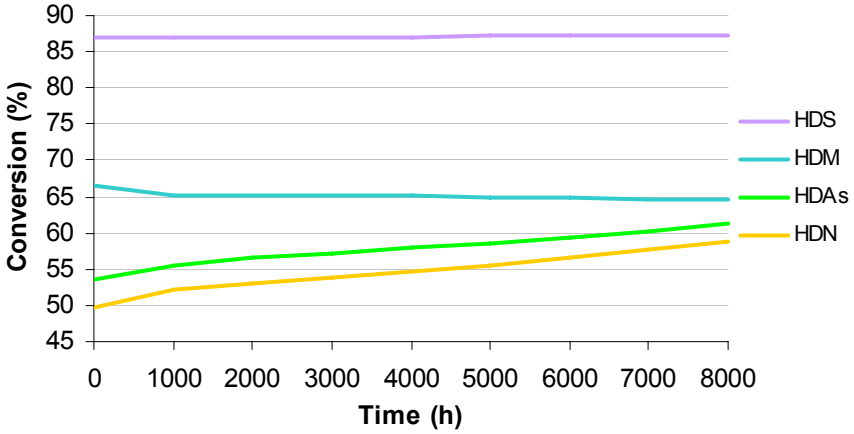

Figure 7.6 Variation in HDS, HDM, HDAs and HDN reactor performances along the time

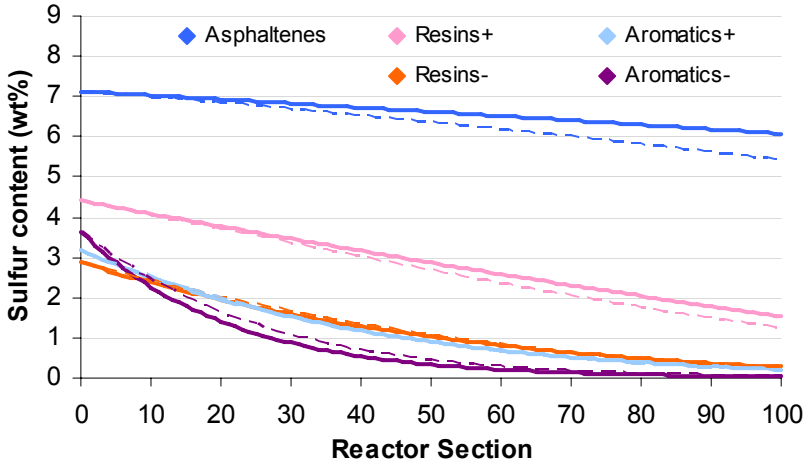

Figure 7.7 Evolution of the sulfur content in families of compounds along the reactor. The dashed and full lines respectively correspond to the profiles at the begin and the end of a 12 month run